MAGNON SPIN TRANSPORT IN MAGNETIC HETEROSTRUCTURES

by

Yihong Cheng

A Dissertation Submitted to the Faculty of the

DEPARTMENT OF PHYSICS

In Partial Fulfillment of the Requirements

For the Degree of

DOCTOR OF PHILOSOPHY

In the Graduate College

THE UNIVERSITY OF ARIZONA

2020

THE UNIVERSITY OF ARIZONA
GRADUATE COLLEGE

As members of the Dissertation Committee, we certify that we have read the dissertation prepared by: Yihong Cheng
titled:

and recommend that it be accepted as fulfilling the dissertation requirement for the Degree of Doctor of Philosophy.

Shufeng Zhang — Date: Mar 31, 2020
Shufeng Zhang

R. Binder — Date: Mar 31, 2020
R. Binder

Charles William Wolgemuth — Date: Apr 1, 2020
Charles William Wolgemuth

Arvinder Sandhu — Date: Mar 31, 2020
Arvinder Sandhu

Weigang Wang — Date: Mar 31, 2020
Weigang Wang

Final approval and acceptance of this dissertation is contingent upon the candidate's submission of the final copies of the dissertation to the Graduate College.

I hereby certify that I have read this dissertation prepared under my direction and recommend that it be accepted as fulfilling the dissertation requirement.

Shufeng Zhang — Date: Mar 31, 2020
Shufeng Zhang
Physics

ACKNOWLEDGEMENTS

The journey at the University of Arizona over the last six years pursuing the doctoral degree in Physics is memorable and rewarding to me. However, the lifestyle as being a Ph.D. student finally comes to the end and I would always remember this special period in my whole life. Here, I would take this opportunity to express my gratitude to all those people who tutored, helped and accompanied me during my graduate school.

Foremost, I would like to express my deepest gratitude to my advisor, Dr. Shufeng Zhang for his guidance and support. I am so fortunate to have had one of the very best advisors to learn physics from and do physics with. I am always impressed by his insight, passion and hardworking in working with physics. Throughout my graduate studies, Dr. Zhang has motivated and guided me to have completed several research projects and I am so grateful that I could have the opportunity to explore the world of physics with his help.

Besides, I would also want to thank my dissertation committee members, Dr. Weigang Wang, Dr. Rudolf Binder, Dr. Arvinder Sandhu, and Dr. Charles Wolgemuth for their support during my graduate years. Especially, I would like to thank Dr. Wang for being an excellent collaborator. I am also very grateful to my group members and fellow students for all the helpful discussions, Dr. Kai Chen, Dr. Anirban Kundu, Dr. Fei Huang, Meng Xu, Tiankui Zhang, Adam Wallace, Dr. Xiaolin Xu, Ping Tang and many more inside the department.

Finally, I thank my wife Yanan Liu, my parents Shineng Zhang and Yatun Zhu and all the other family members for their endless love, help and support alone this journey. I am truly indebted to them forever.

DEDICATION

To my wife Yanan Liu,

my parents Shineng Zhang and Yatun Zhu,

and my family.

TABLE OF CONTENTS

List of Figures

Abstract

In the study of spintronics, one of the most important issues is to identify and manipulate spin currents. The two most profound effects in spintronics, giant magnetoresistance and spin-transfer torque, are the results of the interplay between spin-polarized electron transport and magnetization dynamics. On the other hand, the magnons are also capable of carrying angular momentum currents or spin currents. Magnons are quantized low-energy collective excitations of magnetic materials. Besides the finite energy and crystal momentum, each quasi-particle magnon is also known to have an angular momentum $\hbar$. This dissertation summarizes my doctoral study about the magnon spin transport in magnetic heterostructures.

The first part of my dissertation is devoted to the interplay of magnon and electron currents in heterostructure of ferromagnetic metals. We theoretically formulate the spin-magnon coupled transport by explicitly taking into account the exchange coupling between the conduction electrons and magnons. The intrinsic strong $s-d$ exchange coupling in itinerant ferromagnets inevitably leads to substantial magnon current, in addition to the polarized electron current. Even for a uniformly magnetized conducting ferromagnet, we find an electric charge current is always accompanied with a magnon current at finite temperature.

The second part is the study of incoherent magnon transport in heterostructure of magnetic insulators. We propose an insulating spin valve, which is made of an antiferromagnetic insulator sandwiched between two ferromagnetic insulator layers. Instead of conduction electrons, the incoherent magnons in this structure serve as angular momentum carriers. We predict two transport phenomena in such structure in the presence of a temperature gradient: the giant magneto-spin-Seebeck effect and

the magnon transfer torque.

In the third part, we explore the spin-transfer torques in magnetic tunnel junctions with an antiferromagnetic insulator as the tunnel barrier. The voltage bias induced asymmetric heating would create a magnon current flowing across the antiferromagnetic layer, resulting a magnon transfer torque in addition to the electron spin-transfer torque. This study presents a potential method to realize more energy efficient switching in spin-transfer torque induced magnetization switching in magnetic tunnel junctions.

At last, we study the magnon spin transport property in non-collinear antiferromagnets. In such system, the magnon spectra displays non-trivial multi-band structure with unconventional spin-momentum locking. We study the roles of these magnons on the charge and spin transport properties. The magnon spin conductivity tensor has a more complicated symmetry properties compared to the spin Hall conductivity tensor in non-magnetic metals.

Chapter 1

Introduction

1.1 Background and overview

Spin is an intrinsic form of angular momentum carried by elementary particles. In the past three to four decades, the study of spin transport in magnetic materials has emerged as a relatively new research area known as spintronics [5–7]. One of the central issues in spintronics is the identification and manipulation of spin degrees of freedom in solid-state nanostructures. So far, the methods that have been used to generate nonequilibrium accumulation and current of spin polarization involve transport, optical and resonance, e.g. ferromagnetic resonance.

Although the importance of the electron's spin in controlling transport properties was already emphasized by Nevill Mott in 1936 [8] to understand electrical conductivities of transition metals and their alloys, the remarkable scientific and technological breakthroughs in this field all started from the discovery of giant magnetoresistance (GMR) [9, 10] in metallic magnetic multilayers Fe/Cr by Albert Fert and Peter Grünberg back in 1988. They find the electrical resistance of such multilayer structure has a significant change depending on whether the magnetization of adjacent ferromagnetic layers are in a parallel or an antiparallel configuration. Their seminal works were later recognized by the 2007 Nobel Prize in Physics.

Since the discovery of GMR, the spin-dependent transport in solids has attracted many other fundamental research interests as well as many possibilities of applica-

tions. For example, the large and reproducible tunneling magnetoresistance (TMR) of the magnetic tunnel junctions (MTJs) were demonstrated by Miyazaki's and Moodera's groups in 1995 [11, 12]. The MTJs are tunnel junctions with non-magnetic very thin insulating layer sandwiched by ferromagnetic electrodes. Similar to metallic magnetic multilayers, their resistance depends on the relative orientation of the two magnetizations of ferromagnetic electrodes. The MgO barrier-based MTJs [13, 14] show a very large TMR ratio, making them a ideal platform in many experiments and devices.

Another important prediction and discovery in the development of spintronics is the so-called spin-transfer torque (STT) effect [15–20], which is first introduced by J.C. Slonczewski and L. Berger, gives means to field-free electrically manipulate the magnetic moment of a ferromagnet. The idea is that the spin-polarized charge current can transfer its spin angular momentum to the localized magnetization.

Even in non-magnetic materials, a transverse pure spin current can be generated by longitudinal electrical current through relativistic spin-orbit coupling (SOC), known as spin Hall effect (SHE) [21–25]. The inverse spin Hall effect (ISHE) [26, 27], where a transverse charge current can be induced by the injection of spin current in heavy metals, is a powerful method to detect spin current in spintronics. We will discuss these important developments that are introduced so far in Sec. 1.1.1 in more detail.

From technological point of view, GMR's and later on TMR's application to the read heads of the hard disk drives (HDDs) has led to a solid increase of the areal recording density for many years [28]. The magnetic random-access memory (MRAM) [28–30] utilizes the MTJs as the memory cell to achieve nonvolatile memory operations with short access time. Advances in MRAM technology have been closely linked with advances in the study of spintronics: the magnetic state is read through large TMR and usually written by STT method.

On the other hand, magnetic excitations in magnetically ordered system, spin waves (SWs) or magnons [31–33], are an ideal spin current carrier in spintronics. Magnons are quantized low-energy elementary excitations in ferromagnets (FMs)

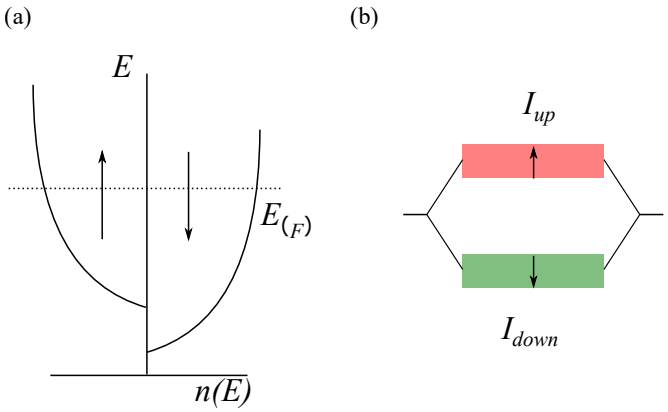

Figure 1.1: (a) Schematic band structure of a ferromagnetic transition metal. The dashed line shows the Fermi level. (b) Schematic for two-current model. Spin-up and spin-down conduction channels are almost independent in the limit of very small spin-flip scattering.

and antiferromagnets (AFMs). In addition to their energy and crystal momentum, magnons are known to have intrinsic angular momentum. Therefore, the translational flow of quasiparticle magnons can be identified as pure spin current since magnons are naturally chargeless.

Although magnons are a well-known concept for many years, the theoretical and experimental study of magnon spin transport in spintronics has emerged as a hot topic recently. For example, spin Seebeck effect (SSE) [34–37] shows a temperature gradient in magnetic materials could drive magnon spin current, in analogy to the thermoelectric Seebeck effect where a charge current is generated by a temperature gradient in solid. Magnons in ferromagnetic insulators (FIs) and AFMs could transport spin information in various structures [38–45]. The proposed magnon valve structure and magnon transfer torque induced magnetization switching [46–48] open new possibilities in the study of solely magnon-related phenomenon in spintronics. This dissertation is majorly focused the study of magnon spin transport in magnetic materials and structures, and we will discuss magnons in more detail in Sec. 1.1.2.

1.1.1 Spin-dependent electron transport in magnetic materials

The spin nature of electron offers new degree of freedom in the study of electron transport properties in solids. It was highlighted long ago by Sir Nevill Mott [8] that electron's spin plays an important role in controlling its transport properties. Mott proposed the concept of two-current model to understand the electrical resistivity of ferromagnetic metals and their alloy, which is shown in Fig. 1.1. In such theory, transition metals such as Fe shows band splitting feature between the majority (up) spin and minority (down) spin projections along the quantization axis or the magne direction, as shown in Fig. 1.1(a). The electrons at Fermi level are therefore in different states and exhibit different conduction properties, e.g. the scattering rate of these two channels are spin-dependent and quite different. Mott also argues that the spin-flip scattering rate is metals in normally small as compared to the spin-conserved scattering rate. This means that spin-up and spin-down electrons do not mix and therefore, electrical conduction occurs in parallel for the two spin channels, as illustrated in Fig. 1.1(b). With the applied electric field, the two-current model can be simply written as

$$j_{\uparrow} = \sigma_{\uparrow} E \tag{1.1a}$$

$$j_{\downarrow} = \sigma_{\downarrow} E \tag{1.1b}$$

with spin-dependent conductivities $\sigma_{\uparrow,\downarrow}$ and in general, $\sigma_{\uparrow} \neq \sigma_{\downarrow}$. Although this picture is too simplified, it forms a useful basis for a qualitative understanding of the spin-dependent transport in ferromagnetic metals. If we add up these two current channels, we would get charge current J_e

$$J_e = (\sigma_{\uparrow} + \sigma_{\downarrow}) E \tag{1.2}$$

, and their difference would be the usually defined spin-polarized charge current J_s in FMs

$$J_s = (\sigma_{\uparrow} - \sigma_{\downarrow}) E \tag{1.3}$$

The GMR effect [9, 10] refers to the observation that the resistance of ferromagnetic multilayers is low (high) when the magnetization between adjacent magnetic layers are in parallel (antiparallel), with current flowing either in the film plane (CIP geometry) or perpendicular to the film plane (CPP geometry), as shown in Fig. 1.2(a). The two-current model can be utilized to explain GMR quite straightforwardly, as demonstrated in Fig. 1.2(b). We assume that scattering is weak (strong) for majority (minority) spin up (down) electrons. For parallel magnetic configuration, spin up (down) electrons pass the adjacent layers feeling two low (high) resistance, while for antiparallel case, both spin up and spin down electrons see one high and one low resistance. Since conduction occurs in parallel for the two spin channels with the assumption that spin mixing is negligible, the series-resistor theory tells us the total resistance is low (high) for parallel (antiparallel) magnetic configuration. The GMR ratio is characterized as

$$\mathrm{GMR} = \frac{R_{\mathrm{AP}} - R_{\mathrm{P}}}{R_{\mathrm{P}}} \tag{1.4}$$

where R_{P} and R_{AP} is the parallel and antiparallel resistance.

The MR in CIP geometry of magnetic multilayers quickly vanishes as one increase the layer thickness to more than the very short electron mean free path. While for the CPP geometry, the much longer electron spin diffusion length, as compared to mean free path, makes the CPP-GMR even exist in structures with relatively thick layers. As discussed in [49], the spin accumulation effect in the diffusive transport regime plays an essential role in the CPP-GMR geometry. The nonequilibrium electron spin accumulation μ_s can be described as the difference in electrochemical potentials for spin up $\mu_\uparrow$ and spin down electrons $\mu_\downarrow$

$$\mu_s = \mu_\uparrow - \mu_\downarrow \tag{1.5}$$

The accumulation of spins is not a conserved quantity since random scattering of electrons can flip its spin. Therefore, Valet and Fert [49] proposed the spin diffusion equation

$$\nabla^2 \mu_s = \frac{\mu_s}{\lambda_s^2} \tag{1.6}$$

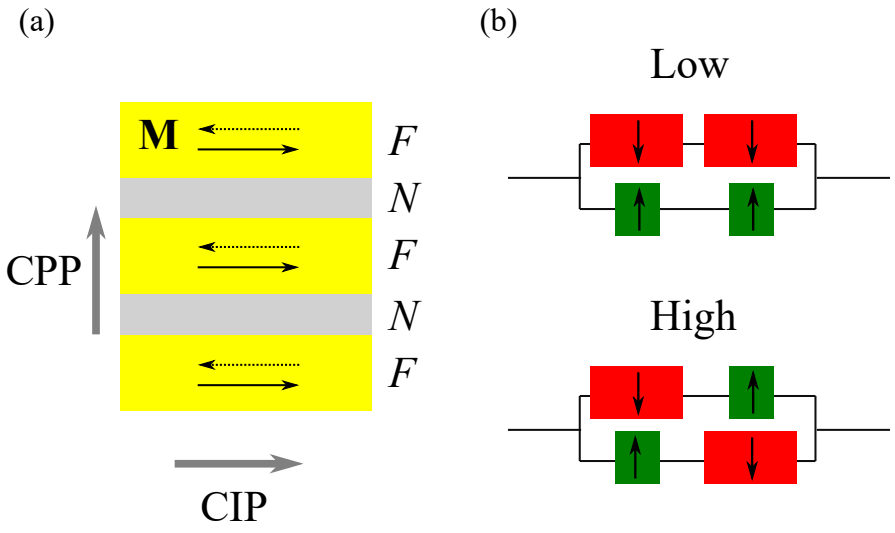

Figure 1.2: (a) A multilayer thin film structure composed of ferromagnets (F) and non-magnetic metals (N). The magnetizations of ferromagnets all lie in the film plane and can point either in the right or left directions. The arrows outside show the current direction for CIP and CPP geometries. (b) The resistor network representative of GMR effect within the two-current model. The total resistance of ferromagnetic multilayer is low for parallel state and high for antiparallel state.

where λ_s is the spin diffusion length and the diffusive spin current induced by the accumulation of spins is

$$J_s = \sigma_s \nabla \mu_s \tag{1.7}$$

with σ_s is the electron spin conductivity.

If one replaces the non-magnetic (NM) metallic layer in such FM/NM/FM spin valves (SVs) to insulating material like alumina or MgO but keeps the ferromagnetic electrodes, one would have the so-called magnetic tunnel junctions (MTJs). The tunneling resistance (TMR) of MTJs with perpendicularly applied bias voltage is also found to be different for the parallel and antiparallel magnetic configurations of their ferromagnetic electrodes [11, 12, 50]. TMR is a consequence of spin-dependent tunneling, and in a broader sense, is another manifestation of spin-dependent transport

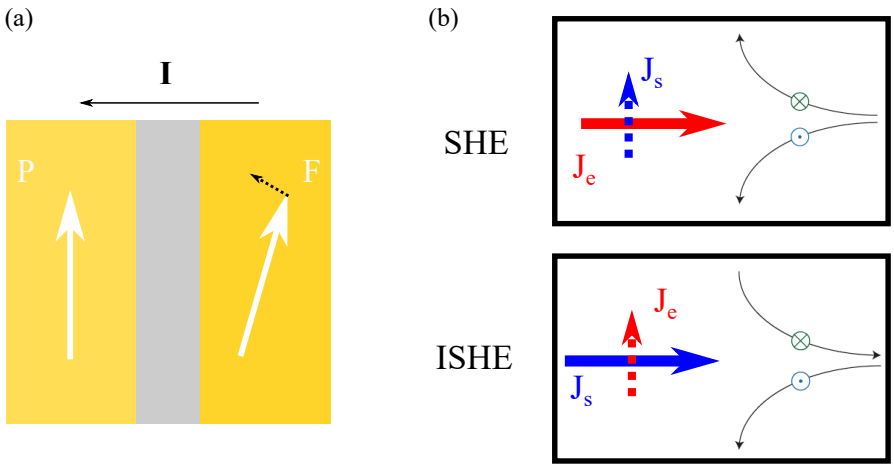

Figure 1.3: (a) STT effect in magnetic multilayers. The current is applied perpendicular to the film plane. The magnetization of the left magnetic layer here is pinned (P) and the magnetization of the right layer is free (F). The non-magnetic spacer layer (gray) can be either metallic or insulating. The dash arrow in the free layer represents the spin torque, and its direction depends on the polarity of current. Therefore, the relative orientation of two magnetizations can be switched between parallel and antiparallel configurations. (b) SHE and ISHE effects. Upper: an injected charge current J_e induces a transverse pure spin current J_s via SHE. Lower: an injected pure spin current J_s induces a transverse charge current via ISHE. Solid arrows represent the driving current and dotted arrows represent the induced current. The spin polarization of J_s is always defined perpendicular to the paper plane.

that is related to GMR. The TMR ratio is similarly defined as

$$\mathrm{TMR} = \frac{R_{\mathrm{AP}} - R_{\mathrm{P}}}{R_{\mathrm{P}}} \tag{1.8}$$

Compared to the metallic SVs, the MgO-based MTJs can reach much higher magnetoresistance (MR) ratio at room temperature and can also be scaled to smaller lateral size. Therefore, MTJs show a potential great advantage in the application point of view.

While the GMR and TMR that we have discussed refer to the fact that the relative orientation of the magnetic moments in magnetic multilayers can affect its electrical transport properties, here we discuss the spin current's effect on magnetization dy-

namics.

The well-known Landau-Lifshitz-Gilbert (LLG) equation describes the magnetization $\mathbf{M}$ dynamics of a FM under an effective magnetic field $\mathbf{H}_{eff}$ and intrinsic Gilbert magnetization damping

$$\frac{d\mathbf{M}}{dt} = -\gamma \mathbf{M} \times \mathbf{H}_{eff} + \alpha \mathbf{M} \times \frac{d\mathbf{M}}{dt} \tag{1.9}$$

where γ is the gyromagnetic ratio, α is the phenomenological Gilbert damping parameter. This model can be expanded to account for the spin current induced effect on magnetization dynamics.

The so-called spin-transfer torque (STT) phenomenon [15, 16, 19, 20] is sometimes regarded as inverse effect to the GMR and TMR. As illustrated in Fig. 1.3(a), Slonczewski and Berger argue that if the two magnetizations in SVs or MTJs are not collinear, the transverse component of the spin-polarization of the current from the magnetization pinned layer can transfer its spin to the magnetization free layer, therefore behaves like a torque acting to the free magnetization, and this torque can reorient or switch the direction of the free magnetization. STT is a novel method to actively control and manipulate the magnetization direction of a magnetic layer (both in SVs and MTJs) by simply using a perpendicular electrical current, in contrast to the conventional method with the use of an external magnetic field. Theoretically, the spin torque can be written as this form

$$\boldsymbol{\tau}_{\mathrm{STT}} \simeq a_J \mathbf{M}_F \times (\mathbf{M}_F \times \mathbf{M}_P) + b_J \mathbf{M}_F \times \mathbf{M}_P \tag{1.10}$$

with $\mathbf{M}_F$ and $\mathbf{M}_P$ are the magnetization of the free layer and pinned layer, a_J is the damping-like term and b_J is the field-like term, while both transverse to the direction of free magnetization.

Spin Hall effect (SHE) [21–25] is another distinct method to generate spin current in spintronics, especially pure spin current. Basically, in SHE as shown in Fig. 1.3(b), a longitudinal charge current can generate a transverse flowing pure spin current, and the induced spin current is polarized perpendicular to the plane defined by the flowing

directions of charge and spin current. The magnitude relation between charge current and spin current is often written phenomenologically as

$$J_s = \theta_{SH} J_e \tag{1.11}$$

where θ_{SH} is the spin Hall angle (SHA), sometimes regarded as a measure of the strength of SOC in the SHE material. The physics behind SHE is that there is a left-right scattering asymmetry to the electron spins due to strong SOC in heavy metals (HMs) and some semiconductors, e.g. spin up electrons get scattered more to the left while spin down electrons get scattered more to the right, as shown in Fig. 1.3(b).

The spin current that is induced by SHE is usually used to switch the magnetization in FM/HM bilayer structure, known as SHE induced spin-orbit torque (SOT) switching in spintronics. The spin current that is generated in HMs can build up a spin accumulation in the vicinity of HM/FM interface. If the polarization direction of this spin accumulation is not collinear to the magnetization direction of the FM, the transverse spin accumulation can induce a spin torque to the magnetization [51].

Fig. 1.3(b) also shows the reciprocal effect of SHE, the inverse SHE (ISHE) [26, 27]

$$J_e = \theta_{SH} J_s \tag{1.12}$$

where a pure spin current injected into the same material like HMs generates a transverse charge current. Such ISHE is often used as a convenient and efficient way to detect spin current electronically.

The discovery of above introduced GMR (TMR) and STT (SOT) makes all electrical manipulation and detection of magnetic states possible in spintronics: GMR or TMR allows us to electrically detect the different magnetic states, while STT or SOT enables the switching between different magnetic configurations with simply a charge current.

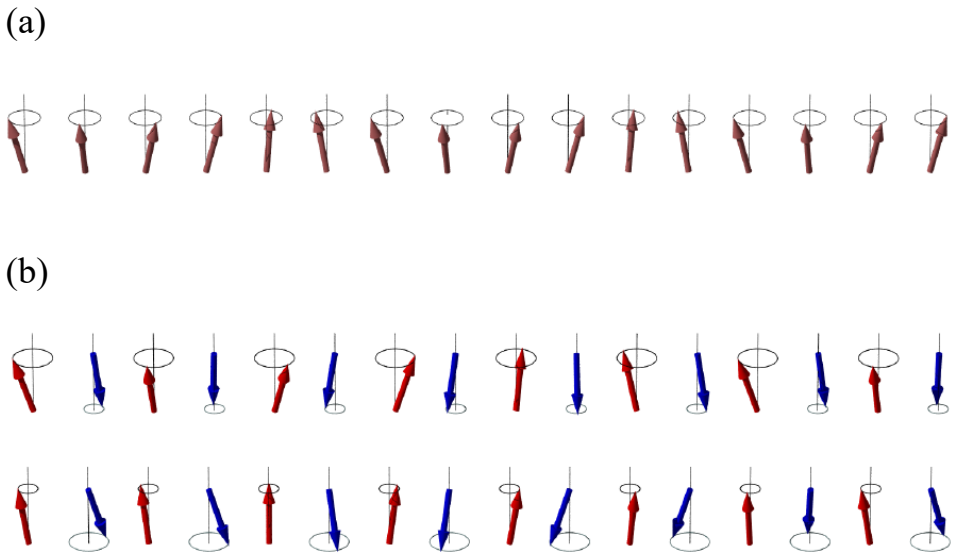

Figure 1.4: SWs or magnons in ferromagnets (a) and collinear bipartite antiferromagnets (b). The arrows represent the spin direction. In (b), the red and blue colors (up and down arrows) represent the A sublattice and B sublattice of AFMs. The upper part is the antiferromagnetic α mode magnon with spin $-\hbar$ and the lower part is the β mode magnon with spin $\hbar$. (From [1] with permission.)

1.1.2 Magnons in ferromagnets and antiferromagnets

Historically, the concept of spin waves (SWs) as collective excitations in magnetic materials was introduced in 1930 by Felix Bloch [31, 52–55] in order to explain the temperature dependent reduction of the spontaneous magnetization in a ferromagnet. Classically, SW represents a phase-coherent precession of magnetic moments or spins of magnetically ordered system, as illustrated in Fig. 1.4. Compared to one single spin flip, the energy of this spin excited wavelike state has a much lower energy. Holstein and Primakoff [56] introduced the second quantization of SWs in terms of bosonic operators, which are later called magnons, the quanta of SWs. Magnons carry a fixed amount of energy, lattice momentum, and spin in collinear FMs and AFMs. They behave as weakly interacting quasiparticles obeying Bose–Einstein statistics.

Here in this subsection, we briefly discuss the microscopic modeling of both ferromagnetic and collinear antiferromagnetic magnons.

The quantum Heisenberg ferromagnet is specified by the Hamiltonian

$$\hat{H}_{\mathrm{F}} = -J \sum_{\langle i,j \rangle} \hat{\mathbf{S}}_i \cdot \hat{\mathbf{S}}_j \tag{1.13}$$

where $J > 0$ is the exchange energy, $\hat{\mathbf{S}}_i$ represents the quantum mechanical spin operator at lattice site i, and $\langle i, j \rangle$ denotes summation over neighboring sites. At zero temperature, the Hamiltonian favors a ground state where the spins at neighboring sites are all aligned in the same direction.

We can further introduce the Holstein–Primakoff (HP) transformation [56] in which the spin operators are specified in terms of bosonic operators,

$$\hat{\mathbf{S}}_i^{+} = \hat{\mathbf{S}}_i^{x} + i\hat{\mathbf{S}}_i^{y} = \left(2S - a_i^{\dagger} a_i\right)^{1/2} a_i \tag{1.14a}$$

$$\hat{\mathbf{S}}_i^{-} = \hat{\mathbf{S}}_i^{x} - i\hat{\mathbf{S}}_i^{y} = a_i^{\dagger} \left(2S - a_i^{\dagger} a_i\right)^{1/2} \tag{1.14b}$$

$$\hat{\mathbf{S}}_i^{z} = S - a_i^{\dagger} a_i \tag{1.14c}$$

where $\hat{\mathbf{S}}_i^{+}$ ($\hat{\mathbf{S}}_i^{-}$) are spin raising (lowering) operators at lattice site i, and they have the commutation relation

$$\begin{aligned} \left[\hat{\mathbf{S}}_i^{z}, \hat{\mathbf{S}}_j^{\pm}\right] &= \pm\delta_{ij} \hat{\mathbf{S}}_i^{\pm} \\ \left[\hat{\mathbf{S}}_i^{+}, \hat{\mathbf{S}}_j^{-}\right] &= 2\delta_{ij} \hat{\mathbf{S}}_i^{z} \end{aligned} \tag{1.15}$$

$a_i^{\dagger}$ (a_i) are magnon creation (annihilation) operators satisfying

$$\begin{aligned} \left[a_i, a_j^{\dagger}\right] &= \delta_{ij} \\ \left[a_i, a_j\right] &= \left[a_i^{\dagger}, a_j^{\dagger}\right] = 0 \end{aligned} \tag{1.16}$$

In the limit that spin is large $S \gg 1$ thus

$$\hat{\mathbf{S}}_i^+ \simeq \sqrt{2S} a_i \tag{1.17a}$$

$$\hat{\mathbf{S}}_i^- \simeq \sqrt{2S} a_i^\dagger \tag{1.17b}$$

$$\hat{\mathbf{S}}_i^z = S - a_i^\dagger a_i \tag{1.17c}$$

and by only keeping the quadratic terms, the Heisenberg Hamiltonian takes the form

$$\begin{aligned} \hat{H}_{\mathrm{F}} &= -J \sum_{\langle i,j \rangle} \hat{\mathbf{S}}_i^z \hat{\mathbf{S}}_j^z + \frac{1}{2} \left(\hat{\mathbf{S}}_i^+ \hat{\mathbf{S}}_j^- + \hat{\mathbf{S}}_i^- \hat{\mathbf{S}}_j^+ \right) \\ &= -J \sum_{\langle i,j \rangle} \left[S^2 - \left(a_i^\dagger - a_j^\dagger \right) \left(a_i - a_j \right) \right] \end{aligned} \tag{1.18}$$

After Fourier transformation of the magnon operators,

$$a_i^\dagger = N^{-1/2} \sum_{\mathbf{q}} e^{-i\mathbf{q}\cdot\mathbf{R}_i} a_{\mathbf{q}}^\dagger \tag{1.19a}$$

$$a_i = N^{-1/2} \sum_{\mathbf{q}} e^{i\mathbf{q}\cdot\mathbf{R}_i} a_{\mathbf{q}} \tag{1.19b}$$

one can readily obtain the Hamiltonian as

$$\hat{H}_{\mathrm{F}} = \sum_{\mathbf{q}} \varepsilon_{\mathbf{q}} a_{\mathbf{q}}^\dagger a_{\mathbf{q}} \tag{1.20}$$

Here, $\varepsilon_{\mathbf{q}} = 2JSZ \left(1 - \gamma_{\mathbf{q}} \right)$ represents the dispersion relation of the spin excitations, where Z is the number of nearest neighbors and $\gamma_{\mathbf{q}} = 1/Z \sum_{\boldsymbol{\delta}} e^{i\mathbf{q}\cdot\boldsymbol{\delta}}$ with $\boldsymbol{\delta}$ runs over all nearest neighboring positions. In particular, in the limit $\mathbf{q} \to 0$, the dispersion relation is quadratic $\varepsilon_{\mathbf{q}} \propto q^2$. If we take into account terms of more than quadratic number of magnon operators, one can find the magnon-magnon interaction terms. One can also prove ferromagnetic magnons would be spin-1 since

$$\sum_i \hat{\mathbf{S}}_i^z a_{\mathbf{q}}^\dagger |0\rangle = \hbar a_{\mathbf{q}}^\dagger |0\rangle \tag{1.21}$$

with $|0\rangle$ is the ground state with zero magnons. As is shown in Fig. 1.4(a), these

small fluctuations of the spins around their quantization direction decrease the total spin by one.

Having discussed the magnon spectrum of the ferromagnets, we now turn to AFMs, as a significant majority of magnetic ordered systems in natural are AFMs [57–63]. Here, we shall consider the simplest case, collinear Heisenberg AFMs with two sublattices A and B,

$$\hat{H}_{\mathrm{AF}} = J \sum_{\langle i\in A, j\in B\rangle} \hat{\mathbf{S}}_i \cdot \hat{\mathbf{S}}_j \tag{1.22}$$

where, once again, $J > 0$. The ground states of the bipartite lattice are close to a staggered spin configuration, known as a Néel order [52, 64] , where all neighboring spins are antiparallel, as shown in Fig. 1.4(b). By using the HP transformation in the linear spin-wave approximation for both sublattices

$$\begin{aligned} \hat{\mathbf{S}}_i^+ &= \sqrt{2S}a_i \qquad \hat{\mathbf{S}}_j^+ = \sqrt{2S}b_j^\dagger \\ \hat{\mathbf{S}}_i^- &= \sqrt{2S}a_i^\dagger \qquad \hat{\mathbf{S}}_j^- = \sqrt{2S}b_j \\ \hat{\mathbf{S}}_i^z &= S - a_i^\dagger a_i \quad \hat{\mathbf{S}}_j^z = -S + b_j^\dagger b_j \end{aligned} \tag{1.23}$$

the Hamiltonian reads

$$\hat{H}_{\mathrm{AF}} = J \sum_{\langle i\in A, j\in B\rangle} \left[-S^2 + S\left(b_j^\dagger b_j + a_i^\dagger a_i + a_i^\dagger b_j^\dagger + a_i b_j\right)\right] \tag{1.24}$$

After Fourier transformation the Hamiltonian take the form

$$\hat{H}_{\mathrm{AF}} = \frac{JS}{2}\sum_{\mathbf{q}} \begin{pmatrix} a_{\mathbf{q}}^\dagger & b_{\mathbf{q}}^\dagger & a_{-\mathbf{q}} & b_{-\mathbf{q}} \end{pmatrix} \cdot H(\mathbf{q}) \cdot \begin{pmatrix} a_{\mathbf{q}} \\ b_{\mathbf{q}} \\ a_{-\mathbf{q}}^\dagger \\ b_{-\mathbf{q}}^\dagger \end{pmatrix} \tag{1.25}$$

with

$$H(\mathbf{q}) = \begin{pmatrix} 1 & 0 & 0 & \gamma_{\mathbf{q}} \\ 0 & 1 & \gamma_{\mathbf{q}} & 0 \\ 0 & \gamma_{\mathbf{q}} & 1 & 0 \\ \gamma_{\mathbf{q}} & 0 & 0 & 1 \end{pmatrix} \tag{1.26}$$

In order to diagonalize $H(\mathbf{q})$, or in other words, to remove the non-particle-number conserving contributions in the Hamiltonian, e.g. $a^{\dagger}_{\mathbf{q}} b^{\dagger}_{-\mathbf{q}}$ and $a_{-\mathbf{q}} b_{\mathbf{q}}$, one introduce a canonical transformation called Bogoliubov transformation to new defined magnon operators

$$\begin{aligned} a_{\mathbf{q}} &= u_{\mathbf{q}} \alpha_{\mathbf{q}} - v_{\mathbf{q}} \beta^{\dagger}_{-\mathbf{q}} \\ b^{\dagger}_{-\mathbf{q}} &= -v_{\mathbf{q}} \alpha_{\mathbf{q}} + u_{\mathbf{q}} \beta^{\dagger}_{-\mathbf{q}} \\ a^{\dagger}_{\mathbf{q}} &= u_{\mathbf{q}} \alpha^{\dagger}_{\mathbf{q}} - v_{\mathbf{q}} \beta_{-\mathbf{q}} \\ b_{\mathbf{q}} &= -v_{-\mathbf{q}} \alpha^{\dagger}_{-\mathbf{q}} + u_{-\mathbf{q}} \beta_{\mathbf{q}} \end{aligned} \tag{1.27}$$

where $\alpha^{\dagger}_{\mathbf{q}}$, $\alpha_{\mathbf{q}}$ and $\beta^{\dagger}_{\mathbf{q}}$, $\beta_{\mathbf{q}}$ are the new defined creation and annihilation operators for the two magnon modes α and β, which also satisfy the boson commutation rules. With these transformations, the Hamiltonian becomes

$$\hat{H}_{\mathrm{AF}} = \sum_{\mathbf{q}} \varepsilon^{\alpha}_{\mathbf{q}} \alpha^{\dagger}_{\mathbf{q}} \alpha_{\mathbf{q}} + \varepsilon^{\beta}_{\mathbf{q}} \beta^{\dagger}_{\mathbf{q}} \beta_{\mathbf{q}} \tag{1.28}$$

In the absence of the external magnetic field, α and β magnons are degenerate, they have exactly the same energy $\varepsilon^{\alpha}_{\mathbf{q}} = \varepsilon^{\beta}_{\mathbf{q}} = 2JSZ\sqrt{1-\gamma^2_{\mathbf{q}}}$. In contrast to the ferromagnets, the band of the collinear antiferromagnets displays a linear spectrum in the long wavelength limit, $\varepsilon_{\mathbf{q}} \propto q$ as $\mathbf{q} \to 0$. As for the spin of α and β magnons, one can find

$$\begin{aligned} \left(\sum_{i \in A} \hat{\mathbf{S}}^z_i + \sum_{j \in B} \hat{\mathbf{S}}^z_j \right) \alpha^{\dagger}_{\mathbf{q}} |0\rangle &= -\hbar \alpha^{\dagger}_{\mathbf{q}} |0\rangle \\ \left(\sum_{i \in A} \hat{\mathbf{S}}^z_i + \sum_{j \in B} \hat{\mathbf{S}}^z_j \right) \beta^{\dagger}_{\mathbf{q}} |0\rangle &= \hbar \beta^{\dagger}_{\mathbf{q}} |0\rangle \end{aligned} \tag{1.29}$$

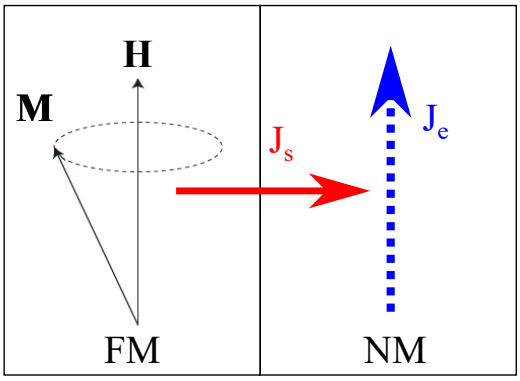

Figure 1.5: Spin pumping effect: The magnetization of FM layer precesses around the external dc magnetic field direction under FMR. When the FM in resonance is in contact with a NM, the magnetization precession can pump a spin current J_s into adjacent NM layer. A charge current J_e is generated in NM via ISHE.

The α and β magnons are quantized in the direction either parallel or antiparallel to the Néel vector, with $-\hbar$ or $+\hbar$ spins, as demonstrated in Fig. 1.4(b). By contrast, on frustrated lattices such as the triangular lattice, spin arrangement of non-collinear antiferromagnetic magnons becomes much more complicated because the lattice frustration [65–72]. We will discuss the magnons in non-collinear antiferromagnets in the later Chap. 5.

The name SWs are usually used to describe the phase-coherent, long wavelength excitations of the magnetic material. The ferromagnetic resonance (FMR) technique is a powerful way to excite SW with wavevector $\mathbf{q} = 0$. For example, the spin pumping refers to the observation that the FM under FMR condition can effectively pump spin current into the adjacent non-magnetic layer, as illustrated in Fig. 1.5. The applied microwave-frequency ac magnetic field makes the magnetization in FM go into a uniform precessional mode. This $\mathbf{q} = 0$ SW excitation therefore will emit a pure spin current into the adjacent NM layer [26, 73–75]

$$J_s = \frac{\hbar}{4\pi} G_{\text{mix}} \mathbf{m} \times \frac{d\mathbf{m}}{dt} \tag{1.30}$$

where G_{mix} is the spin mixing conductance, $\mathbf{m}$ is the unit magnetization vector. The

pumped spin current is DC in the second order of precession angle, making them electrically measurable in the attached NM layer through ISHE.

As we have discussed before, STT and SHE induced SOT can be used to reorient magnetization of the free layer in FM/spacer/FM sandwich structure and FM/NM bilayer structure. The direction of the STT and SOT depends on the polarization of the spin current, and once the damping like torque induced by STT is in antiparallel to the Gilbert damping term, the STT leads to auto-oscillation of the magnetization free layer, which is known as spin-torque oscillator (STO). Therefore, the spin pumping effect we discussed here, is sometimes regarded as the opposite of the STT effect, since spin pumping addresses the spin current generation by precessional magnetization, while STT regards the fact that spin current can drive the magnetization to precess. These two effects are shown to be the Onsager reciprocal relation to each other [76–78].

On the other hand, the study of incoherent magnon spin transport in spintronics has became a hot subject recently, especially in magnetic insulators. Incoherent magnons are usually referred to the short-wavelength, high energy thermal magnons. At finite temperature, the incoherent magnons are naturally present in the magnetic materials and in equilibrium obeying Bose-Einstein statistics

$$N_m^0(\varepsilon_{\mathbf{q}}) = \frac{1}{\exp\left(\frac{\varepsilon_{\mathbf{q}}}{k_B T}\right) - 1} \tag{1.31}$$

where $\varepsilon_{\mathbf{q}}$ is the magnon energy, k_B is the Boltzmann constant and T is the temperature. The magnon density is calculated as

$$n_m = \int d\varepsilon_{\mathbf{q}} N_m^0(\varepsilon_{\mathbf{q}}) D(\varepsilon_{\mathbf{q}}) \tag{1.32}$$

where $D(\varepsilon_{\mathbf{q}})$ is the magnon density of states.

So far, two effective methods to generate nonequilibrium incoherent magnons in spintronics have been electrically and thermally. We briefly discuss these two experimental methods in the following.

The $s-d$ exchange interaction between itinerant spins and localized spins couples

conduction electrons and magnons together

$$\hat{H}_{sd} = -J_{sd} \sum_i \boldsymbol{\sigma} \cdot \mathbf{S}_i \tag{1.33}$$

where J_{sd} is exchange energy, $\boldsymbol{\sigma}$ is the itinerant spin and $\mathbf{S}_i$ is the localized spin. Through this exchange coupling, the electron spin accumulation that is created for example, by SHE in non-magnetic metal, can be converted into magnon spin current through the interfacial $s-d$ exchange coupling in such NM/ferromagnetic insulator (FI) bilayer structure [44, 45, 79, 80].

The proposed incoherent magnon mediated electric charge current drag effect in such NM/FI/NM utilize the magnon as spin information carrier in the spacer FI layer, as shown in Fig. 1.6(a). In such sandwich structure, the electron charge current J_e in the left NM layer create a perpendicular flowing electron spin current J_s by SHE. This J_s can therefore be converted to the magnon spin current J_m in the spacer FI layer. On the right NM, J_m is converted back to the J_s through the interfacial coupling, and therefore can be electrically detected through ISHE by voltage signal. Here, the incoherent magnons in the middle ferromagnetic insulating layer play an essential role in conducting spin from one NM layer to the other NM layer.

In addition to the electrical magnon injection method, magnon spin current can also be generated thermally. The so-called spin Seebeck effect (SSE) [34–37, 81–83] utilizes a temperature gradient in a ferromagnetic material to generate magnon spin current, such that the thermal magnon density is non-uniform and magnons would diffuse from high to low temperature region, leading to a diffusive magnon current, as shown in Fig. 1.6(b). If a magnetic insulator is subject to a temperature gradient, the magnon density n_m becomes position-dependent

$$n_m(\mathbf{r}) = \int d\varepsilon_{\mathbf{q}} N_m(\mathbf{r}, \varepsilon_{\mathbf{q}}) D(\varepsilon_{\mathbf{q}}) \tag{1.34}$$

where

$$N_m(\mathbf{r}, \varepsilon_{\mathbf{q}}) = \frac{1}{\exp\left(\frac{\varepsilon_{\mathbf{q}} - \mu_m(\mathbf{r})}{k_B T(\mathbf{r})}\right) - 1} \tag{1.35}$$

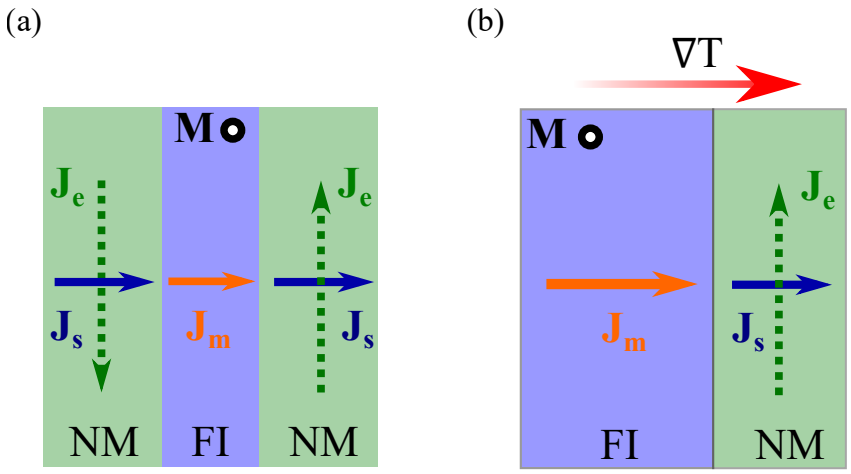

Figure 1.6: (a) Magnon mediated electric charge current drag in NM/FI/NM trilayer structure. The charge current J_e in the left NM layer will induce a electron spin current J_s flowing into the FI layer by SHE. Magnons in FI layer can conduct spin current by J_m. Similar to left NM layer, the electron spin current J_s in the right NM layer can induce charge current J_e in that layer. Therefore, the charge current in the left NM can drag another charge current in the right NM layer, although the middle spacer layer is insulating. (b) Spin Seebeck effect in FI/NM bilayer structure. The temperature gradient that drives the magnon spin current is applied perpendicular to the film plane. The magnon current J_m can be converted to electron spin current J_s in the adjacent non-magnetic heavy metals. Through the ISHE, a voltage signal J_e can be detected in the lateral direction.

Here we have used the position dependent magnon chemical potential $\mu_m(\mathbf{r})$ to characterize the nonequilibrium magnon accumulation. Similar to the electron spin diffusion equation, for magnons we have

$$\nabla^2 \mu_m = \frac{\mu_m}{\lambda_m^2} \tag{1.36}$$

where λ_m is the magnon spin diffusion length that gives the length scale over which the magnon chemical potential exponentially relax to equilibrium value. Consequently, the diffusive magnon spin current can be directly calculated

$$J_m = \sigma_m \nabla \mu_m \tag{1.37}$$

where σ_m is the magnon spin conductivity. In such FI/NM bilayer of Fig. 1.6(b), the magnon spin current that is generated by temperature gradient can be electrically detected in the adjacent non-magnetic layer through ISHE. While the thermal gradient could in principle works for all ferromagnetic materials, it is usually less efficient for magnetic metals due to practical difficulties in maintaining a large thermal gradient with a well-defined heat flow direction [84].

1.2 Outline of dissertation

In this Ph.D. dissertation, we theoretically explore the magnon spin transport in magnetic heterostructure. The dissertation is organized as follows.

In Chapter 2, we formulate the spin-magnon transport by explicitly taking into account the exchange coupling between the conduction spin and magnon in magnetic metals. The intrinsic strong $s-d$ exchange coupling in itinerant ferromagnets inevitably leads to substantial magnon spin current. Even for a uniformly magnetized conducting ferromagnet, an electric charge current is always accompanied with a magnon spin current at finite temperature. Up until now, the study of electric and spin transport has mostly neglected the role of the magnon spin current in ferromagnetic metals. Experimentally, several measured phenomena such as the spin accumulation and spin transfer directly depend on the total angular momentum current in which the magnon current is a part of. Other phenomena, such as the giant magnetoresistance and spin Hall effect, are sensitive to the electron spin current and seemingly independent of the magnon spin current. However, we will show that the presence of the magnon spin current could indirectly modify key parameters for electron spin transport. Thus, a schematic investigation on the correlation between spin current and magnon current would lead to a better understanding of angular momentum transport in general. At present, theoretical studies on the coupling and conversion between magnon and electron spin currents are mostly focused on the interface.

In Chapter 3, we study magnon transport in an insulating spin valve made of an

antiferromagnetic insulator sandwiched between two ferromagnetic insulator layers. In the conventional metal-based spin valve, the electron spins propagate between two metallic ferromagnetic layers, giving rise to giant magnetoresistance and spin-transfer torque. Here, the incoherent magnons in the insulating spin valve serve as angular momentum carriers and are responsible for the angular momentum transport between two ferromagnetic insulator layers across the antiferromagnetic spacer. We predict two transport phenomena in the presence of a temperature gradient: a giant magneto-spin-Seebeck effect in which the output voltage signal is controlled by the relative orientation of the two ferromagnetic insulator layers and magnon transfer torque that can be used for switching the magnetization of the ferromagnetic insulator layers with a temperature gradient of the order of 0.1 Kelvin per nanometer.

In Chapter 4, we study spin-transfer torques in magnetic tunnel junctions with an antiferromagnetic insulator as the tunnel barrier. When a finite voltage bias is applied to the magnetic tunnel junction, the energy relaxation of the tunnel electrons leads to asymmetric heating of two metallic layers. Consequently, there would be a magnon current flowing across the antiferromagnetic insulator layer, resulting a magnon transfer torque in addition to the electron spin-transfer torque. Comparing to magnetic tunnel junctions with a nonmagnetic insulator which prohibits the magnon transmission, we find the magnon transfer torque with an antiferromagnetic insulator barrier could be several times larger than the conventional spin-transfer torque of the tunnel electrons. This study presents a potential method to realize more efficient switching in magnetic tunnel junctions and provides a motivation of experimental search for antiferromagnetic insulator-based magnetic tunnel junctions.

In Chapter 5, we address the magnon spin transport in non-collinear antiferromagnets. For non-collinear antiferromagnetic metals, the magnon spectra displays non-trivial multi-band structure with the property of unconventional spin-momentum locking of magnons. We study the roles of these magnons on the charge and spin transport properties by taking into account the momentum and angular momentum transfer between conduction electrons and magnons. We show that the unpolarized electron current driven by an electric field can efficiently induce a magnon spin

current. The resulting magnon spin conductivity tensor has a more complicated symmetry properties compared to the spin Hall conductivity tensor in non-magnetic metals or in collinear antiferromagnetic materials. The temperature dependence of the magnon spin conductivity is also calculated.

Chapter 2

Interplay of magnon and electron currents in magnetic heterostructure

2.1 Background and motivation

One of the most important issues in spintronics is to identify and manipulate spin currents. As we have mentioned previously, in magnetic materials, both electrons and magnons have intrinsic angular momenta, and the translational flow of these particles (or quasiparticles) lead to a spin current or angular momentum current. Most of studies on the spin current has been focused on the electron spin current due to direct connections between the electron spin current and measurable physical phenomena. For example, the giant magnetoresistance (GMR) and the spin-transfer torque (STT) are proportional to the spin current or spin polarization of conduction electrons in the magnetic multilayers and at the interfaces. By experimentally measuring GMR and STT for a given structure, the quantitative values of electron spin current can be obtained. The magnon current, on the other hand, is much harder to experimentally quantify. Since a magnon is chargeless and it does not couple with the external electrical field, both generation and detection of magnon accumulation and magnon current are experimentally challenging.

At present, the magnon current has been generated by two methods. The spin Seebeck effect [34–37] utilizes a temperature gradient in a ferromagnetic material such that the thermal magnon density is non-uniform and magnons would diffuse from

high to low temperature region, leading to a diffusive magnon current. While the thermal gradient could in principle works for all ferromagnetic materials, it is usually less efficient for magnetic metals due to practical difficulties in maintaining a large thermal gradient with a well-defined heat flow direction [84]. Another method is to utilize spin injection from the neighboring layer. For example, in a bilayer consisting of a heavy metal and a magnetic insulator, e.g., Pt/Yttrium iron garnet (YIG) bilayer, an in-plane electron charge current in the Pt layer could induce a magnon current in YIG layer via the conversion of the electron spin current to the magnon current [40, 44, 45, 85]. In this case, the electron spin current and the magnon current are located in different spatial regions (electron spin current in Pt and magnon current in YIG, respectively), and the interaction between electron spin and magnon occurs only at the interface.

In this chapter, we theoretically formulate the spin-magnon transport by explicitly taking into account the exchange coupling between the conduction electrons and magnons in magnetic metals. The intrinsic strong exchange coupling in itinerant ferromagnets inevitably leads to substantial magnon current. Even for a uniformly magnetized conducting ferromagnet, an electric charge current is always accompanied with a magnon current at finite temperature. Up until now, the study of electric and spin transport has mostly neglected the role of the magnon current. Experimentally, several measured phenomena such as the spin accumulation and spin transfer directly depend on the total angular momentum current in which the magnon current is a part of. Other phenomena, such as the GMR and spin Hall effect, are sensitive to the electron spin current and seemingly independent of the magnon current. However, we will show that the presence of the magnon current could indirectly modify key parameters for electron spin transport. Thus, a schematic investigation on the correlation between spin current and magnon current would lead to a better understanding of angular momentum transport in general. At present, theoretical studies on the coupling and conversion between magnon and electron spin currents are mostly focused on the interface [80, 85–89].

2.2 Derivation of magnon and electron spin diffusion equations

We shall first clarify that the magnon current we study here is the translational *flow* of quasi-particle magnons. The direction of the angular momentum of the magnon current is always *parallel* to the magnetization (or order parameter) because the magnon is defined as a quantum state without a transverse component relative to the quantization axis (magnetization direction). The spin-wave spin-current [90], sometimes referred as spin supercurrent [91], considers spatial and temporal dependence of the classical magnetization which is described by Landau-Lifshitz-Gilbert equation for transverse magnetization dynamics. A clear distinction of these magnon currents was discussed in Ref. [92].

We start with a magnetic metal in which the exchange interaction between conduction electron spin $\boldsymbol{\sigma}$ and localized spin $\mathbf{S}_i$ at site i takes an isotropic form

$$\hat{H}_{sd} = -J_{sd} \sum_i \boldsymbol{\sigma} \cdot \mathbf{S}_i \tag{2.1}$$

where J_{sd} is given by the exchange integral. In the spin-wave approximation, $\hat{H}_{sd}$ is written as [93, 94]

$$\hat{H}_{sd} = -\left(J_{sd} \sqrt{\frac{S}{2N}} \right) \sum_{\mathbf{kq}} \left(a^\dagger_{\mathbf{q}} c^\dagger_{\mathbf{k}\uparrow} c_{\mathbf{k+q}\downarrow} + a_{\mathbf{q}} c^\dagger_{\mathbf{k+q}\downarrow} c_{\mathbf{k}\uparrow} \right), \tag{2.2}$$

where N is the number of atomic sites, S is the spin per site, $c_{\mathbf{k}}$ ($c^\dagger_{\mathbf{k}}$) and $a_{\mathbf{q}}$ ($a^\dagger_{\mathbf{q}}$) represent the annihilation (creation) operators for the electrons and the magnons. The first term describes one spin down electron scatters to one spin up electron by creating one magnon, and the second terms describe the reverse process where one spin up electron scatters to one spin down electron by destroying one magnon.

The linearized Boltzmann equation for the electrons in a layered structure, in

which the spatial dependence is only one-dimensional, is [95, 96]

$$v_{k_z}\frac{\partial f_\sigma(z,\mathbf{k})}{\partial z} - eE(z)v_{k_z}\frac{\partial f^0}{\partial \varepsilon_{\mathbf{k}}} = - \frac{f_\sigma(z,\mathbf{k}) - \overline{f_\sigma}(z)}{\tau_\sigma} - \frac{f_\sigma(z,\mathbf{k}) - \overline{f_{\sigma'}}(z)}{\tau_{\uparrow\downarrow}} + \left[\frac{\partial f_\sigma(z,\mathbf{k})}{\partial t}\right]_{sd} \tag{2.3}$$

where $f_\sigma(z,\mathbf{k})$ is the position dependent electron distribution function for spin $\sigma = \uparrow, \downarrow$ (or $\pm$), z is the coordination normal to the plane of the layers, τ_σ and $\tau_{\uparrow\downarrow}$ represents spin conserving and spin-flip scattering relaxation times, the overbar on the distribution function is the average over the momentum $\mathbf{k}$, and the last term is due to the exchange interaction $\hat{H}_{sd}$ [97–99],

$$\begin{aligned}\left[\frac{\partial f_\uparrow(z,\mathbf{k})}{\partial t}\right]_{sd} &= J_{sd}^2\frac{\beta\pi S}{N\hbar}\sum_{\mathbf{q}}\delta\left(\varepsilon_{\mathbf{k}} + \varepsilon_{\mathbf{q}}^m - \varepsilon_{\mathbf{k}+\mathbf{q}}\right) \\ &\times\left[1 - f^0\left(\varepsilon_{\mathbf{k}+\mathbf{q}}\right)\right] f^0\left(\varepsilon_{\mathbf{k}}\right) N_m^0\left(\varepsilon_{\mathbf{q}}^m\right) \\ &\times\left\{\left[\delta\mu_\downarrow(z) - \delta\mu_\uparrow(z) - \delta\mu_m(z)\right] + \left[g_\downarrow(z,\mathbf{k}+\mathbf{q}) - g_\uparrow(z,\mathbf{k}) - g_m(z,\mathbf{q})\right]\right\}\end{aligned} \tag{2.4a}$$

$$\begin{aligned}\left[\frac{\partial f_\downarrow(z,\mathbf{k})}{\partial t}\right]_{sd} &= J_{sd}^2\frac{\beta\pi S}{N\hbar}\sum_{\mathbf{q}}\delta\left(\varepsilon_{\mathbf{k}} - \varepsilon_{\mathbf{k}-\mathbf{q}} - \varepsilon_{\mathbf{q}}^m\right) \\ &\times\left[1 - f^0\left(\varepsilon_{\mathbf{k}-\mathbf{q}}\right)\right] f^0\left(\varepsilon_{\mathbf{k}}\right)\left[N_m^0\left(\varepsilon_{\mathbf{q}}^m\right) + 1\right] \\ &\times\left\{\left[\delta\mu_\uparrow(z) - \delta\mu_\downarrow(z) + \delta\mu_m(z)\right] + \left[g_\uparrow(z,\mathbf{k}-\mathbf{q}) - g_\downarrow(z,\mathbf{k}) + g_m(z,\mathbf{q})\right]\right\}\end{aligned} \tag{2.4b}$$

where $\beta = (k_B T)^{-1}$ is the inverse of the temperature, f^0 and N_m^0 are the equilibrium distribution functions of the electron and the magnon, $\varepsilon_{\mathbf{k}}$ and $\varepsilon_{\mathbf{q}}^m$ are the dispersion relations for the electron and for the magnon, and we have separated the distribution functions into the sum of the equilibrium and nonequilibrium parts,

$$f_\sigma(z,\mathbf{k}) = f^0(\mathbf{k}) - \frac{\partial f^0(\mathbf{k})}{\partial \varepsilon_{\mathbf{k}}}\left[\delta\mu_\sigma(z) + g_\sigma(z,\mathbf{k})\right] \tag{2.5a}$$

$$N_m(z,\mathbf{q}) = N_m^0(\mathbf{q}) - \frac{\partial N_m^0(\mathbf{q})}{\partial \varepsilon_{\mathbf{q}}^m}\left[\delta\mu_m(z) + g_m(z,\mathbf{q})\right], \tag{2.5b}$$

in which nonequilibrium parts are further separated into the isotropic term $\delta\mu_{\sigma,m}(z)$ and anisotropic term $g_\sigma(z,\mathbf{k})$ $[g_m(z,\mathbf{q})]$ with respect to the momentum, i.e.,

$$\int d\mathbf{k} g_\sigma(z,\mathbf{k}) = \int d\mathbf{q} g_m(z,\mathbf{q}) = 0 \tag{2.6}$$

We should point out that in the conventional Boltzmann equation for electrons, the spin-magnon interaction is phenomenologically included as a part of relaxation times (τ_s and $\tau_{\uparrow\downarrow}$) [100]. The explicit spin-magnon scattering in Eq. (2.3) would allow us to fully address both spin and magnon currents.

Similarly, the Boltzmann equation for the magnon is

$$v_{q_z}\frac{\partial N_m(z,\mathbf{q})}{\partial z} = -\frac{N_m(z,\mathbf{q}) - \overline{N_m}(z)}{\tau_m} - \frac{N_m(z,\mathbf{q}) - N_m^0}{\tau_{th}} + \left[\frac{\partial N_m(z,\mathbf{q})}{\partial t}\right]_{sd} \tag{2.7}$$

where τ_m and τ_{th} represent the magnon number conserving and non-conserving relaxation times [79], respectively, and the last term is the momentum transfer between electron and magnon,

$$\begin{aligned}\left[\frac{\partial N_m(z,\mathbf{q})}{\partial t}\right]_{sd} = {} & J_{sd}^2\frac{\beta\pi S}{N\hbar}\sum_{\mathbf{k}}\delta\left(\varepsilon_{\mathbf{k}+\mathbf{q}} - \varepsilon_{\mathbf{k}} - \varepsilon_{\mathbf{q}}^m\right) \\ & \times\left[1 - f^0\left(\varepsilon_{\mathbf{k}+\mathbf{q}}\right)\right] f^0\left(\varepsilon_{\mathbf{k}}\right) N_m^0\left(\varepsilon_{\mathbf{q}}^m\right) \\ & \times\left\{\left[\delta\mu_\downarrow(z) - \delta\mu_\uparrow(z) - \delta\mu_m(z)\right] + \left[g_\downarrow(z,\mathbf{k}+\mathbf{q}) - g_\uparrow(z,\mathbf{k}) - g_m(z,\mathbf{q})\right]\right\}\end{aligned} \tag{2.8}$$

Comparing Eq. (2.3) and (2.7), we notice that there is no drift term in Eq. (2.7); this is because the magnon has no charge and the electric field does not drive the magnon motion. If no thermal gradient is applied, the magnon current would come from the momentum transfer from the electron, i.e., the last term in Eq. (2.7) becomes a source term for the magnon current.

The solutions of the above Boltzmann equations in mutilayered structures depend on many parameters including the band dispersions, momentum and spin relaxations for electrons and magnons, and also detailed boundary conditions at the interface.

Thus, it would be less physical rewarding to numerically solve the equations. A more physically meaningful approach is to simplify Eqs. (2.3) and (2.7) to a set of macroscopic equations such that the experimentally measurable quantities can be directly compared with. In the absence of the electron-magnon coupling, such simplifications have led to a set of spin diffusion equations of electrons [49], which provide a powerful tool to analyze experimental data for the GMR of magnetic multilayers with the current perpendicular to the plane of the layers [101]. We should extend this approach by explicitly taking into account the coupling between spin and magnon.

Four macroscopic variables are spin accumulation $\delta n_s(z)$, electron spin current $j_s(z)$, magnon accumulation $\delta n_m(z)$, and magnon current $j_m(z)$:

$$\delta n_s(z) \equiv (2\pi)^{-3} \int d\mathbf{k} \left[f_\uparrow(z,\mathbf{k}) - f_\downarrow(z,\mathbf{k}) \right], \tag{2.9a}$$

$$j_s(z) \equiv (2\pi)^{-3} \int d\mathbf{k} v_{k_z} \left[f_\uparrow(z,\mathbf{k}) - f_\downarrow(z,\mathbf{k}) \right], \tag{2.9b}$$

$$\delta n_m(z) \equiv (2\pi)^{-3} \int d\mathbf{q} \left[N_m(z,\mathbf{q}) - N_m^0(\mathbf{q}) \right], \tag{2.9c}$$

$$j_m(z) \equiv (2\pi)^{-3} \int d\mathbf{q} v_{q_z} N_m(z,\mathbf{q}) \tag{2.9d}$$

Note that we have used the spin/magnon accumulation in the unit of the particle number per volume, and spin/magnon current in the unit of the particle number density current. To convert into the angular momentum current, charge current, or accumulation, one can simply multiply the resulting variables by $\hbar$, e, or μ_B. To obtain the macroscopic equations for these variables, a number of approximations are needed. We provide the detail of these approximations in Appendix A.1. The resulting spin-magnon diffusion equations and the extended Ohm's law are,

$$\frac{d^2}{dz^2}\begin{pmatrix}\delta n_s(z)\\ \delta n_m(z)\end{pmatrix} = \begin{pmatrix}\lambda_s^{-2} & \lambda_{sm}^{-2}\\ \lambda_{ms}^{-2} & \lambda_m^{-2}\end{pmatrix}\begin{pmatrix}\delta n_s(z)\\ \delta n_m(z)\end{pmatrix} \tag{2.10}$$

and

$$\begin{pmatrix}j_s(z)\\ j_m(z)\end{pmatrix} = j_e\begin{pmatrix}P_s\\ P_m\end{pmatrix} + \begin{pmatrix}-\sigma_s & \sigma_{ms}\\ \sigma_{sm} & -\sigma_m\end{pmatrix}\frac{d}{dz}\begin{pmatrix}\delta n_s(z)\\ \delta n_m(z)\end{pmatrix}, \tag{2.11}$$

where all coefficients in the above equations are given in the Appendix A.1. We shall briefly discuss the physical meaning of these coefficients here. The two lengths λ_s and λ_m in Eq. (2.10) are spin and magnon diffusion lengths. As usual, λ_s are related to the geometry mean of the momentum and spin-flip relaxation times $\sqrt{\tau_e \tau_{\uparrow\downarrow}}$ ($\tau_e^{-1} = \tau_\uparrow^{-1} + \tau_\downarrow^{-1}$) and λ_m is similarly related to $\sqrt{\tau_{th}\tau_m}$. However, due to coupling between spins and magnons, these lengths are modified by the interactions, see Appendix A.1. The off-diagonal matrix elements λ_{sm} and λ_{ms} describe the conversions between the spin and magnon accumulations, and both λ_{sm} and λ_{ms} are inversely proportional to J_{sd}^2, as expected. The generalized Ohm's law, Eq. (2.11), describes the drift spin/magnon current (first term) by an applied charge current $j_e \left(\equiv j_\uparrow + j_\downarrow\right)$ and the diffusive spin/magnon current (second term) due to spin-magnon accumulation in an inhomogeneous structure. Clearly, in the absence of spin-magnon coupling, $\sigma_{ms} = \sigma_{sm} = 0$ and $P_m = 0$ since the electric field cannot drive a magnon current, and $P_s = P_0 \equiv (\tau_\uparrow - \tau_\downarrow)/(\tau_\uparrow + \tau_\downarrow)$ is the spin polarization of the ferromagnet. With the spin-magnon coupling, both P_s and P_m depend on a number of scattering parameters, e.g. J_{sd}, τ_e, τ_m, see Appendix A.1 in detail. Finally, the spin-magnon conductivity is a 2×2 matrix whose diagonal elements are the electron spin conductivity σ_s and the magnon conductivity σ_m, and the off-diagonal element $\sigma_{ms}\,(\sigma_{sm})$ is the inter-conductivity induced by the exchange coupling and is proportional to J_{sd}^2.

Equations (2.10) and (2.11) are our main results in this chapter. The diffusion equation, Eq. (2.10), explicitly describes how the electron spin diffusion is affected by the magnon diffusion. When there is no coupling, i.e., $\lambda_{sm}^{-1} = \lambda_{ms}^{-1} = 0$, spin and magnon have their own diffusion lengths. When the coupling becomes strong, these two length scales become mutually dependent. We will study the diffusion properties of the coupled system in layered structure in the later Sections. The extended Ohm's law, Eq. (2.11), indicates a non-zero drift term for the magnon current $P_m j_e \neq 0$. The origin comes from the momentum transfer rather than the angular momentum transfer from the spin to the magnon. To see this, we consider the case $P_0 = 0$ and we still have a finite magnon current since the first term in P_m would still survive. Then, the question is how a charge current j_e without spin polarization induce a magnon

current? The answer becomes obvious when we consider the electron spin and magnon together: the magnon current induced by momentum transfer of the electron will in turn create a spin polarization of the electron and thus P_s is no longer zero, as shown in the Appendix A.1. The induced P_s, though it is small, is proportional to the electron momentum relaxation time τ_e, rather than the spin-flip relaxation times $\tau_{\uparrow\downarrow}$, further illustrating that the momentum transfer is responsible for creating a magnon current even for $P_0 = 0$.

2.3 Applications to the magnetic multilayers

2.3.1 Two-angular momentum current model

The conventional two-current model in spintronics [8] refers to a charge-current carried by spin-up and spin-down conduction electrons. For a ferromagnetic conductor such as NiFe, the spin-up and spin-down electrons have a different density of states at the Fermi level and a different scattering rate (or relaxation time). One may define a conductivity for each of the spin channel (up and down) such that the Ohm's law is applied to each spin channels. Alternatively, one can introduce a charge current, which is the sum of the two spin channel currents, and a spin current, the difference of the two. Since the charge current is conserved, the conventional two current model in fact reduces to just one spin current model. In the present case, we are dealing with truly two-angular momentum current model: both electron spin and magnon currents are carrying angular moments and neither of them is conserved. Next, we shall estimate a relative magnitude of the spin and magnon current in a conventional magnetic metal.

We show in Fig. 2.1 the spin current and the magnon current relative to the applied charge current, $P_s = j_s/j_e$ and $P_m = j_m/j_e$ for several plausible parameters closely related to the transition magnetic metals such as Ni, Co, Fe, and their alloys. As the exchange coupling J_{sd} increases, the magnon current increases, and in a large coupling limiting case, the magnon current becomes saturated. The saturated magnon current is limited by the magnon scattering rate: even if the transfer of the

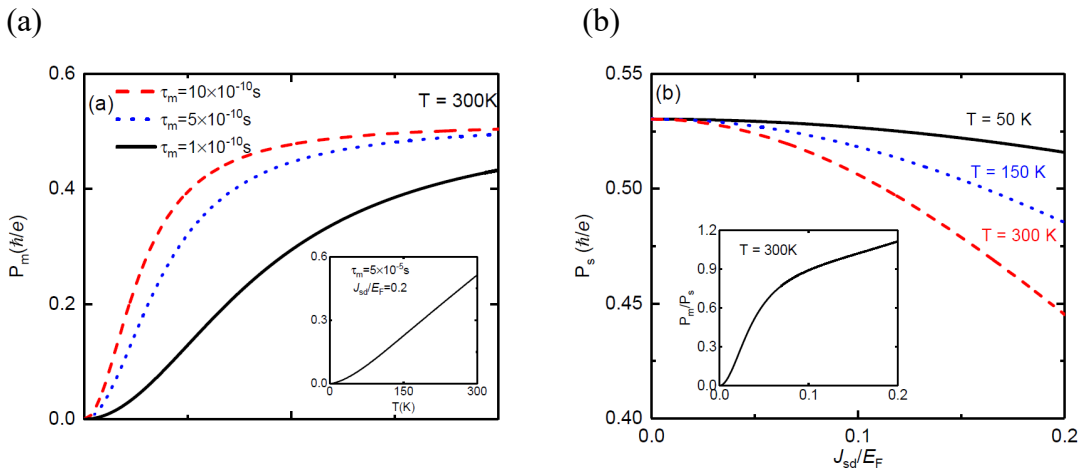

Figure 2.1: (a) The ratio of the magnon current to the charge current and (b) the ratio of the spin current to the charge current, as a function of the exchange coupling magnitude for several different magnon momentum relaxation times and temperatures. The insert in (a) shows the temperature dependence at a fixed $J_{sd}/E_F = 0.2$, and the insert in (b) shows the ratio of the magnon current to the spin current at a fixed temperature $T = 300K$. Other parameters are $E_F = 5$ eV, $T_C = 550$ K, $\tau_e = 7 \times 10^{-16}$ s.

spin-magnon is efficient for a large J_{sd}, the steady-state magnon current would be a balance between the magnon momentum relaxation and the momentum transfer from the electron current. On the other hand, the electron spin current decays as the coupling increases due to increased spin angular momentum loss from the electron to the magnon. The spin and magnon currents are highly temperature dependent because the number of magnon carriers increase with the temperature and thus the transfer between the electron current and magnon current is more efficiency at high temperatures. From Fig.2.1, we conclude that the magnon current is comparable to the spin current at the room temperature and consequently, the total angular momentum current must include the magnon current when one studies the angular momentum transfer in multilayered systems, which we will discuss next.

2.3.2 Spin and magnon accumulation in layered structure

In this subsection, we determine the spin/magnon accumulation for a hypothetical bilayer where two identical ferromagnetic layers are in contact at $z = 0$, with their magnetization antiparallel aligned. Experimentally, a thin nonmagnetic layer is needed to separate the magnetic coupling between two layers such that the antiparallel of the two layers can be achieved. This simple example would provide insights on the spatial and temperature dependence of the spin and magnon distributions. We should first solve the spin-magnon diffusion equations, Eq. (2.10), for each layer:

$$\delta n_s(z) = A_L \exp\left(\frac{z}{\lambda_+}\right) + B_L \exp\left(\frac{z}{\lambda_-}\right) \tag{2.12}$$

for $z < 0$ and

$$\delta n_s(z) = A_R \exp\left(-\frac{z}{\lambda_+}\right) + B_R \exp\left(-\frac{z}{\lambda_-}\right) \tag{2.13}$$

for $z < 0$, where the two characteristic lengths are given by

$$\frac{1}{\lambda_\pm^2} = \frac{1}{2}\left(\frac{1}{\lambda_s^2} + \frac{1}{\lambda_m^2}\right) \pm \frac{1}{2}\sqrt{\left(\frac{1}{\lambda_s^2} - \frac{1}{\lambda_m^2}\right)^2 + \frac{4}{\lambda_{sm}^2\lambda_{ms}^2}} \tag{2.14}$$

and A_L, B_L, A_R and B_R are four constants of the integration to be determined by the boundary conditions. The magnon accumulation $\delta n_m(z)$ can be similarly obtained without a new constant of the integration since $\delta n_m(z)$ can be expressed by $\delta n_s(z)$ from Eq. (2.10), namely,

$$\delta n_m(z) = \lambda_{sm}^2[\delta n_s''(z) - \lambda_s^{-2}\delta n_s(z)] \tag{2.15}$$

By using the extended Ohm's law, Eq. (2.11), the spin and magnon current can also be expressed in terms of these constants. For the perfect interface, the continuity of the spin and magnon currents and accumulations gives four boundary equations at $z = 0$, and thus we are able to completely determine these four constants (A_L, B_L, A_R and B_R) and therefore the position dependent spin and magnon accumulations and currents. The explicit solution could be found in Appendix A.2.

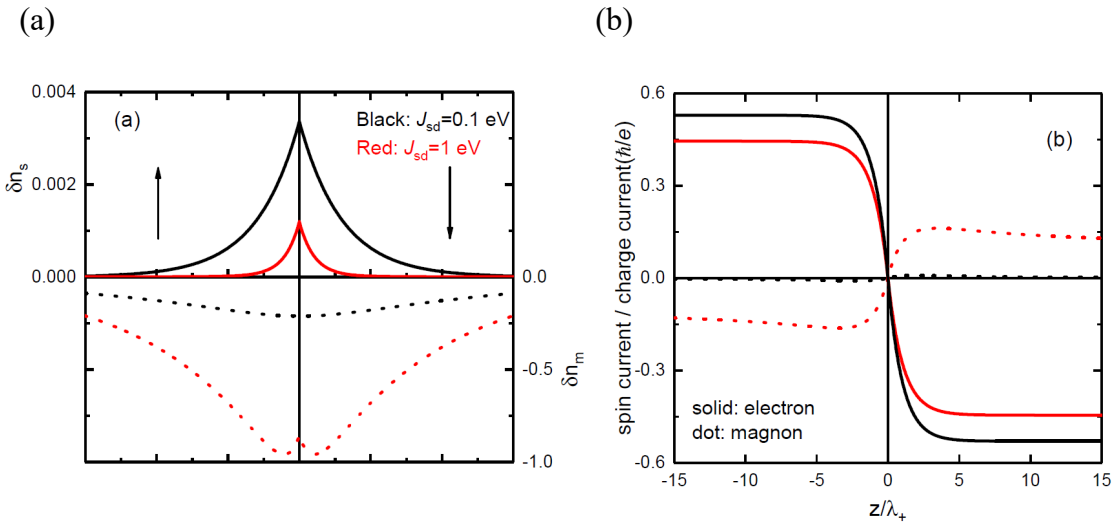

Figure 2.2: (a) The position dependence of the spin and magnon accumulation. (b) The position dependence of the spin current and magnon current. The parameters are the same as used in Fig. 2.1.

In Figure. 2.2, we show the spatial distribution of the spin and magnon accumulations and currents near the interface. When the coupling J_{sd}/E_F is small, the magnon accumulation and magnon currents are small, as expected. The magnon accumulation increases as J_{sd} increases since the source the nonequilibrium is through the coupling. On the other hand, the electron spin accumulation decreases due to additional electrons relaxations to the magnons. Interestingly, the magnon accumulation displays a non-monotonic behavior near the interface. The origin comes from the interplay between two length scales (λ_+ and λ_-) in the solution of the accumulation, see Eq. (2.12)-(2.14), and Appendix A.2. The supposition of the two exponential functions leads to a local extrema at the position between these two lengths. Similarly, the magnon current also displays a non-monotonic function. The maximum value could even exceed the value of the uniform layer without the interface.

2.3.3 Magnetoresistance

Magnetoresistance of magnetic multilayers for the current perpendicular (CPP) to the layers has been theoretically modeled using Valet-Fert's [49] spin diffusion

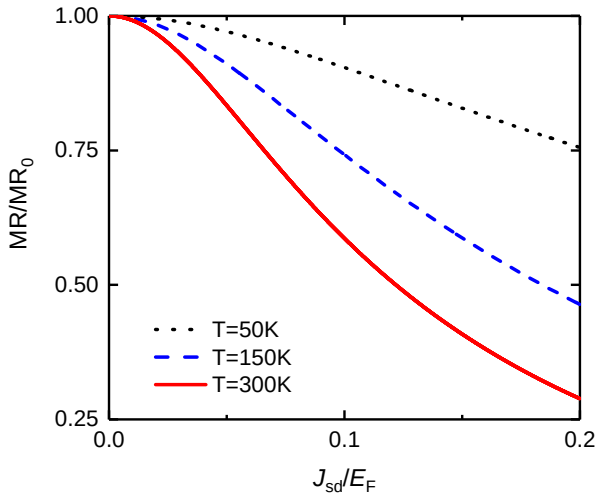

Figure 2.3: Magnetoresistance of the magnetic bilayer, normalized to the classical value without the spin-magnon coupling, as function of the exchange coupling for several different temperatures. We have used a temperature-independent relaxation time in order to single out the temperature dependent contribution from the magnon accumulation.

equations for electrons at zero temperature. The essential physics picture is that the spin accumulation creates an additional interface resistance. Since the spin accumulation depends on the magnetization configurations in magnetic multilayers, the resulting resistance varies with the relative magnetization of each layer. In the above example of the bilayer, there is no spin accumulation when the magnetizations of the two magnetic layers are parallel. The maximum spin accumulation is created for the antiparallel magnetization. Without taking into count the coupling between electrons and magnons, Valet-Fert's model immediately leads to a magnetoresistance ΔR, defined as the resistance difference between the antiparallel and parallel aligned magnetization,

$$\Delta R = P_0^2 \lambda_s \rho_F \tag{2.16}$$

where ρ_F is the resistivity of the magnetic layer. The above Valet-Fert spin diffusion theory successfully provides an essential method for analyzing the CPP magnetoresistance at low temperatures [101]. At higher temperatures, the magnons become

important and the above simple expression breaks down. Indeed, the experimental findings on strong temperature dependence of the CPP GMR [102, 103] have not been satisfactorily explained. With our formalism, the electron spin accumulation would be decreased due to electron-magnon angular momentum transfer and thus provides a plausible explanation for the temperature dependent GMR. Unfortunately, the analytical expression of CPP GMR becomes rather cumbersome due to the multiple diffusion lengths as well as additional scattering channels involving magnons, see Appendix A.2. However, the essential physical picture remains intact: the magnetoresistance comes from the additional resistance generated by the spin accumulation which is strongly affected by the electron-magnon coupling at high temperatures. In Fig. 2.3, we show the magnetoresistance as function of the exchange coupling at several temperatures.

2.4 Summary and outlook

We have established the macroscopic diffusion equations for nonequilibrium electron spins and magnons of conducting ferromagnets. The essential conclusion is that the magnon current is always accompanied with the charge and spin electron current. The magnon current is the result of the momentum and angular momentum transfer from the conducting electrons. In magnetic multilayers, both spins and magnons are accumulated near the interfaces. As a result, the spin and magnon currents are spatially varying on length scales determined by multiple scattering mechanisms and by the coupling between spins and magnons. The spin-magnon diffusion equations can be broadly applied to various spintronics systems.

Experimental determination of our predicted magnon accumulation and magnon currents are certainly challenging due to the lack of proper experimental tools that can directly couple to the magnon accumulation. Aside from the indirect methods such as converting the magnon current to the spin current or the spin-transfer torques, a direct measuring the magnon accumulation might be possible as well because the magnon accumulation is much larger than the electron spin accumulation. At present,

the electron or hole spin accumulation is only measured in a semiconductor system [23]. For metallic magnets, the spin accumulation is too small even for the current density as high as 10^8 A/cm^2. The magnon accumulation might offer a possible route for directly observing the accumulation of the magnetic moment.

Chapter 3

Giant magneto-spin-Seebeck effect and magnon transfer torques in insulating spin valves

3.1 Motivation

In spintronics, spin current plays an essential role in delivering angular momentum from one layer to another. For example, a conventional spin valve (SV), consisting of two metallic ferromagnets separated by either a metallic or insulating non-magnetic layer, can effectively manipulate the spin current by changing the relative orientations of magnetization of the two magnetic layers. By propagating through two magnetic layers across the non-magnetic spacer, the spin of the conduction electrons interacts with both magnetic layers and leads to two most profound effects: giant magnetoresistance (GMR) [9, 10] and spin-transfer torque (STT) [15, 16]. For both GMR and STT effects, the magnetic layers must be metallic since the conduction electrons are essential for providing spin transport.

Besides the electron spin, each quasi-particle magnon is also known to have an angular momentum $\hbar$. Magnons are quantized low-energy excitations of magnetic materials. Since magnons are charge neutral, an electric field would not be able to directly drive a magnon current. A temperature gradient, however, can create a magnon current via magnon diffusing from high to low temperature in space. Conse-

quently, the magnon current can transfer its angular momentum to an electron spin current of a heavy metal in contact with the magnetic insulator. Due to the inverse spin Hall effect (ISHE) [26], this electron spin current generates an electric current or voltage in the heavy metal that can be directly measured; this is also known as the spin Seebeck effect [34–37].

Another demonstration of magnons as the angular momentum carriers had recently been achieved in a trilayer Pt/YIG/Pt where the electron spin current in one of the Pt layers can propagate to the other Pt layer mediated by the magnon current in the insulating ferromagnetic YIG layer [40, 44, 45]. In addition to the magnon transport in ferromagnets, magnons in antiferromagnetic materials such as NiO are also capable of carrying an angular momentum current as reported in trilayer structure YIG/NiO/Pt [38, 39, 41–43].

Besides above experiments, there are a number of existing theoretical studies on magnon transport [79, 88, 89, 104, 105]. Slonczewski [106] discussed the spin-transfer torque initiated by thermal transport of magnons. In the Slonczewski's model, the magnons induced by thermal gradient are to excite conduction electron spins. Thus, the role of the thermal magnons is to initiate spin-dependent electron transport in metal. In our study, the magnon transport in all insulating spin valves does not involve conduction electrons. In terms of STT magnitude, both Slonczewski and our work have estimated that the temperature gradient of the order of 1 Kelvin across interface would generate magnetic torque that is 1-2 order larger than the conventional STT. However, the thermal gradient is more difficult to maintain in metals than in insulators, and thus the all-insulator structure we proposed here would be more relevant for experimental verification of magnon transport.

All these findings motivate us to investigate an all-insulator spin valve structure, namely a trilayer consisting of two ferromagnetic insulators (FI) separated by an antiferromagnetic insulator (AFI), subject to a temperature gradient across the layers, as illustrated in Fig. 3.1. In this structure, the magnons are expected to travel between two FIs through the AFI spacer and the magnon current would depend on the relative orientations of the two FIs. As the consequence, we show that the magnon

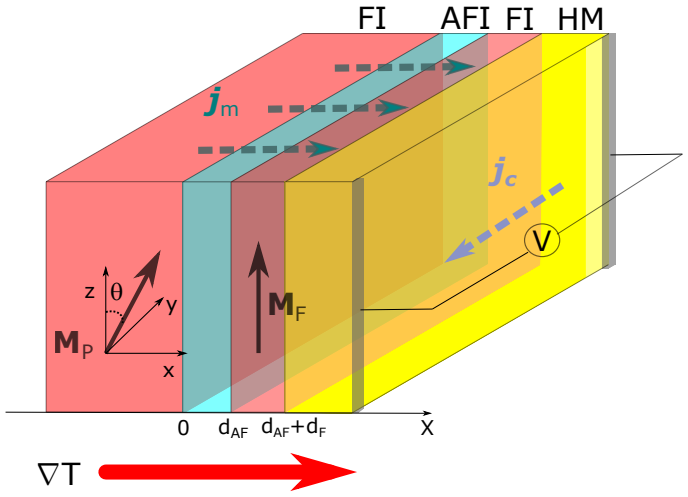

Figure 3.1: Schematics of the proposed all-insulating spin valve. Two FI layers are separated by an AFI layer. The attached heavy metal layer is used to read out the magnon current in the ISV. The temperature gradient is applied perpendicular to the layer and we assume it is uniform in magnetic layers but zero in the HM layer. In our calculation of GMSSE and MTT, we fixed the direction of the free layer while allowing the direction of the pinned layer to rotate from 0 to π.

valve proposed here display two distinct phenomena: the giant magneto spin-Seebeck effect (GMSSE) and the magnon transfer torque (MTT).

For the GMSSE, the voltage signal detected by the heavy metal (HM) layer attached to one of the FI layer, as shown in Fig. 3.1, is proportional to the total spin current near the interface of the HM and the thin FI free layer ($\mathbf{M}_F$) via ISHE. When the magnetization of the two FI layers are in parallel (antiparallel), the magnon current induced by the temperature gradient in each FI layer is additive (subtractive), leading to a voltage difference between parallel and antiparallel magnetization alignments. By properly choosing the thickness of the free FI layer, one is able to achieve a 100% GMSSE ratio (the spin current generated by antiparallel configuration is zero).

For the MTT, when the magnetization of the two FI layers are not collinear, the thin FI free layer would absorb the transverse component of the magnon current generated in the thick FI pinned layer ($\mathbf{M}_P$), similar to conventional STT phenomenon. If the MTT is sufficiently large, the magnetization of free FI layer can be switched.

We have estimated that a thermal gradient about 0.1 Kelvin per nanometer could produce a magnon transfer torque of the order of $10^9 \mathrm{A/m}^2(\hbar/e)$ (e is the electron charge), a comparable magnitude for the electron current induced STT switching [107–109]. We present our theory below.

3.2 Derivation of magnon diffusive transport

We start by considering a simplest heat profile with a uniform temperature gradient $\nabla_x T$ across the insulating spin valve (ISV), i.e., the thermal conductivity is same for all insulator layers. The temperature gradient in the heavy metal layer is negligibly small. At equilibrium, the average number of magnons in each layer obeys the Bose-Einstein distribution with zero chemical potential. When a thermal gradient exists, magnons would diffuse across the layers and a nonequilibrium magnon distribution would be established. A simplest way to describe the magnon diffusive transport is to introduce an effective magnon chemical potential $\boldsymbol{\mu}_m^{\mathrm{F}}$ that characterizes the local magnon spin accumulation [79, 80, 88, 110]. Similar to the case in ferromagnetic metals, the direction of the magnon chemical potential $\boldsymbol{\mu}_m^{\mathrm{F}}$ and magnon current $\mathbf{J}_m^{\mathrm{F}}$ are always parallel to the local magnetization $\hat{\mathbf{M}}$, i.e., $\boldsymbol{\mu}_m^{\mathrm{F}} = \mu_m^{\mathrm{F}}\hat{\mathbf{M}}$ and $\mathbf{J}_m^{\mathrm{F}} = J_m^{\mathrm{F}}\hat{\mathbf{M}}$ (in units of $\mathrm{J/m}^2$), and thus we may write the magnon Ohm's law in a simple scalar form [88]

$$J_m^{\mathrm{F}} = -S_m^x \nabla_x T - \sigma_m^{\mathrm{F}} \frac{d\mu_m^{\mathrm{F}}}{dx} \tag{3.1}$$

where we have defined the magnon thermal conductivity S_m^x and magnon spin conductivity σ_m^{F} as

$$S_m^x = \frac{\hbar\tau_m}{(2\pi)^3 T} \int d^3q v_{q_x}^2 \frac{\varepsilon_{\mathbf{q}}}{k_B T} \mathrm{csch}^2 \frac{\varepsilon_{\mathbf{q}}}{2k_B T} \tag{3.2}$$

$$\sigma_m^{\mathrm{F}} = \frac{\hbar\tau_m}{(2\pi)^3} \int d^3q \frac{v_q^2}{3} \frac{\partial N_m^0(\mathbf{q})}{\partial \varepsilon_{\mathbf{q}}} \tag{3.3}$$

where $\mathbf{v_q}$ is the magnon velocity, τ_m is the magnon relaxation time, $\varepsilon_{\mathbf{q}}$ is the magnon energy and $N_m^0(\mathbf{q}) = [\exp(\beta\varepsilon_{\mathbf{q}}) - \mathbf{1}]^{-\mathbf{1}}$ is the equilibrium magnon distribution. The

magnon accumulation in Eq. 3.1 satisfies the diffusion equation,

$$\frac{d^2\mu_m^{\mathrm{F}}}{dx^2} = \frac{\mu_m^{\mathrm{F}}}{(\lambda_m^{\mathrm{F}})^2} \tag{3.4}$$

where λ_m^{F} is the magnon diffusion length.

For the AFI, magnon diffusion is generally more complicated. If the AFI is a single crystal with collinear magnetic moments for two sublattices, the magnon spectra contain two degenerate branches with each magnon carrying either $\hbar$ or $-\hbar$ with respect to the order parameter (the staggered magnetization direction). For a polycrystalline AFI layer, there are multiple directions for the order parameter and the description of the magnon transport would be very cumbersome and difficult.

Here, we shall consider a simple realization in which the order parameter of the AFI may be distributed randomly; this is certainly an oversimplification for modelling a polycrystalline AFI, but the problem becomes trackable. In this picture, the magnon propagation in the AFI is similar to the electron spin transport in a non-magnetic metal in which the spin or magnon currents can be oriented in any direction dictated by the spin/magnon injection from the neighboring magnetic layer. Thus, magnon Ohm's law in the AFI may be similarly defined as

$$J_m^{\mathrm{AF}} = -\sigma_m^{\mathrm{AF}} \frac{d\mu_m^{\mathrm{AF}}}{dx} \tag{3.5}$$

where σ_m^{AF} is the magnon spin conductivity of AFI; for a collinear AF spin structure σ_m^{AF} has already been calculated [111]. It is noted that the AFI has no drift term associated with the temperature gradient since the magnon current from the two degenerated magnon spectra cancels out [54, 111, 112] ; this is analogous to the electron spin transport where an electric field induces a spin current drift term in ferromagnetic metal, but not in non-magnetic metal. The magnon chemical potential in AFI layer also satisfies the diffusion equation,

$$\frac{d^2\mu_m^{\mathrm{AF}}}{dx^2} = \frac{\mu_m^{\mathrm{AF}}}{(\lambda_m^{\mathrm{AF}})^2} \tag{3.6}$$

where λ_m^{AF} is the magnon diffusion length of AFI layer. Since $\boldsymbol{\mu}_m^{\mathrm{AF}}$ can take any direction, the general solution of μ_m^{AF} is

$$\boldsymbol{\mu}_m^{\mathrm{AF}}(x) = \mathbf{A}\exp\left(\frac{x}{\lambda_m^{\mathrm{AF}}}\right) + \mathbf{B}\exp\left(-\frac{x}{\lambda_m^{\mathrm{AF}}}\right) \tag{3.7}$$

where $\mathbf{A}$ and $\mathbf{B}$ are the vectoral constants of the integrations. Clearly, when the magnetization $\mathbf{M}_P$ and $\mathbf{M}_F$ are not collinear, the direction of $\boldsymbol{\mu}_m^{\mathrm{AF}}$ is neither parallel to $\mathbf{M}_P$ nor to $\mathbf{M}_F$. The constant vectors $\mathbf{A}$ and $\mathbf{B}$ would be determined by the boundary conditions given below.

The first set of the boundary conditions involves the longitudinal magnon chemical potential and magnon current. When neglecting the interfacial spin memory loss, the longitudinal spin current is continuous across the FI/AFI interfaces, i.e.,

$$\begin{aligned} J_m^{\mathrm{F}}(0^-) &= \hat{\mathbf{M}}_P \cdot \mathbf{J}_m^{\mathrm{AF}}(0^+) \\ J_m^{\mathrm{F}}(d_{\mathrm{AF}}^+) &= \hat{\mathbf{M}}_F \cdot \mathbf{J}_m^{\mathrm{AF}}(d_{\mathrm{AF}}^-) \end{aligned} \tag{3.8}$$

The magnon current across the interfaces is also related with the difference of the magnon chemical potential at the two sides of the interface,

$$J_m(0) = \frac{G_{\mathrm{A/F}}^{\parallel}}{2\pi}\left[\mu_m^{\mathrm{F}}(0^-) - \boldsymbol{\mu}_m^{\mathrm{AF}}(0^+)\cdot\hat{\mathbf{M}}_P\right] \tag{3.9}$$

where $G_{\mathrm{A/F}}^{\parallel}$ is the conductance addressing spin convertance efficiency across interfaces [89, 104]. A similar expression at the interface $x = d_{\mathrm{AF}}$ can also be written.

The second set of the boundary conditions relates the magnon chemical potential and magnon current perpendicular to the local magnetization of the FI layers. Similar to the ferromagnetic metal case where the electron spin chemical potential and spin current transverse to the magnetization direction are zero [19, 113] , the transverse magnon chemical potential and magnon current vanish in the FI layers as well. Thus, the transverse magnon current and chemical potential at the boundaries are

$$\hat{\mathbf{M}}_P \times \left[\hat{\mathbf{M}}_P \times \mathbf{J}_m^{\mathrm{AF}}(0^+)\right] = -\frac{G_{\mathrm{A/F}}^{\perp}}{2\pi}\hat{\mathbf{M}}_P \times \left[\hat{\mathbf{M}}_P \times \boldsymbol{\mu}_m^{\mathrm{AF}}(0^+)\right] \tag{3.10}$$

and the similar expression for the interface at $x = d_{\mathrm{AF}}$.

The thermal driven interfacial magnon conductance for the transverse component $G^{\perp}_{\mathrm{A/F}}$ is analogous to the mixing conductance of electron spin [74, 114] , and it differs from the longitudinal one $G^{\parallel}_{\mathrm{A/F}}$. Finally, the boundary conditions at the interface of the FI and HM layers involve the conversion between the magnon current and the electron spin current of the HM layer; it has been previously formulated in Ref. [89].

With these boundary conditions, the magnon chemical potential and magnon current are determined in each layer. In the calculation shown below, we shall take the thickness of pinned layer much larger than the magnon diffusion length λ_m^{F} and the thickness of the antiferromagnetic layer much less than the magnon diffusion length λ_m^{AF}.

3.3 Results

3.3.1 Giant magneto-spin-Seebeck effect

Figure 3.2 shows the thickness dependence of the giant magneto spin-Seebeck spin current signal for the two magnetic layers in parallel and in antiparallel configurations. In the parallel alignment, the magnon current at the HM interface is the sum of the magnon sources from both FI layers. At a small thickness of the free layer, the main contribution is from the pinned layer whose magnon current travels through two AFI/FI interfaces. As the thickness increases, the contribution from the free layer increases, that from the pinned layer decreases because the magnon current from it is further away from the FI/HM interface with a higher probability to be scattered by the free layer.

To see the relative contribution of the magnon current from the two FI layers, we turn off the temperature gradient either in the pinned or in the free layer, as shown in the inset of Fig. 3.2(a). The decrease of the magnon current from the pinned layer is steeper than the increase from the free layer for small thickness of free layer. For the magnon current generated in the fixed layer, the exponential decaying length involves multiple interface scattering in addition to the scattering in the free layer,

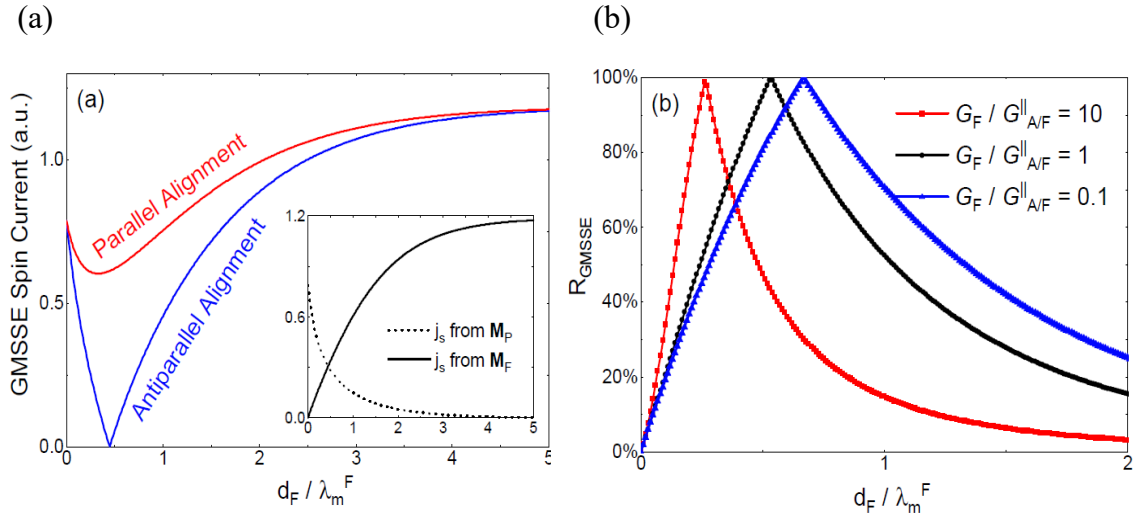

Figure 3.2: Thickness dependence of the GMSSE. (a) The GMSSE spin current (arbitrary unit) is shown for the parallel (red solid line) and antiparallel (blue solid line) aligned FI layers and (b) the GMSSE ratio. The parameters used in the figure are: magnon spin conductance for FI layer $G_{\rm F} \equiv \sigma_m^{\rm F}/\lambda_m^{\rm F} = 2.1 \times 10^{18}{\rm m}^{-2}$, electron spin conductance for NM layer $G_{\rm N} = 7.7 \times 10^{18}{\rm m}^{-2}$ and spin conductance for FI/NM interface $G_{\rm F/N} = 0.3 \times 10^{18}{\rm m}^{-2}$.

while the magnon current generated in the free layer is linearly increasing with its thickness; this explains the initial reduction of the total magnon current at small thickness of Fig. 3.2(a). When the thickness becomes larger, the contribution from the free layer is more important and eventually dominates the entire magnon current for the thickness much larger than the magnon diffusion length.

For the antiparallel alignment, the magnon current from the pinned layer is always opposite to that from the free layer. As the thickness of the free layer increases, the magnitude of the total magnon current first decreases due to partial cancellation of the contributions from the two magnetic layers. At a certain critical thickness $d_{\rm cr}$, the magnon currents from two layers are exactly cancelled and the total magnon current becomes identically zero. In this case, we completely achieved an off-state in which the ISHE voltage is zero. If we define a giant magneto spin-Seebeck ratio by $R_{\rm GMSSE} = (j_s^P - j_s^{AP})/j_s^P$, where j_s^P and j_s^{AP} are the magnon spin current magnitudes for parallel and antiparallel alignments of the FI layers, we arrive the thickness dependence of

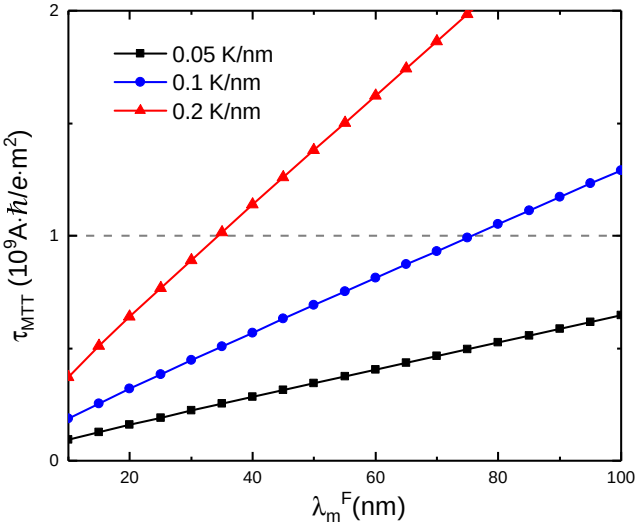

Figure 3.3: The magnon transfer torque as a function of the magnon diffusion length at room temperature. The parameters used in the figure are: $G^{\perp}_{\mathrm{A/F}} = 1\times10^{17}\mathrm{m}^{-2}$, $G^{\parallel}_{\mathrm{A/F}} = 1\times10^{18}\mathrm{m}^{-2}$, G_{F}, G_{N} and $G_{\mathrm{F/N}}$ are same as used in Fig. 3.2.

R_{GMSSE} shown in Fig. 3.2(b). It is noted that the 100% giant magneto spin-Seebeck effect is always possible by choosing a proper thickness of the free layer.

3.3.2 Magnon transfer torques

We next calculate the magnon transfer torque $\boldsymbol{\tau}_{\mathrm{MTT}}$ on the free layer. At the interface between AFI and free layer, the transverse part of the spin current of the AFI layer is unable to penetrate into the free layer. Similar to the conventional spin transfer torque, one may identify the MTT as the transverse magnon current density at the AFI side of the interface, namely,

$$\boldsymbol{\tau}_{\mathrm{MTT}} = \hat{\mathbf{M}}_F \times \left(\mathbf{J}_m^{\mathrm{AF}}(d_{\mathrm{AF}}^-) \times \hat{\mathbf{M}}_F\right) \tag{3.11}$$

In Figure 3.3, we show the MTT for the perpendicularly aligned two AFI layers as a function of the magnon diffusion length λ_m^{F} for $d_{\mathrm{F}} = 3$ nm and for several temperature gradients. The nearly linear relation between the MTT and the diffusion length is

due to the fact that we have chosen the pinned layer infinitely thick such that the spin current flowing from the pinned layer to free layer scales as $k_B \nabla_x T \lambda_m^{\rm F}$ [89]. If the thickness is finite, the linear relation for a large $\lambda_m^{\rm F}$ will no longer be held. In determining the absolute value of the MTT in Fig. 3.3, we have used the following plausible parameters relevant to typical magnetic insulators of YIG [80] and YIG/NiO interface: $T_C = 550$ K, $a_{\rm YIG} = 1.39$ nm, quadratic dispersion relation $\varepsilon_{\mathbf{q}} = Aq^2 + \Delta_g$ with exchange stiffness $A = 6$ meV $\cdot$ nm^2 and magnon gap $\Delta_g = 10^{-6}$ eV, and $G^{\parallel}_{\rm YIG/NiO} = 1 \times 10^{18}{\rm m}^{-2}$.

It is interesting to compare the absolute values of the MTT with the STT. In the conventional STT devices, one needs a critical electric current density on the order of $J_c \sim 10^{10}{\rm A/m}^2$ [107–109] to switch a metallic ferromagnetic layer. Assuming the electric current is 100% spin polarized, the angular momentum current would be $(\hbar/e)J_c$. For switching an insulating ferromagnet which typically has a smaller Gilbert damping parameter and lower saturation magnetization, we would expect an order of magnitude smaller critical angular momentum current. In Fig. 3.3, the horizontal dotted line represents this hypothetical critical value for the magnetization switching. Thus, we estimate that a temperature gradient of the order of 0.1 K/nm for $\lambda_m^{\rm F} = 80$ nm [45, 88] is capable of achieving the magnetization switching.

If we write the MTT in the vector form

$$\boldsymbol{\tau}_{\rm MTT} = \tau^0_{\rm MTT} \hat{\mathbf{M}}_F \times (\hat{\mathbf{M}}_P \times \hat{\mathbf{M}}_F) \tag{3.12}$$

magnitude $\tau^0_{\rm MTT}$ is the transverse component of $\mathbf{J}_m^{\rm AF}(d^-_{\rm AF})$ which depends on the relative angle between two magnetic layers. In Fig. 3.4, we show the angular dependence of the MTT; this behavior is similar to that of the spin torque in the conventional metal-based SV [113].

3.4 Summary and outlook

We emphasize some of the key features in our proposed magnon valves. First, the GMSSE and the MTT phenomena proposed here are strongly temperature de-

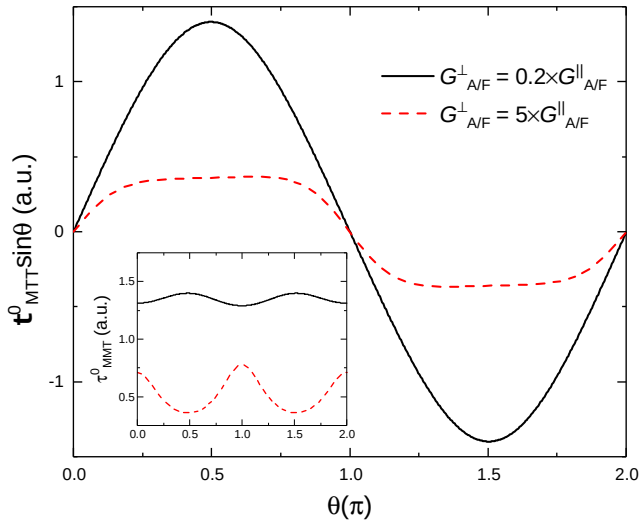

Figure 3.4: The angular dependence of the magnon transfer torque where θ is the angle between the magnetization of $\mathbf{M}_P$ and $\mathbf{M}_F$ layers. In the insert, we show the angular dependence of the MTT without $\sin\theta$.

pendent. Since the number of magnons in the FI and AFI is much robust at high temperature, we expect the predicted GMSSE and MTT to be diminished at low temperature. This temperature dependence is rather general for all magnon driven transport phenomena and has been reported in various experiments related to magnon transport. Second, the modeling of the magnon transport in AFI is oversimplified. We have used a simple magnon dispersion relation with an ideal collinear sublattice AF Hamiltonian and we further assume that the AFI can transmit any direction of the spin current. These simplifications lead to uncertainty in the estimation of the MTT. More specific models relevant to experimental materials should be used to give rise a better estimation. Third, the interaction at the interface between the AFI and FI could have profound effects. The exchange bias and coercivity enhancement would complicate the interface magnon conductance compared to that for an ideal atomically flat interface and furthermore, other effects of the MTT on the magnetization switching could emerge.

In summary, we have proposed a magnon valve structure based on insulating magnetic materials. Similar to the giant magnetoresistance and the spin transfer torque

in the conventional spin valve, we predict two phenomena in the giant magneto spin-Seebeck effect and magnon transfer torque. From the viewpoint of fundamental study of spin transport, the ISV offers an ideal platform for magnon angular momentum transport, without the complications of metal-based SV where both magnons and electrons are involved in the transport. In terms of device application, the ISV guarantees zero Joule energy lost for minimizing power consumption and lower damping for faster magnetization switching. On the other hand, controlling the direction of bi-polar heat flow and determining the temperature gradient at the nanometer scale for reversibly switching magnetization may present a challenge for device designs.

Chapter 4

Amplification of spin-transfer torque in magnetic tunnel junctions with an antiferromagnetic barrier

4.1 Introduction

In today's spin-based information storage technology, magnetic tunnel junctions (MTJs) [11, 12, 50, 115] have been arguably the most important building blocks. Since the discovery of large tunnel magnetoresistance (TMR) in the MgO-based MTJs about 14 years ago [13, 14, 116, 117] , research and development on MTJs have almost exclusively focused on MgO barriers. Indeed, MgO tunnel barriers have shown tremendous advantages over other insulating barriers such as amorphous Al_2O_3. The superior epitaxial growth of MgO barrier with transition metal ferromagnet (FM) electrodes makes the tunnel resistance rather tunable to meet the different requirement of specific devices, e.g. magnetic reading heads and magnetic random-access memories (MRAMs) [118]. Most importantly, TMR of MgO-based MTJs is as large as 600% at room temperature [119] , far exceeding other known tunnel barriers.

While the large TMR value of MgO-based MTJs provides unprecedented efficiency for magnetic reading, switching the magnetization direction of MTJs for the writing remains challenging. In the first generation of MRAM devices, an external magnetic field is used for magnetization switching; this method is not scalable and would fail

for high density MRAMs [29]. The second generation takes advantage of spin transfer torque (STT) where a sufficient large electric current across the tunnel barrier can reorient the relative magnetizations of two magnetic layers in parallel or antiparallel, depending on the polarity of the current [15, 16, 107, 120–123].

Up until now, the critical switching current density (j_c) is very high, of the order of 10^6 A cm^{-2}. In the STT switching, the spin angular momentum of tunnel electrons from one electrode to the other determines the total magnetic torque. Under a typical switching voltage across the junction about 0.5 V, each tunneling electron transfers its spin angular momentum at maximum of $\hbar/2$, but the accompanied energy of 0.5 eV is completely wasted. Thus, the STT switching by tunnel electrons are not energy efficient.

In this chapter, we theoretically investigate the tunnel transport with an antiferromagnetic insulator (AFI) as tunnel barrier. Our central idea and motivation for replacing MgO by an AFI barrier are outlined below.

Consider a tunnel junction made of two ferromagnetic metals separated by a thin antiferromagnetic insulator, as shown in Fig. 4.1. When a voltage is applied across the tunnel barrier, electrons tunnel from the electrode with the lower voltage to that with the higher voltage. While the tunneling electron will relax its energy in both electrodes, the majority of the energy is relaxed in the electrode receiving the tunnel electron. Since the inelastic mean free path is only a few angstroms for the tunnel electron with the energy about 0.5 eV above the Fermi level [124, 125] , the heat is generated near the vicinity of the interface. The heat is subsequently diffusing into the interior of the electrode as well as across the barrier. In the steady state condition, a temperature gradient is established in the structure and one expects a temperature difference would be created at the two sides of the barrier.

It has been experimentally and theoretically shown that the temperature difference could reach a fraction of a Kelvin degree for a bias voltage of 0.5-1 V [126, 127]. Consequently, a magnon current would flow across the AFI barrier from one FM electrode to the other, exerting a magnon transfer torque on the free magnetization layer. Theoretically, the magnon current driven by temperature gradient has already

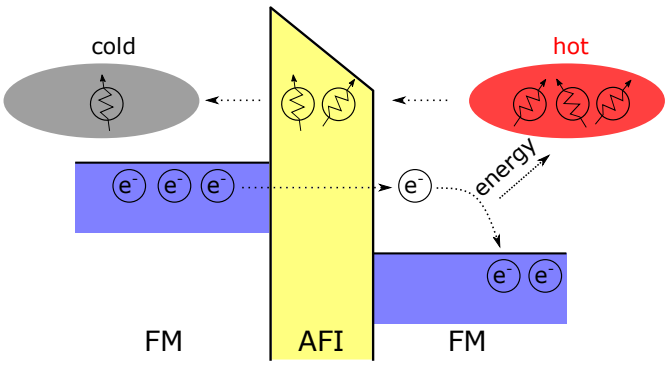

Figure 4.1: Schematics of the proposed AFI-MTJ. Two FM layers are separated by an AFI barrier and they are biased by a negative voltage of the order of several hundreds of mV. Hot electrons tunnel from the left FM electrode to the right FM electrode and the excess energy is dissipated over inelastic scattering length to heat up magnons on the right. The resulting magnons would diffuse from right (hot) to left (cold) mediated by the magnons in AFI.

studied in details [86, 88, 128–130].

The above discussion leads us to critically examine whether it is possible to recycle the wasted energy of tunnel electrons for magnetization switching. Since a magnetic barrier is required for magnon propagation, both ferromagnetic and antiferromagnetic insulators would be barrier candidates. However, the ferromagnetic insulator would be strongly coupled with ferromagnetic electrodes and thus it is difficult to freely rotate the relative orientation of the magnetization of two electrodes. An antiferromagnetic barrier would be ideal: one can control and minimize the exchange bias and the antiferromagnetic material is theoretically and experimentally proven materials which can efficiently propagate the magnon current [38, 39, 41–43, 59, 87, 111, 112].

4.2 Heat transport and temperature profile

To model the temperature profile, we specify the geometrical parameters in Fig. 4.2(a): the MTJ, made of a pinned magnetic layer FM1, an AFI barrier, and a free magnetic layer FM2, is sandwiched by two non-magnetic (NM) layers (representing

the overlayer and underlayer of MTJs) so that the temperature profile is not simply limited within the MTJ. Thicknesses of the layers are labeled in Fig. 4.2(b). A time-dependent electric current $j_e(t)$ flows perpendicularly to the layers with a bias voltage $V(t)$ across the junction. The sign convention for the current is $j_e(t) < 0$ (or equivalently $V(t) < 0$) corresponding to net electron tunneling from FM1 to FM2.

We model the heat transport by using the layer-by-layer approach. In each layer, the heat diffusion equation reads,

$$\rho_i C_i \frac{\partial T(t,x)}{\partial t} - \kappa_i \frac{\partial^2 T(t,x)}{\partial x^2} = P_i(t,x) \tag{4.1}$$

where ρ_i, C_i and κ_i are the mass density, heat capacity and thermal conductivity of the i-th layer, $P_i(t,x)$ is the power of heat source generated by the electric current. The Joule heating, j_e^2/σ_i, is always present for each metallic layer where σ_i is electric conductivity. In the tunnel junction, as illustrated in Fig. 4.1, the main energy relaxation of the tunnel electrons occurs near the interface. For the electrode receiving the tunnel electrons, the energy of tunnel electrons is above the Fermi level up to the bias voltage $V(t)$. These hot electrons have short mean free paths, of the order of 1 nm. For the electrode emitting electrons, the holes left by the tunnel electrons, are also short-lived and thus, the annihilation of holes takes place near the interface as well.

Therefore, we may parameterize the heat generation by tunnel electrons as [126, 127],

$$P_{\text{re}}(t,x) = \alpha \frac{j_e(t)V(t)}{\lambda_{\text{inel}}} \exp\left(-|x|/\lambda_{\text{inel}}\right) \tag{4.2a}$$

$$P_{\text{em}}(t,x) = (1-\alpha) \frac{j_e(t)V(t)}{\lambda_{\text{inel}}} \exp\left(-|x|/\lambda_{\text{inel}}\right) \tag{4.2b}$$

where $|x|$ is the stack position from AFI/FM interface, α is to parameterize the relative heat power generated in two electrodes, and λ_{inel} is the inelastic scattering mean free path. The parameter α is always larger than 0.5, i.e., the electron-receiving electrode generates more heat; this is because the tunnel probability is larger for

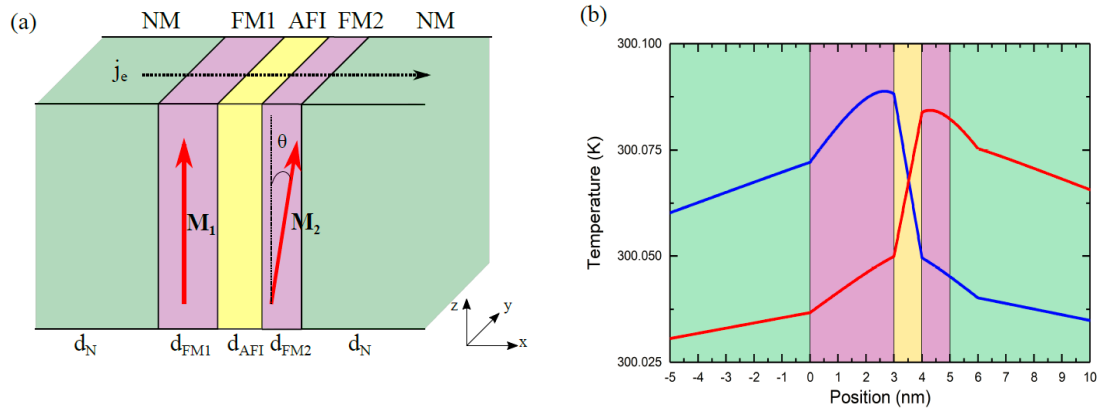

Figure 4.2: a) Proposed AFI-MTJ structure and b) Temperature profiles for both directions of the current. The yellow (purple, green) area is AFI (FM, NM). Red (blue) solid line in (b) denotes electrons tunnel from left (right) to right (left). The current density used in (b) is $j_e = 2 \times 10^6$ A cm^{-2} and the voltage is $V = 0.2$ V. Other material parameters are [2, 3] : $d_{\rm FM1} = 2d_{\rm FM2} = 3d_{\rm AFI} = 3$ nm, $d_{\rm N} = 30$ nm, $\kappa^{\rm N} = 401$ Wm^{-1}K^{-1}, $\kappa^{\rm F} = 91$ Wm^{-1}K^{-1}, $\kappa^{\rm AF} = 20$ Wm^{-1}K^{-1}, $\sigma^{\rm F} = 1.43 \times 10^7$ Sm^{-1}, $\sigma^{\rm N} = 5.96 \times 10^7$ Sm^{-1}, $\lambda_{\rm inel} = 1$ nm and $\alpha = 0.9$ with the choice of Ni as FM, NiO as AFI and Cu as NM. The temperatures at the outer boundaries of MTJ are kept at 300 K.

tunnel electrons with higher energy.

Since the characteristic time of magnetization dynamics (about picoseconds) is much longer than the electron-electron and electron-phonon collision times (about tens of femtoseconds) which control the rate of change of the temperature [131] , we shall solve the above heat diffusion in the steady state condition, i.e., we assume that the source and temperature become constant once an electric current is turned on. Equation (4.1) becomes a simple differential form and we are able to find the general solutions for each layer. The integration constants are then determined by boundary conditions in which we use the continuity of the temperature and heat current across the interfaces. In Fig. 4.2(b), we show the typical temperature profile of tunnel junction by using the materials parameters in bulk form, as indicated in the caption. Since we assume an asymmetric heating parameter $\alpha = 0.9$, i.e., 90% of the Joule

heating is generated at the electron receiving electrode, the temperature is always higher for the high voltage side of the junction. The temperature difference across tunnel barrier could reach tens of mK for current density of $j_e = 2 \times 10^6$ A cm^{-2} and voltage of 0.2 V. The actual temperature gradient across the barrier can be even larger when the stack structure and the passivation materials used in the MTJ device are optimized [132].

4.3 Magnon current and magnon transfer torques

With our calculated temperature profile, we now turn to the calculation of magnon current and its induced torque on the free layer. We have previously calculated the giant magneto-spin-Seebeck effect and the magnon transfer torque in all-insulating spin valves in the presence of temperature gradient in Chap. 3. It is rather straightforward to extend our calculation for the magnon current in structure made of an antiferromagnetic insulator and magnetic metals.

The magnon current in the presence of a temperature gradient in FM may be written as

$$\mathbf{j}_m^{\mathrm{F}}(x) = -\hbar S_m \nabla_x T(x) \hat{\mathbf{M}}_{\mathrm{F}} - \sigma_m^{\mathrm{F}} \nabla_x \mu_m(x) \hat{\mathbf{M}}_{\mathrm{F}} \tag{4.3}$$

where S_m is the spin Seebeck coefficient [46, 88] , σ_m^{F} is the magnon conductivity [46, 88] and we use the effective magnon chemical potential $\boldsymbol{\mu}_m(x)$ to describe the nonequilibrium magnon accumulation [46, 79, 88, 110] , and $\hat{\mathbf{M}}_{\mathrm{F}}$ is the FM magnetization. Within the AFI layer with two sublattices, the magnon Ohm's law is

$$\mathbf{j}_m^{\mathrm{AF}}(x) = -\sigma_m^{\mathrm{AF}} \nabla_x \boldsymbol{\mu}_m(x) \tag{4.4}$$

where σ_m^{AF} is the AFI magnon conductivity. It is noted that since we consider easy-axis collinear AFI, two degenerate magnon branches cancels out therefore we don't consider magnon spin Seebeck effect in AFI [112, 133].

The exchange interaction at AFI/FM interface is responsible for the magnon trans-

mission

$$H_{\text{int}} = -J_{\text{int}} \sum_{i} \mathbf{S}_{i,\text{F}} \cdot \mathbf{S}_{i,a(b)} \tag{4.5}$$

where J_{int} is the interface exchange constant, $\mathbf{S}_{i,\text{F}}$ represents the spin at the interface of FM layer and $\mathbf{S}_{i,a(b)}$ is the spin of two sublattices of AFI. We here consider that (1) both FM and AFI have in-plane uniaxial anisotropy, and (2) the AFI interface is a compensated one such that the exchange coupling between the ferromagnetic spin and either sublattice spin of the AFI is modeled by the same J_{int}. The order parameter of AFI is assumed to have a angle to the magnetization of FM, thus the second quantization of Eq. (4.5) would be

$$H_{\text{int}} = -J_{\text{int}} \sum_{\mathbf{kq}} (S_{\text{F}} S_{\text{AF}})^{1/2} \left[C_{\mathbf{q}} A_{\mathbf{k}} \alpha_{\mathbf{q}}^{\dagger} (1 + \hat{\mathbf{n}} \cdot \hat{\mathbf{M}}_{\text{F}}) + C_{\mathbf{q}} A_{\mathbf{k}} \beta_{\mathbf{q}}^{\dagger} (1 - \hat{\mathbf{n}} \cdot \hat{\mathbf{M}}_{\text{F}}) + \text{H.c.} \right] \delta_{\mathbf{k},\mathbf{q}} \tag{4.6}$$

where $\hat{\mathbf{n}}$ is the AFI order parameter, $A_{\mathbf{k}}$ ($A_{\mathbf{k}}^{\dagger}$) represents the annihilation (creation) operators for the FM magnons, $\alpha_{\mathbf{q}}^{\dagger}$, $\alpha_{\mathbf{q}}$ and $\beta_{\mathbf{q}}^{\dagger}$, $\beta_{\mathbf{q}}$ are the creation and annihilation operators for the two magnon branches of AFI, $C_{\mathbf{q}} = u_{\mathbf{q}} - v_{\mathbf{q}}$ where $u_{\mathbf{q}}$ and $v_{\mathbf{q}}$ are the Bogoliubov transformation coefficients of AFI magnons, $S_{\text{F(AF)}}$ is the magnitude of FM (AFI) spin and we have neglected the high order magnon interactions.

Two sets of boundary conditions at interfaces are needed to determine the integration constants from the Eq. (4.3) and Eq. (4.4). The first one is that the longitudinal magnon spin current is continuous across the FM/AFI interface,

$$j_m^{\text{F}} = \hat{\mathbf{M}}_{\text{F}} \cdot \mathbf{j}_m^{\text{AF}} \tag{4.7}$$

and their magnitude is related to the difference of magnon chemical potential at two sides of the interface

$$j_m = G_{\text{A/F}}^{\parallel} \left[\mu_m^{\text{F}} - \boldsymbol{\mu}_m^{\text{AF}} \cdot \hat{\mathbf{M}}_{\text{F}} \right] \tag{4.8}$$

where $G_{\text{A/F}}^{\parallel}$ is the longitudinal magnon spin conductance. For the $\hat{\mathbf{n}} \cdot \hat{\mathbf{M}}_{\text{F}} = 1$ case, the interface exchange interaction in the form of $J_{\text{int}} A_{\mathbf{k}} \alpha_{\mathbf{q}}^{\dagger}$ leads to a spin current across the interface. The longitudinal magnon spin conductance has already been calculated

in Ref. [89] and for temperature much lower than the Curie and Néel temperatures, it scales with $\frac{J_{\rm int}^2}{(k_B T_{\rm C})(k_B T_{\rm N})}\left(\frac{T}{T_{\rm C}}\right)^{1/2}\left(\frac{T}{T_{\rm N}}\right)^2$.

For the case of which the quantization axis of AFI that is perpendicular to local magnetization of FM, e.g. $\hat{\mathbf{n}}\cdot\hat{\mathbf{M}}_{\rm F}=0$ we have both $\alpha_{\mathbf{q}}$ and $\beta_{\mathbf{q}}$ that can create a FM magnon with the interaction $J_{\rm int}A_{\mathbf{k}}^{\dagger}(\alpha_{\mathbf{q}}+\beta_{\mathbf{q}})$. Since $\alpha_{\mathbf{q}}$ and$\beta_{\mathbf{q}}$ have opposite spin direction, the non-equal accumulations of these two magnons would create a transverse spin torque on FM. The second boundary condition would be

$$\hat{\mathbf{M}}_{\rm F}\times\left[\hat{\mathbf{M}}_{\rm F}\times\mathbf{j}_m^{\rm AF}\right]=-G_{\rm A/F}^{\perp}\hat{\mathbf{M}}_{\rm F}\times\left[\hat{\mathbf{M}}_{\rm F}\times\boldsymbol{\mu}_m^{\rm AF}\right] \tag{4.9}$$

where $G_{\rm A/F}^{\perp}$ is analogous to the mixing conductance and its magnitude is half the longitudinal one. We show the detailed derivation in Appendix B. Note that the magnon current in FM layers is always parallel to the direction of the magnetization, as in the case of the electron spin current.

With these boundary conditions and the temperature profile we have numerically solved in Sec. 4.2, we can determine the magnon accumulation and magnon current in each layer. The magnon torque on the free layer FM2 is simply identified as the transverse component (relative to the magnetization vector of the FM2) of the magnon current at the AFI/FM2 interface.

4.4 Amplification of spin torques

To quantitatively estimate the enhancement of the spin torque by using AFI barrier, we numerically calculate the magnon current and obtain the magnon spin torque due to the temperature difference generated by the tunnel electrons.

To be more concrete, we choose the critical torque $\tau_{\rm cr}$ for the switching of the free layer that is equivalent to the critical electric current $j_{\rm cr}^{(0)}=5\times10^6\ \mathrm{A\,cm^{-2}}$ in the absence of the magnon spin torque. When the magnon spin torque is turned on, we numerically determine the new critical electric current density $j_{\rm cr}^{(m)}$ needed to generate the *same amount* of torque $\tau_{\rm cr}$. As the magnon torque is directly related to the Joule heating, the relative contribution between magnon current and electron

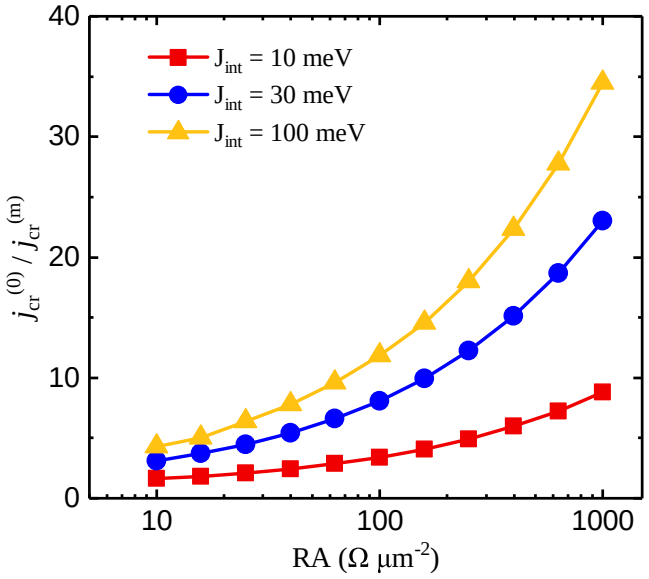

Figure 4.3: The dependence of the ratio of the switching current density without and with the magnon spin torques on tunnel resistance area product (RA) at different interface exchange coupling strength. We assume the critical electric current $j_{\rm cr}^{(0)} = 5 \times 10^6$ A cm^{-2} with polarization $P = 0.5$ in the absence of the magnon spin torque. The RA value scales exponentially with the barrier thickness, RA $= 10\,\Omega\,\mu$m^2 at $d_{\rm AFI} = 1$ nm and RA $= 10^3$ $\Omega\,\mu$m^2 at $d_{\rm AFI} = 2$ nm. Other parameters used in this figure are such: $d_{\rm FM1} = 2d_{\rm FM2} = 3$ nm, $T_{\rm C} = 630$ K, $T_{\rm N} = 530$ K, $a_{\rm F} = 0.35$ nm, $a_{\rm AF} = 0.417$ nm, $S_{\rm F} = S_{\rm AF} = 2$.

spin current depends highly on the tunnel resistance. The larger the voltage (or the resistance), the greater the magnon torque relative to the electron spin torque.

In Fig. 4.3 we show the dependence of the ratio of the switching current density without and with the magnon spin torques on tunnel resistance area product (RA) for $\theta = \pi/2$ (the angle between the magnetization directions of the two magnetic layers) at different interface exchange coupling strengths. We note that, in Fig. 4.3, all lines represent the exact same total torque $\tau_{\rm cr}$: as the resistance and the exchange coupling increase, the magnon spin torque increases, and thus the electric current needed to generate the same total torque reduces.

Clearly, a large tunnel resistance generates a larger magnon spin torque and therefore a thicker tunnel barrier is favored. A thick barrier thickness usually improves

the tunnel magnetoresistance. However, for device applications, the tunnel resistance has to match with other parts of the electronics and thus we cannot increase the resistance indefinitely.

4.5 Discussions and conclusions

The spin currents, or the angular momentum currents, of tunnel electrons and diffusive magnons, are not always additive. One may simply understand the relative sign of spin and magnon currents as follows. Consider the magnetization of two magnetic electrodes in parallel. If the majority electrons have a larger tunnel conductance than the minority electrons, the electron spin current would be additive to the magnon current, because the spin direction of magnons is always antiparallel to the majority electrons and the flow direction of magnons from asymmetric tunneling heating is opposite to the (spin) electron current. Thus, it is essential to choose a MTJ in which majority electron tunneling dominates.

We have shown in this paper that there is a theoretical possibility that an AFI-based MTJ could significantly reduce the critical current density compared to non-magnetic barrier based MTJ, particularly, the MgO based MTJ. The major challenge is to identify an AFI barrier that displays a large TMR and other technologically friendly parameters such as tunable tunnel resistance, favorable temperature and bias dependence of TMR, and high transparent AFI for magnons to propagate across. We recall that at the early stage of MTJ development, Ni/NiO/Co junction was reported to have small TMR at low temperature [134]. When the Al_2O_3-based MTJ with more than 10% room temperature TMR was discovered in 1995, many experimental groups were racing to find better MTJs with a larger TMR value. After the MgO-based MTJs were discovered in 2004, the search for new tunnel junctions was no longer interested in many groups. Research effort has been focused on optimizing MgO-based MTJs which become the exclusive material choice for all spintronics applications. This work illustrates a need for a completely different MTJ in which the barrier is an antiferromagnetic material. There are many classes of antiferromagnetic insulators

and the present work provides a strong motivation for experimental search of AFI-based MTJs.

Our simplified model illustrates the possible advantage of using AFI barrier based MTJs. However, there are a number of complications. As we have learned that a large TMR of MgO based MTJ has its origin in the electronic state matching between the MgO layer and the ferromagnetic electrodes for a particular spin channel [116] , it is unclear whether a particular AF material would also have this spin-dependent electronic state matching such that an extremely large TMR can be found. We also expect that the orientations of the crystalline and staggered magnetic moments would play an important role for both TMR and the spin/magnon transfer torques. In addition, our study completely ignores the influence of the inelastic scattering in the AFI barrier.

In conclusion, we have demonstrated theoretically that an AFI barrier based MTJ can achieve a much lower switching current density by "reuse" the wasted energy of tunnel electrons. The advantage of AFI over NM barrier is that the AFI barrier provides a magnon propagating gateway for additional spin transfer torques created by the tunnel electrons induced thermal gradient. If a proper AFI based MTJ is realized experimentally, one would generate a new perspective of lowering switching current density of spin transfer torque based MRAMs.

Chapter 5

Spin transport in non-collinear antiferromagnetic metals

5.1 Introduction

Antiferromagnets (AFMs) are of great interest for the study of spintronics recently [58, 59, 135, 136]. Most studies on spin transport phenomenon so far have focused on collinear AFMs, i.e., two magnetic sublattices have an opposite direction of magnetic moment. For example, the spin Seebeck [41, 111, 112, 133] and spin pumping effects [38, 137] in AFMs, the magnon transfer torque in FM/AFM/FM sandwich structure [47, 48] and spin Hall effect in AFMs [138, 139].

More recently, the non-collinear AFMs have shown qualitatively and quantitatively different transport properties compared to those of collinear AFMs. The non-collinear antiferromagnetic system Mn_3Z (Z = Sn, Ir, and Ge) has been found to have a strong anomalous Hall effect [4, 140–142] compared to ferromagnetic metals. The interfacial spin transfer between non-collinear AFMs and normal metals has been theoretically demonstrated [143]. In insulating non-collinear AFMs, studies have established the evidence of the thermal Hall effect [144, 145] , spin Seebeck and spin Nernst effects [146]. Also, the spin Hall and inverse spin Hall effects [147, 148] have been reported in Mn_3Sn, where previous research has focused mainly on non-magnetic heavy metals.

Both collinear and non-collinear AFMs have zero net magnetization without a

magnetic field. However, they fundamentally differ in the magnon spectra. For a collinear AFM, one may define a Néel vector, representing the difference between two antiparallel magnetic moments of two sublattices. The magnons, which are quasi-particles of the low-energy excitations, are then quantized in the direction parallel or antiparallel to the Néel vector, i.e., the magnon spectra have two doubly degenerated branches with each magnon's angular momentum either parallel or antiparallel to the Néel vector. In this case, the spin direction of the magnon is fixed by the Néel vector, independent of the momentum of the magnon.

For non-collinear AFMs, however, the Néel vector is ill-defined. We will show that each magnon is no longer an eigenstate of the spin angular momentum. The average value of the angular momentum for a given magnon depends on the momentum of the magnon. This spin-momentum locking of magnon is similar to the electron band with spin-orbit coupling in which the electron's spin is locked in the direction perpendicular to the electron momentum. In the non-collinear AFMs, the locking of magnon's spin and momentum is more complicated [149].

The above spin-momentum locking of magnons would strongly affect the electrical and magnetoelectrical transport properties of non-collinear antiferromagnetic metals. Magnons and conduction electrons are two main angular momentum carriers that determine the total spin current. Although an applied electric field only drives the charge current of the conduction electrons, the magnon current can be induced by electron-magnon scattering such that the electron transfers its momentum to the magnons, as demonstrated in Chap. 2. The resulting net momentum of magnons, along with the intrinsic angular momentum of each magnons, generates a magnon spin current.

In this chapter, we show that the novel types of magnon spin currents can be efficiently generated by purely electrical means in non-collinear AFMs. The paper is organized as follows. In Sec. 5.2, we propose a two-dimensional spin Hamiltonian of a kagome lattice with nearest antiferromagnetic exchange interaction, including a Dzyaloshinskii-Moriya interaction (DMI) interaction and on-site anisotropic term. We solve the magnon spectra of the Hamiltonian and determine the spin-momentum

locking pattern in momentum space. In Sec. 5.3, we propose an exchange Hamiltonian between the conduction electrons and local spins of the non-collinear AFMs and calculate the magnon spin current under external electric field. In Sec. 5.4, we discuss key results of this chapter.

5.2 Magnon bands and spin-momentum locking

We start with a two-dimensional (2D) kagome antiferromagnetic metal, consisting the unpolarized conduction electrons and local magnetic spins. The antiferromagnetic exchange coupling of the local spins yields classical spin-fluctuation ground state in which the spins in the three sublattices $\mathbf{S}_A$, $\mathbf{S}_B$ and $\mathbf{S}_C$, forming 120° angle to each other, as shown in Fig. 5.1(a). Note that the ground state is highly degenerate with a number of different spin configurations if the isotropic antiferromagnetic exchange coupling is the only spin Hamiltonian. To freeze the ground state spin configurations, we include two additional anisotropic terms to model the Hamiltonian [150–152],

$$\hat{H} = \sum_{\langle i,j \rangle} \left[J_{\text{ex}} \mathbf{S}_i \cdot \mathbf{S}_j + \mathbf{D}_{ij} \cdot \left(\mathbf{S}_i \times \mathbf{S}_j \right) \right] - K \sum_i \left(\mathbf{S}_i \cdot \mathbf{z}_i' \right)^2 \tag{5.1}$$

where $\langle i, j \rangle$ is the summation over nearest neighbors, $J_{\text{ex}} > 0$ is the antiferromagnetic Heisenberg exchange, $\mathbf{D}_{ij} = D_z \hat{\mathbf{z}}$ is the DMI which is assumed perpendicular to the 2D plane, K is the single-ion anisotropy with the anisotropic axis $\mathbf{z}_i'$ defined as the unit vector whose direction is parallel to the spin orientations of the frozen classical ground-state, see Fig. 5.1(a). Without these anisotropies, the theorem of Mermin and Wagner [153] would prevent the formation of the long range antiferromagnetic ordering. Throughout this paper, we have taken the anisotropic terms much smaller than the exchange energy. The other part of the Hamiltonian involves the interaction between conduction electrons and the local spins, which will be explicitly included when we discuss the magnon spin conductivity. In this Section, we shall determine the low-energy excitations from Eq. (5.1), i.e., the magnon dispersions or the magnon bands.

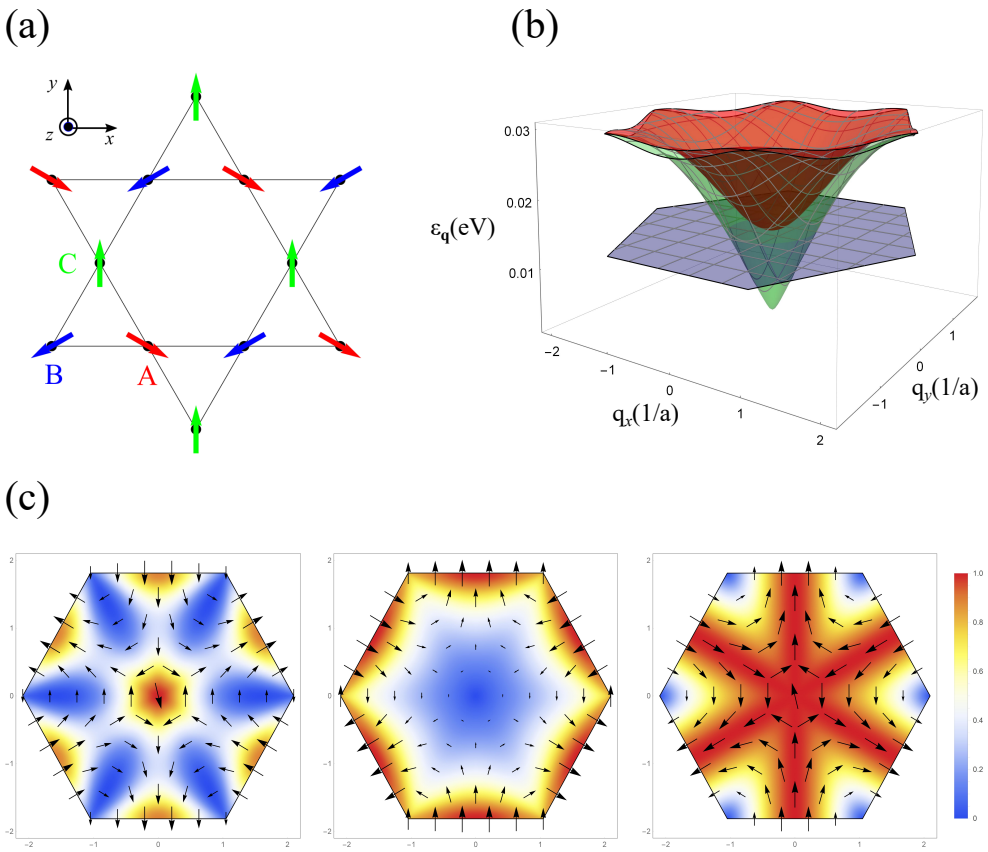

Figure 5.1: (a) The kagome antiferromagnetic lattice with three sublattices, labeled A, B and C. (b) The magnon dispersion relations in the first Brillouin zone. Here the parameters are such: $J_{\text{ex}} = 10$ meV, $D_z = 1/10 J_{\text{ex}}$ and $K = 1/1000 J_{\text{ex}}$. At small $\mathbf{q}$, the red band is quadratic, the green band is linear, and the blue band is finite and flat over the entire first Brillouin zone. Note the red band and blue band touch each other at $\mathbf{q} = 0$. (c) The $\mathbf{q}$ resolved magnon spins. From the left to right: red, green and blue bands. The arrows represent the direction of the magnon spins and the color represents the magnitude.

Following the conventional linear spin-wave approach, we introduce the Holstein-Primakoff (HP) transformation

$$\mathbf{S}_{i\alpha} = \mathbf{z}'_{i\alpha}(S - b^\dagger_{i\alpha} b_{i\alpha}) + \mathbf{x}'_{i\alpha}\sqrt{\frac{S}{2}}(b_{i\alpha} + b^\dagger_{i\alpha}) - \mathbf{y}'_{i\alpha} i\sqrt{\frac{S}{2}}(b_{i\alpha} - b^\dagger_{i\alpha}) \tag{5.2}$$

where S is the spin, $b_{i\alpha}^{\dagger}$ ($b_{i\alpha}$) is the magnon creation (annihilation) operator of the sublattice α ($\alpha = A, B, C$) at unit cell i, $\mathbf{x}'_{i\alpha}\mathbf{y}'_{i\alpha}\mathbf{z}'_{i\alpha}$ denotes the local Cartesian coordinate system. By replacing Eq. (5.2) into (5.1), and discarding terms with more than the second order in the HP bosons, we find, after Fourier transformation, the spin Hamiltonian can be written in a compact form,

$$\hat{H} = \sum_{\mathbf{q}} \begin{pmatrix} b_{\mathbf{q}}^{\dagger} & b_{-\mathbf{q}} \end{pmatrix} \cdot H(\mathbf{q}) \cdot \begin{pmatrix} b_{\mathbf{q}} \\ b_{-\mathbf{q}}^{\dagger} \end{pmatrix} \tag{5.3}$$

where $b_{\mathbf{q}}^{\dagger} = \begin{pmatrix} b_{A\mathbf{q}}^{\dagger} & b_{B\mathbf{q}}^{\dagger} & b_{C\mathbf{q}}^{\dagger} \end{pmatrix}$ and $H(\mathbf{q})$ is a 6×6 bosonic Bogoliubov–de Gennes matrix whose explicit expression is rather cumbersome, but it was straightforwardly obtained by simple but tedious algebra. To obtain the eigenenergies and eigenstates, we need to diagonalize the matrix $H(\mathbf{q})$. A standard procedure is to carry the Bogoliubov transformation, i.e.,

$$b_{\alpha\mathbf{q}} = \sum_{\nu} \left(M_{\nu\mathbf{q}}^{\alpha} b_{\nu\mathbf{q}} + N_{\nu\mathbf{q}}^{\alpha} b_{\nu-\mathbf{q}}^{\dagger} \right) \tag{5.4}$$

where $\nu = 1, 2, 3$ represents three band indices. By placing Eq. (5.4) into (5.3), and by utilizing the commutator properties of the boson operators, we numerically determine the transformation matrices $M_{\nu\mathbf{q}}^{\alpha}$ and $N_{\nu\mathbf{q}}^{\alpha}$ and obtain the diagonalized Hamiltonian,

$$\hat{H} = \sum_{\nu\mathbf{q}} \varepsilon_{\nu\mathbf{q}} b_{\nu\mathbf{q}}^{\dagger} b_{\nu\mathbf{q}} \tag{5.5}$$

where $\varepsilon_{\nu\mathbf{q}}$ is the magnon dispersion relation. The three magnon dispersions in the first Brillouin zone are shown in Fig. 5.1(b) where three branches of the magnons color codes with red, green and blue. Interestingly, for small wave number $\mathbf{q}$, the red band is quadratic, the green band is linear, and the blue is a flat band with finite energy. Note that the Goldstone mode, which is the zero energy mode of bosons, does not show up in the magnon bands here since we introduce an anisotropy in Eq. (5.1), i.e., the magnons are gapped at $\mathbf{q} = 0$ for the green band.

In collinear AFMs, two band indices represent the magnon spin state, i.e., the

magnon in one band has the angular momentum parallel to the Néel vector and in the other band, antiparallel to the Néel vector. In the present case, the transformation to diagonalize the matrix $H(\mathbf{q})$, Eq. (5.4), mixes spin states in three sublattices. Consequently, the magnons in three bands are no longer an eigenstate of the angular momentum. To determine the angular momentum transfer between conduction electrons and magnons in the next Section, we define the spin of a magnon by its average value of all spins,

$$\mathbf{S}_{\nu\mathbf{q}} = \langle \nu\mathbf{q}| \sum_{i\alpha} \mathbf{S}_{i\alpha} |\nu\mathbf{q}\rangle \tag{5.6}$$

where $|\nu\mathbf{q}\rangle$ is the wavefunction of the magnon. In Fig. 5.1(c) we show the $\mathbf{q}$-dependent magnon spin for the three bands. For a given magnon $b^\dagger_{\nu\mathbf{q}}$, its spin direction is uniquely defined. We shall emphasize that the spin-momentum locking for magnons differs from that for conventional conduction electrons in two aspects: 1) The electron spins are usually locked in the directions perpendicular or parallel to the momentum, while the magnon spins have a wide range of angle distribution relative to the magnon momentum, and 2) Both spin and momentum are good quantum numbers (eigenstate) for conduction electrons in spin-orbit coupled system, while for non-collinear antiferromagnetic magnons, only momentum, but not spin, is the good quantum number. Consequently, the magnitude of the spin for different magnons is different and is no longer quantized as well, as illustrated in Fig. 5.1(c).

5.3 Electron-magnon scattering and magnon spin conductivity

To study the roles of above magnons in charge and spin transport, we consider the conduction electrons interacting with magnons via $s-d$ exchange coupling given below,

$$\hat{H}_{\rm sd} = -J_{\rm sd} \sum_{i\alpha} \boldsymbol{\sigma}_{i\alpha} \cdot \mathbf{S}_{i\alpha} \tag{5.7}$$

where $J_{\rm sd}$ is the $s-d$ exchange coupling, $\boldsymbol{\sigma}$ is the electron spin, index i and α are similarly defined as previous. The second quantized form of electron-magnon coupling

can be further derived as [143]

$$\hat{H}_{\rm sd} = \sum_{\sigma\sigma'\nu\mathbf{q}\mathbf{k}} \sum_{n=1}^{3} \left[V_{\nu\mathbf{q}}^{(n)} b_{\nu\mathbf{q}}^{\dagger} c_{\mathbf{k}-\mathbf{q}\sigma'}^{\dagger} L_{\sigma'\sigma}^{(n)} c_{\mathbf{k}\sigma} + \text{H.c} \right] \tag{5.8}$$

where $c_{\mathbf{k}}^{\dagger}$ ($c_{\mathbf{k}}$) is the electron creation (annihilation) operator,

$$L_{\sigma'\sigma} = \{\sigma^{+} + \sigma^{-}, \sigma^{+} - \sigma^{-}, 2\sigma^{z}\} \tag{5.9}$$

and the coupling strength is

$$V_{\nu\mathbf{q}}^{(n)} = -\sqrt{2S} J_{\rm sd} \sum_{\alpha} e^{i\mathbf{q}\cdot\boldsymbol{\delta}_{\alpha}} \times \left(f_{n\alpha}^{*} M_{\nu\mathbf{q}}^{\alpha} + f_{n\alpha} N_{\nu-\mathbf{q}}^{\alpha} \right) \tag{5.10}$$

with $\boldsymbol{\delta}_{\alpha}$ is the position of the αth site within the unit cell, $f_{1\alpha} = \sin\theta_{\alpha}$, $f_{2\alpha} = i\cos\theta_{\alpha}$, $f_{3\alpha} = 2i$ and θ_{α} is the angle of the classical orientation of the αth site spin in global frame of reference.

Magnons are quasiparticles without electric charges and thus an applied electric field can not directly drive magnon current. We have shown previously that the magnons can obtain its spin current in two essential ways – spin transfer and momentum transfer from conduction electrons to magnons in Chap. 2. As in the case of ferromagnetic metals, the electrons are spin polarized and thus there is always a magnon spin current in addition to the electron spin current. If the conduction electron is not spin polarized, e.g., a collinear antiferromagnetic metal, the electron-magnon scattering would not lead to magnon spin current since the magnon momentum is independent of the spin and thus the sum over two degenerate magnon modes remains zero. In the present case, however, the spin and the momentum of magnons in the non-collinear AFMs are locked and therefore, the transferred momentum from the conduction electrons could generate magnon spin current. More quantitatively, we use Boltzmann transport formalism of the electrons and magnons to estimate the induced magnon spin current under external electric field. We assume that the charge current is spin-unpolarized for simplicity so that we discard the spin angular momentum transfer.

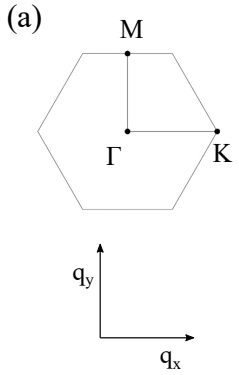

(b)

$$\sigma^i_{jx} = \begin{pmatrix} 0 & \sigma^x_{yx} \\ \sigma^y_{xx} & 0 \end{pmatrix}$$

$$\sigma^i_{jy} = \begin{pmatrix} \sigma^x_{xy} & 0 \\ 0 & -\sigma^y_{yy} \end{pmatrix}$$

Figure 5.2: (a) First Brillouin zone of the kagome AFM. Two high-symmetry axes are indicated with ΓK and ΓM. (b) The symmetry determined magnon spin conductivity tensor for ΓK and ΓM direction. The tensor $(\sigma_m)^i_{jx}$ is off-diagonal while $(\sigma_m)^i_{jy}$ is diagonal.

We start with the magnon Boltzmann equation

$$0 = -\frac{N_\nu(\mathbf{q}) - N^0_\nu(\mathbf{q})}{\tau_\nu} + \left(\frac{\partial N_\nu(\mathbf{q})}{\partial t}\right)_{\text{sd}} \tag{5.11}$$

where $N_\nu(\mathbf{q})$ is magnon distribution function, τ_ν is the magnon relaxation time due to lattice and $\left(\frac{\partial N_\nu(\mathbf{q})}{\partial t}\right)_{\text{sd}}$ is the electron-magnon scattering term which provides the nonequilibrium magnon distribution.

We separate the magnon distribution function into equilibrium and nonequilibrium parts

$$N_\nu(\mathbf{q}) = N^0_\nu(\mathbf{q}) + \frac{\partial N^0_\nu}{\partial \varepsilon_{\nu\mathbf{q}}} g_\nu(\mathbf{q}) \tag{5.12}$$

where $g_\nu(\mathbf{q})$ is the nonequilibrium part that is going to be solved.

The electron-magnon scattering term is calculated via Fermi-Golden rule

$$\left(\frac{\partial N_\nu(\mathbf{q})}{\partial t}\right)_{\text{sd}} = W_{\nu\mathbf{q}} \sum_{\mathbf{k}} \delta\left(\epsilon_{\mathbf{k}+\mathbf{q}} - \epsilon_{\mathbf{k}} - \varepsilon_{\nu\mathbf{q}}\right) \tag{5.13}$$

$$\times \{[N_\nu(\mathbf{q}) + 1][1 - f(\mathbf{k})] f(\mathbf{k}+\mathbf{q}) \tag{5.14}$$

$$- N_\nu(\mathbf{q})[1 - f(\mathbf{k}+\mathbf{q})] f(\mathbf{k})\} \tag{5.15}$$

where $f(\mathbf{k})$ is the electron distribution function, and the scattering magnitude is

$$W_{\nu\mathbf{q}} = \frac{\pi}{\hbar}\sum_{n=1}^{3}\left|V_{\nu\mathbf{q}}^{(n)}\right|^2 \tag{5.16}$$

The electron distribution satisfies the Boltzmann equation in which the scattering terms include the electron-magnon scattering and other scattering contribution such as impurities and phonons. In principle, one needs to self-consistently determine $f(\mathbf{k})$ along with the magnon distribution. However, we will take a simplified approach by assuming one single relaxation time τ_e as a parameter to represent all scattering,

$$f(\mathbf{k}) = f^0(\mathbf{k}) - \frac{\partial f^0}{\partial \varepsilon_{\mathbf{k}}}\frac{e\hbar\tau_e}{m}\left(\mathbf{E}\cdot\mathbf{k}\right) \tag{5.17}$$

where e is the electorn charge, m is the electron mass, $\varepsilon_{\mathbf{k}}$ is the electron energy and $\mathbf{E}$ is the electric field. There are a number of justifications for our approximations. First, the effect of the electron-magnon scattering may not be more important for the conduction electrons comparing to other sources of scattering. Second, our essential focus is to study the magnon spin current rather than electron spin current which have been studied extensively earlier. Third, the simple electron distribution allows us to reduce the mathematical complication in obtaining the magnon spin current.

By placing the electron distribution, Eq. (5.17) into the magnon's Boltzmann function, Eq. (5.11), we find the nonequilibrium part of magnons is

$$g_\nu(\mathbf{q}) = -\frac{1}{\left(1+\frac{\tau_\nu^{\mathrm{em}}(\mathbf{q})}{\tau_\nu}\right)}\frac{e\hbar\tau_e}{m}\left(\mathbf{E}\cdot\mathbf{q}\right) \tag{5.18}$$

where the momentum resolved electron-magnon relaxation time for magnons is calculated as

$$\tau_\nu^{\mathrm{em}}(\mathbf{q}) = \frac{N_\nu^0(\mathbf{q})\left[N_\nu^0(\mathbf{q})+1\right]}{W_{\nu\mathbf{q}}\Gamma_{\nu\mathbf{q}}} \tag{5.19}$$

with

$$\Gamma_{\nu\mathbf{q}} = \sum_{\mathbf{k}} N_\nu^0(\mathbf{q}) \left[1 - f^0(\mathbf{k}+\mathbf{q})\right] f^0(\mathbf{k}) \\ \delta\left(\varepsilon_{\mathbf{k}+\mathbf{q}} - \varepsilon_{\mathbf{k}} - \varepsilon_{\nu\mathbf{q}}\right)$$

The magnon spin current is then,

$$(J_m)_j^i = \sum_{\nu\mathbf{q}} \frac{\partial N_\nu^0}{\partial \varepsilon_{\nu\mathbf{q}}} g_\nu(\mathbf{q}) v_{\nu\mathbf{q}}^j S_{\nu\mathbf{q}}^i \tag{5.20}$$

$$\equiv (\sigma_m)_{jk}^i E_k \tag{5.21}$$

where i (j) stands for the polarization (flow) direction of magnon spin current, k is the electric field direction, v is the magnon velocity and σ_m is the magnon spin conductivity (similar defined as electron spin conductivity).

Since the spin-momentum locking is complex, an electric field applied in an arbitrary direction relative to the crystal structure would generate unpredictable magnon spin current. We choose to apply the electric field in two high-symmetry axes, ΓK ($\mathbf{x}$) and ΓM ($\mathbf{y}$), as shown in Fig. 5.2(a). In both cases, the magnon spin current contains longitudinal and transverse parts, that the magnon current flowing parallel and perpendicular to the electric field direction. But they differ fundamentally in the polarization of magnon spin current, due to the different magnon spin-momentum locking along these two axes, as can be seen from Fig. 5.1(c).

For ΓK axis, the magnon spin is always perpendicular to the momentum, while for ΓM axis, they are parallel. Therefore with the electric field applied in the ΓK direction, the magnon spin conductivity tensor has off-diagonal terms, which means that the magnon spin current flowing in the $\mathbf{x}$ direction is polarized in the $\mathbf{y}$ direction (σ_{xx}^y),while for the flowing direction assumed in the $\mathbf{y}$ direction the magnon spin current is polarized in the $\mathbf{x}$ direction (σ_{yx}^x). As for the situation where the field is applied in the ΓM direction, the polarization of the magnon spin current is always in the same direction as the flow direction. In other words, the magnon spin conductivity tensor is diagonal with σ_{xy}^x and σ_{yy}^y components. This symmetry restricted behavior

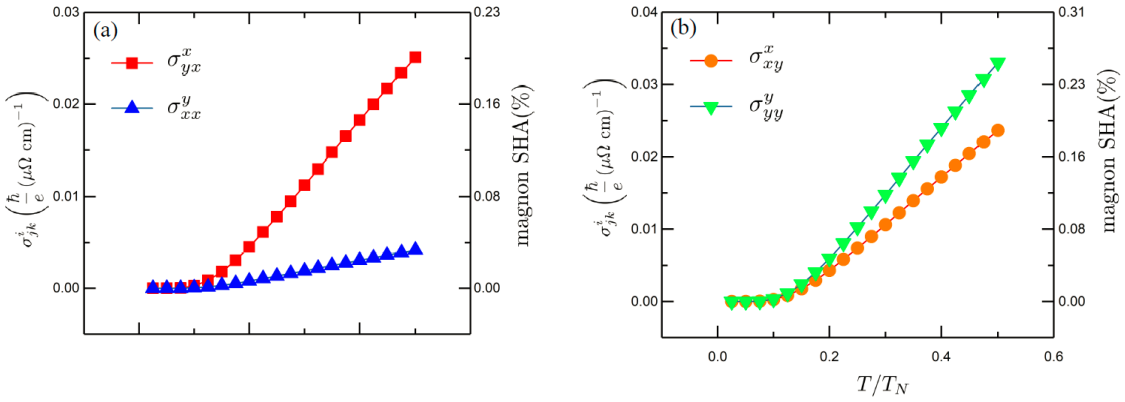

Figure 5.3: Temperature dependence of magnon spin conductivity and magnon SHA for charge current flowing in ΓK (a) or ΓM (b) direction. Material parameters are such: electric resistivity for electron $\rho_e = 320$ μΩ cm [4], $J_{\mathrm{sd}} = 1$ meV, $\tau_\nu = 10^{-6}$ s, Néel temperature $T_{\mathrm{N}} = 420$ K.

of the magnon spin conductivity tensor also has been found in spin-polarized charge current in such system [154]. This unique anisotropic magnon spin current makes non-collinear AFM a more interesting system in the study of charge-spin conversion in zero magnetic field as compared to usual spin-orbit coupling induced phenomena.

One of the major differences between electron spin current and magnon spin current is that the latter is highly temperature dependent. Two major reasons make the temperature essential: the number of magnons increase with the temperature, and the electron-magnon scattering involves inelastic processes that require the thermal energy to be effective. Mathematically, the temperature appears in the equilibrium magnon number, Eq. (5.12) and the scattering term, Eq. (5.15). In addition to the magnon spin conductivity, we further define mangon spin Hall angle (SHA) as $(e/\hbar)\left((\sigma_m)^i_{jk} / (\sigma_e)_{kk}\right)$ where σ_e is the electron electric conductivity, to compare the electric field driven magnon spin current in non-collinear antiferromagnetic metals to the conventional spin Hall effect in non-magnetic metals. We show the magnon spin conductivity and magnon SHA as function of temperature in Fig. 5.3 with field applied either in ΓK (5.3(a)) or ΓM (5.3(b)) direction. Both longitudinal and transverse magnon spin conductivities vanish at low temperatures.

5.4 Discussions and conclusions

In a non-magnetic or collinear antiferromagnetic metal, one would think that the spin current only exists through the spin Hall effect in which the spin-orbit coupling is required. We show in the chapter that the magnon spin current in a non-collinear antiferromagnetic metal is naturally present even though there is no net magnetization and there is no external spin current injection into the AFM.

Two essential mechanisms are responsible for the magnon spin current: the magnon spectra have spin-momentum locking characteristics, and the electron-magnon scattering transfers momentum from conduction electrons to the magnons. Due to complex spin-momentum locking patterns, the resulting magnon spin current tensor is rather difficulty to predict for an applied electric field in an arbitrary direction relative to the lattice orientation. In the case of the electric field applied in the direction with the high symmetric point, K and M, the direction of the magnon spin current could be immediately determined by symmetry analysis.

Another method to generate the magnon spin current is to use thermal gradient. In a collinear AFM, the thermal gradient would not generate any net magnon spin current because the thermal gradient leads to a net magnon momentum and since there is no spin-momentum dependence, the resulting sum over the spin of the degenerated magnons remain zero. The same argument in the last paragraph would lead to a magnon spin current in non-collinear AFMs, which is recently demonstrated as the spin-Seebeck effect of magnons in such system [146].

Magnon spin current may not be directly measurable in the bulk films. As in the measurement for the electron spin current, one needs an additional contact layers that may support magnon accumulation or give rise a magnetic torque. The detailed discussion on the possible realization of the magnon spin torques is beyond the scope of the present paper.

Appendix A

Derivation of electron and magnon currents in magnetic heterostructure

A.1 Spin-magnon diffusion equations and extended Ohm's law

In this Appendix, we specify approximations and calculations leading to Eqs. (2.10) and (2.11). As shown in [49], a key approximation to obtain a closed form for the macroscopic diffusion equations is to expand the nonequilibrium distribution functions into polynomial series P_n, namely,

$$\begin{aligned} g_\sigma(z,\mathbf{k}) &= \sum_n g^{(n)}(z,k)P_n(k_z/k) \\ g_m(z,\mathbf{q}) &= \sum_n g_m^{(n)}(z,k)P_n(q_z/q) \end{aligned} \tag{A.1}$$

, and only keeping the lowest order in expansion ($n = 1$). In the same limiting cases, such approximations are justifiable [49, 88]. By summing over $\mathbf{k}$ in Eq. (2.3) for each spin channel, and by summing over $\mathbf{q}$ in Eq.(2.7), we find, after tedious but stranghtforward calculations,

$$\frac{d}{dz}\begin{pmatrix} j_s(z) \\ j_m(z) \end{pmatrix} = -\begin{pmatrix} \tau_{11}^{-1} & \tau_{12}^{-1} \\ \tau_{21}^{-1} & \tau_{22}^{-1} \end{pmatrix}\begin{pmatrix} \delta n_s(z) \\ \delta n_m(z) \end{pmatrix} \tag{A.2}$$

where the off-diagonal matrix elements of Eq. (A.2) depend on the coupling between spin and magnon and density of states of both quasiparticles. At a temperature much lower than the Curie temperature, the expression reduces to

$$\tau_{12}^{-1} = \left(\frac{J_{sd}}{k_B T_F}\right)^2 \frac{k_B T}{\hbar} \left(\frac{T_C}{T}\right)^{1/2} S\alpha_1 \tag{A.3a}$$

$$\tau_{21}^{-1} = \left(\frac{J_{sd}}{k_B T_C}\right)^2 \frac{k_B T_C}{\hbar} \left(\frac{T}{T_F}\right)^{1/2} S\alpha_2 \tag{A.3b}$$

where α_1 and α_2 are numerical constants. The diagonal parts of the matrix elements are

$$\tau_{11}^{-1} = 2\left(\tau_{\uparrow\downarrow}^{-1} + \tau_{21}^{-1}\right) \tag{A.4a}$$

$$\tau_{22}^{-1} = \left(\tau_{th}^{-1} + \frac{1}{2}\tau_{12}^{-1}\right). \tag{A.4b}$$

Next, we multiply v_{k_z} on both sides of Eq.(2.3) and v_{q_z} on both sides of Eq.(2.7) and sum over momentum, and we find

$$\frac{d}{dz}\begin{pmatrix}\delta n_s(z)\\ \delta n_m(z)\end{pmatrix} = \begin{pmatrix}\zeta_1\\ \zeta_2\end{pmatrix} j_e - \begin{pmatrix}\zeta_{11} & \zeta_{12}\\ \zeta_{21} & \zeta_{22}\end{pmatrix}\begin{pmatrix} j_s(z)\\ j_m(z)\end{pmatrix} \tag{A.5}$$

where

$$\zeta_1 = \frac{3}{v_F^2}\left(P_0\tau_e^{-1} + \tau_{em}^{-1}\right), \qquad \zeta_2 = \frac{1}{2I_m}\tau_{em}^{-1}$$

$$\zeta_{11} = \frac{3}{v_F^2}\left(\tau_e^{-1} + \tau_{em}^{-1}\frac{T_F}{T}\right), \qquad \zeta_{22} = \frac{1}{I_m}\left(\tau_m^{-1} + \tau_{me}^{-1}\right)$$

$$\zeta_{12} = \frac{3}{v_F^2}\tau_{me}^{-1}, \qquad \zeta_{21} = \frac{1}{2I_m}\tau_{em}^{-1}\frac{T_C}{T_F}$$

with

$$\tau_{em}^{-1} = \frac{J_{sd}^2}{\hbar\left(k_B T_C\right)}\left(\frac{T}{T_F}\right)^{1/2} S\alpha_3$$
$$\tau_{me}^{-1} = \frac{J_{sd}^2}{\hbar\left(k_B T_F\right)}\left(\frac{T T_C}{T_F^2}\right)^{1/2} S\alpha_4$$

and v_F is Fermi velocity, the integral is defined as

$$I_m = \int d\mathbf{q}\left(-\partial N_m^0/\partial\varepsilon_{\mathbf{q}}^m\right) / \int d\mathbf{q}\left(-\partial N_m^0/\partial\varepsilon_{\mathbf{q}}^m\right) v_{q_z}^2,$$

α_3 and α_4 are other two numerical constants. From these four equations above, we could easily arrive at the spin-magnon diffusion equations (2.10) and the extended Ohm's law, Eq. (2.11) in the main text. The explicit form of the four length scales in Eq. (2.10) are

$$\lambda_s^{-2} = \zeta_{11}\tau_{11}^{-1}$$
$$\lambda_m^{-2} = \zeta_{22}\tau_{22}^{-1}$$
$$\lambda_{sm}^{-2} = \zeta_{11}\tau_{12}^{-1} + \zeta_{12}\tau_{22}^{-1}$$
$$\lambda_{ms}^{-2} = \zeta_{21}2\tau_{11}^{-1} + \zeta_{22}\tau_{21}^{-1}$$

and the coefficients in extended Ohm's law are

$$
\begin{aligned}
P_s &= \frac{P_0}{1+\chi_s} + \frac{1}{(1+\chi_s)(1+\chi_m)}\frac{\tau_e}{\tau_{em}} \\
P_m &= \frac{1}{2}\frac{1}{(1+\chi_m)}\frac{\tau_m}{\tau_{em}}\left[1 - \frac{P_0}{(1+\chi_s)}\frac{T_C}{T_F}\right] \\
\sigma_s &= \frac{\sigma_s^0}{(1+\chi_s)} \\
\sigma_m &= \frac{\sigma_m^0}{(1+\chi_m)} \\
\sigma_{ms} &= \frac{2}{(1+\chi_s)(1+\chi_m)}\frac{\tau_e}{\tau_{me}}\sigma_m^0 \\
\sigma_{sm} &= \frac{1}{(1+\chi_s)(1+\chi_m)}\frac{\tau_m}{\tau_{em}}\frac{T_F}{T_C}\frac{\sigma_s^0}{2}
\end{aligned}
$$

where

$$
\begin{aligned}
\chi_s &= \frac{\tau_e}{\tau_{em}}\frac{T_F}{T} \\
\chi_m &= \frac{\tau_m}{\tau_{me}}
\end{aligned}
$$

are unitless quantities, which characterize the relative strength of spin-magnon coupling in momentum scattering relaxation time (both proportional to J_{sd}^2 and also temperature dependent), $\sigma_s^0 = 2\tau_e v_F^2/3$ and $\sigma_m^0 = \tau_m I_m$ are electron spin conductivity and the magnon conductivity without considering coupling.

A.2 Characteristic lengths and boundary conditions

The decay length associated with the diffusion equation, Eq. (2.10), can be readily obtained by taking the electron spin and magnon accumulations in the form of $\exp(\pm z/\lambda)$ such that λ satisfies the eigenequations,

$$
\lambda^{-2}\begin{pmatrix}\delta n_s(z)\\ \delta n_m(z)\end{pmatrix} = \begin{pmatrix}\lambda_s^{-2} & \lambda_{sm}^{-2}\\ \lambda_{ms}^{-2} & \lambda_m^{-2}\end{pmatrix}\begin{pmatrix}\delta n_s(z)\\ \delta n_m(z)\end{pmatrix} \tag{A.6}
$$

the nonzero solutions for δn_s and δn_m lead to two new characteristic lengths in Eq. (2.14). If the coupling (J_{sd}) is 0, $\lambda_\pm$ reduces to the original spin diffusion length $\lambda_s^0 = \sqrt{v_F^2 \tau_e \tau_{\uparrow\downarrow}/3}$ and magnon diffusion length $\lambda_m^0 = \sqrt{I_m \tau_m \tau_{th}}$.

In a ferromagnetic bilayer with magnetization antiparallel aligned, we take the perfect interface condition as

$$\delta n_m\left(0^-\right) = \delta n_m\left(0^+\right) \tag{A.7a}$$
$$\delta n_s\left(0^-\right) = \delta n_s\left(0^+\right) \tag{A.7b}$$
$$j_s\left(0^-\right) = j_s\left(0^+\right) \tag{A.7c}$$
$$j_m\left(0^-\right) = j_m\left(0^+\right) \tag{A.7d}$$

and the general solution of accumulation functions are such

$$\delta n_s(z) = A_L \exp\left(\frac{z}{\lambda_+}\right) + B_L \exp\left(\frac{z}{\lambda_-}\right) \tag{A.8a}$$
$$\delta n_m(z) = \alpha A_L \exp\left(\frac{z}{\lambda_+}\right) + \beta B_L \exp\left(\frac{z}{\lambda_-}\right) \tag{A.8b}$$

for $z < 0$ and

$$\delta n_s\left(z\right) = A_R \exp\left(-\frac{z}{\lambda_+}\right) + B_R \exp\left(-\frac{z}{\lambda_-}\right) \tag{A.9a}$$
$$\delta n_m\left(z\right) = \alpha A_R \exp\left(-\frac{z}{\lambda_+}\right) + \beta B_R \exp\left(-\frac{z}{\lambda_-}\right) \tag{A.9b}$$

for $z < 0$, where

$$\alpha = \lambda_{sm}^2\left(\lambda_+^{-2} - \lambda_s^{-2}\right)$$
$$\beta = \lambda_{sm}^2\left(\lambda_-^{-2} - \lambda_s^{-2}\right)$$

The coefficients could be obtained by matching the boundary conditions

$$A_L = A_R = \lambda_+ j_e \frac{P_s\left(\sigma_{sm} - \beta\sigma_m\right) + P_m\left(\sigma_s - \beta\sigma_{ms}\right)}{\left(\alpha - \beta\right)\sigma_s\sigma_m} \tag{A.10a}$$

$$B_L = B_R = -\lambda_- j_e \frac{P_m\left(\sigma_s - \alpha\sigma_{ms}\right) + P_s\left(\sigma_{sm} - \alpha\sigma_m\right)}{\left(\alpha - \beta\right)\sigma_s\sigma_m} \tag{A.10b}$$

then the magnon accumulation, spin current and magnon current would be further determined.

From the Boltzmann equations we could also get an expression for electron current j_e as a total derivative with respect to electron accumulation $\delta n_e(z)$ (which proportional to the summation of electrochemical potentials of two spins), spin accumulation $\delta n_s(z)$ and magnon accumulation $\delta n_m(z)$

$$j_e = \frac{d}{dz}\left[\sigma_e \delta n_e(z) + \sigma_{se}\delta n_s(z) + \sigma_{me}\delta n_m(z)\right] \tag{A.11}$$

By using the continuity requirement of charge current across the interface, we find the magnetoresistance would be

$$\begin{aligned} \delta R &= \frac{\sigma_{se}}{\sigma_e}\left(A_L + B_L\right) + \frac{\sigma_{me}}{\sigma_e}\left(\alpha A_L + \beta B_L\right) \\ &\approx \frac{P_0}{1+\chi_s}\left(A_L + B_L\right) + \frac{1}{1+\chi_m}\left(\alpha A_L + \beta B_L\right) \end{aligned} \tag{A.12}$$

The first term means the magnetoresistance would be largely reduced because both spin polarization and accumulation at the interface would be smaller than the case without coupling, and the second term is a high-order effect coming from the magnon accumulation, which would in turn convert back into electron spin accumulation.

Appendix B

Derivation of the interfacial magnon spin conductance

Consider the exchange interaction at the interface of antiferromagnet and ferromagnet. The Hamiltonian between two spins would be simply,

$$H_{\text{int}} = -J_{\text{int}} \sum_i \mathbf{S}_{i,\text{F}} \cdot \mathbf{S}_{i,a} - J_{\text{int}} \sum_i \mathbf{S}_{i,\text{F}} \cdot \mathbf{S}_{i,b} \tag{B.1}$$

where $\mathbf{S}_{i,\text{F}}$ represents the ferromagnetic spin and $\mathbf{S}_{i,a(b)}$ is the spin of the two sublattices of collinear antiferromagnet.

We choose plane normal as x axis and the easy axis of FM as along z axis. We assume the easy axis of AFI is in y-z plane but having an angle of to z. Therefore we have the spin rotation as

$$S^x_{i,a(b)} = S^{x'}_{i,a(b)} \tag{B.2a}$$

$$S^y_{i,a(b)} = S^{y'}_{i,a(b)} \hat{\mathbf{n}} \cdot \hat{\mathbf{M}}_{\text{F}} - S^{z'}_{i,a(b)} \hat{\mathbf{n}} \times \hat{\mathbf{M}}_{\text{F}} \tag{B.2b}$$

$$S^z_{i,a(b)} = S^{y'}_{i,a(b)} \hat{\mathbf{n}} \times \hat{\mathbf{M}}_{\text{F}} + S^{z'}_{i,a(b)} \hat{\mathbf{n}} \cdot \hat{\mathbf{M}}_{\text{F}} \tag{B.2c}$$

where $\mathbf{n}$ is the Néel order of AFI, $\hat{\mathbf{M}}_{\text{F}}$ is the magnetization of FM, $x'y'z'$ is the local coordinate of AFI and the easy axis of AF is along z' axis.

We first apply transformation that relate the components of the local spin opera-

tors to the creation and annihilation operators of spin deviations,

$$\begin{aligned} H_{\rm int} = & -\frac{J_{\rm int}}{4}\sum_i \Big(S^\dagger_{i,\rm F}S^\dagger_{i,a(b)} + S_{i,\rm F}S_{i,a(b)}\Big)(1-\hat{\mathbf{n}}\cdot\hat{\mathbf{M}}_{\rm F}) \\ & + \Big(S^\dagger_{i,\rm F}S_{i,a(b)} + S_{i,\rm F}S^\dagger_{i,a(b)}\Big)(1+\hat{\mathbf{n}}\cdot\hat{\mathbf{M}}_{\rm F}) + S^z_{i,\rm F}S^{z'}_{i,a(b)}\hat{\mathbf{n}}\cdot\hat{\mathbf{M}}_{\rm F} \\ & + \frac{2}{i}\Big[S^z_{i,\rm F}\Big(S^\dagger_{i,a(b)} - S_{i,a(b)}\Big) - \Big(S^\dagger_{i,\rm F} - S_{i,\rm F}\Big)S^{z'}_{i,a(b)}\Big]\hat{\mathbf{n}}\times\hat{\mathbf{M}}_{\rm F} \end{aligned} \tag{B.3}$$

Within the spin wave approximation, one can express such exchange interaction in terms of boson operators that create or destroy magnons,

$$\begin{aligned} H_{\rm int} = & \frac{-J_{\rm int}}{2}\sum_i \sqrt{S_{\rm F}S_{\rm AF}}\Big\{[A_i(a_i+b^\dagger_i)+{\rm H.c.}](1-\hat{\mathbf{n}}\cdot\hat{\mathbf{M}}_{\rm F}) \\ & + [A_i(a^\dagger_i+b_i)+{\rm H.c.}](1+\hat{\mathbf{n}}\cdot\hat{\mathbf{M}}_{\rm F})\Big\} \\ & - (S_{\rm F}-A^\dagger_iA_i)(a^\dagger_ia_i - b^\dagger_ib_i)\hat{\mathbf{n}}\cdot\hat{\mathbf{M}}_{\rm F} \\ & + \frac{\sqrt{2}}{i}\Big\{\sqrt{S_{\rm F}}(A_i-A^\dagger_i)(a^\dagger_ia_i - b^\dagger_ib_i) \\ & + \sqrt{S_{\rm AF}}[(S_{\rm F}-A^\dagger_iA_i)(a_i+b^\dagger_i-{\rm H.c.})]\Big\}\hat{\mathbf{n}}\times\hat{\mathbf{M}}_{\rm F} \end{aligned} \tag{B.4}$$

where we have used the Holstein-Primakoff transformation in linear approximation: $S^\dagger_{i,\rm F} = \sqrt{2S_{\rm F}}A_i$, $S^z_{i,\rm F} = S_{\rm F} - A^\dagger_iA_i$ for FM and $S^\dagger_{i,a} = \sqrt{2S_{\rm AF}}a_i$, $S^{z'}_{i,a} = S_{\rm AF} - a^\dagger_ia_i$, $S^\dagger_{i,b} = \sqrt{2S_{\rm AF}}b^\dagger_i$, $S^{z'}_{i,b} = -S_{\rm AF} + b^\dagger_ib_i$. The creation ($A^\dagger_i$, $a^\dagger_i$ and $b^\dagger_i$) and destruction ((A_i, a_i and b_i) operators for spin deviations satisfy the common boson commutation rules.

We proceed by introducing the Fourier transform of the collective boson operators

$$A_i = \frac{1}{\sqrt{N}} \sum_{\mathbf{k}} e^{-i\mathbf{q}\cdot\mathbf{R}_i} A_{\mathbf{q}} \tag{B.5a}$$

$$A_i^\dagger = \frac{1}{\sqrt{N}} \sum_{\mathbf{k}} e^{i\mathbf{q}\cdot\mathbf{R}_i} A_{\mathbf{q}}^\dagger \tag{B.5b}$$

$$a_i = \frac{1}{\sqrt{N}} \sum_{\mathbf{k}} e^{-i\mathbf{q}\cdot\mathbf{R}_i} a_{\mathbf{q}} \tag{B.5c}$$

$$b_i = \frac{1}{\sqrt{N}} \sum_{\mathbf{k}} e^{-i\mathbf{q}\cdot\mathbf{R}_i} b_{\mathbf{q}} \tag{B.5d}$$

$$a_i^\dagger = \frac{1}{\sqrt{N}} \sum_{\mathbf{k}} e^{i\mathbf{q}\cdot\mathbf{R}_i} a_{\mathbf{q}}^\dagger \tag{B.5e}$$

$$b_i^\dagger = \frac{1}{\sqrt{N}} \sum_{\mathbf{k}} e^{i\mathbf{q}\cdot\mathbf{R}_i} b_{\mathbf{q}}^\dagger \tag{B.5f}$$

and the diagonalization of the quadratic part of the AF Hamiltonian

$$a_{\mathbf{q}} = u_{\mathbf{q}}\alpha_{\mathbf{q}} - v_{\mathbf{q}}\beta_{-\mathbf{q}}^\dagger \tag{B.6a}$$

$$b_{\mathbf{q}}^\dagger = -v_{-\mathbf{q}}\alpha_{-\mathbf{q}} + u_{-\mathbf{q}}\beta_{\mathbf{q}}^\dagger \tag{B.6b}$$

$$a_{\mathbf{q}}^\dagger = u_{\mathbf{q}}\alpha_{\mathbf{q}}^\dagger - v_{\mathbf{q}}\beta_{-\mathbf{q}} \tag{B.6c}$$

$$b_{\mathbf{q}} = -v_{-\mathbf{q}}\alpha_{-\mathbf{q}}^\dagger + u_{-\mathbf{q}}\beta_{\mathbf{q}} \tag{B.6d}$$

where N is the number of spins and the coefficients satisfies $u_{\mathbf{q}}^2 - v_{\mathbf{q}}^2 = 1$.

Therefore, the second quantization of the interfacial Hamiltonian is

$$\begin{aligned} H_{\text{int}} = &-J_{\text{int}} \sum_{\mathbf{kq}} (S_{\text{F}} S_{\text{AF}})^{1/2} \\ &\left[C_{\mathbf{q}} A_{\mathbf{k}} \alpha_{\mathbf{q}}^\dagger (1 + \hat{\mathbf{n}} \cdot \hat{\mathbf{M}}_{\text{F}}) + C_{\mathbf{q}} A_{\mathbf{k}} \beta_{\mathbf{q}}^\dagger (1 - \hat{\mathbf{n}} \cdot \hat{\mathbf{M}}_{\text{F}}) + \text{H.c.} \right] \delta_{\mathbf{k},\mathbf{q}} \end{aligned} \tag{B.7}$$

where we have neglected the high order magnon interactions.

It would be straightforward to calculate the longitudinal and transverse spin current across AF/F interface (per interface cross area A_{I}) by using the Fermi's golden rule

$$j_{\text{AF/F}} = \left\langle \frac{1}{iA_{\text{I}}} \left[\sum_{\mathbf{q}} a_{\mathbf{q}}^\dagger a_{\mathbf{q}}, H_{\text{int}} \right] \right\rangle \tag{B.8}$$

where <> refers to the thermal averaging over all states. Using the rough interface approximation, we find

$$j^{\parallel}_{\mathrm{AF/F}} = G^{\parallel}_{\mathrm{AF/F}}(\mu^{\mathrm{F}}_m - \mu^{\alpha}_m) \tag{B.9a}$$

$$j^{\perp}_{\mathrm{AF/F}} = G^{\perp}_{\mathrm{AF/F}}[\mu^{\mathrm{F}}_m - (\mu^{\alpha}_m - \mu^{\beta}_m)] \tag{B.9b}$$

where the magnon conductance is

$$\begin{aligned} G^{\parallel}_{\mathrm{AF/F}} = 2G^{\perp}_{\mathrm{AF/F}} =& \frac{\pi S_{\mathrm{F}} S_{\mathrm{AF}} J^2_{\mathrm{int}} a^2_{\mathrm{F}} a^2_{\mathrm{AF}}}{2k_B T} \int d\varepsilon_{\mathbf{q}} d\varepsilon_{\mathbf{q}'} (u_{\mathbf{q}} - v_{\mathbf{q}}) \\ & \times g^{\mathrm{F}}_m(\varepsilon_{\mathbf{q}}) g^{\mathrm{AF}}_m(\varepsilon_{\mathbf{q}}) \times \mathrm{csch}^2 \frac{\varepsilon_{\mathbf{q}}}{2k_B T} \end{aligned} \tag{B.10}$$

where $a_{\mathrm{F(AF)}}$ is the lattice constant of the FM(AFI) material and g_m is the density of states of magnon.

Bibliography

[1] Kai Chen, Spin Transport in Magnetic Nano-Structures, The University of Arizona. (2017).

[2] R.W. Powell, R.P. Tye, and M.J. Hickman, The thermal conductivity of nickel, International Journal of Heat and Mass Transfer **8**, 679 – 688 (1965).

[3] J.E. Keem and J.M. Honig, Selected electrical and thermal properties of undoped nickel oxide, CINDAS Report **52** (1978).

[4] Satoru Nakatsuji, Naoki Kiyohara, and Tomoya Higo, Large anomalous Hall effect in a non-collinear antiferromagnet at room temperature, Nature **527**, 212–215 (2015).

[5] S. A. Wolf, D. D. Awschalom, R. A. Buhrman, J. M. Daughton, S. von Molnár, M. L. Roukes, A. Y. Chtchelkanova, and D. M. Treger, Spintronics: A Spin-Based Electronics Vision for the Future, Science **294**, 1488–1495 (2001).

[6] Igor Žutić, Jaroslav Fabian, and S. Das Sarma, Spintronics: Fundamentals and applications, Rev. Mod. Phys. **76**, 323–410 (2004).

[7] Evgeny Y. Tsymbal and Igor Zutic, eds., *Handbook of spin transport and magnetism* (CRC Press, 2012).

[8] N. F. Mott, The Electrical Conductivity of Transition Metals, Proceedings of the Royal Society of London. Series A-Mathematical and Physical Sciences **153**, 699–717 (1936).

[9] M. N. Baibich, J. M. Broto, A. Fert, F. Nguyen Van Dau, F. Petroff, P. Etienne, G. Creuzet, A. Friederich, and J. Chazelas, Giant Magnetoresistance of (001)Fe/(001)Cr Magnetic Superlattices, Phys. Rev. Lett. **61**, 2472–2475 (1988).

[10] G. Binasch, P. Grünberg, F. Saurenbach, and W. Zinn, Enhanced magnetoresistance in layered magnetic structures with antiferromagnetic interlayer exchange, Phys. Rev. B **39**, 4828–4830 (1989).

[11] T. Miyazaki and N. Tezuka, Giant magnetic tunneling effect in Fe/Al2O3/Fe junction, J. Magn. Magn. Mater. **139**, L231–L234 (1995).

[12] J. S. Moodera, Lisa R. Kinder, Terrilyn M. Wong, and R. Meservey, Large Magnetoresistance at Room Temperature in Ferromagnetic Thin Film Tunnel Junctions, Phys. Rev. Lett. **74**, 3273–3276 (1995).

[13] Stuart S. P. Parkin, Christian Kaiser, Alex Panchula, Philip M. Rice, Brian Hughes, Mahesh Samant, and See-Hun Yang, Giant tunnelling magnetoresistance at room temperature with MgO (100) tunnel barriers, Nat. Mater. **3**, 862–867 (2004).

[14] Shinji Yuasa, Taro Nagahama, Akio Fukushima, Yoshishige Suzuki, and Koji Ando, Giant room-temperature magnetoresistance in single-crystal Fe/MgO/Fe magnetic tunnel junctions, Nat. Mater. **3**, 868–871 (2004).

[15] J. C. Slonczewski, Current-driven excitation of magnetic multilayers, J. Magn. Magn. Mater. **159**, L1–L7 (1996).

[16] L. Berger, Emission of spin waves by a magnetic multilayer traversed by a current, Phys. Rev. B **54**, 9353–9358 (1996).

[17] M. Tsoi, A. G. M. Jansen, J. Bass, W.-C. Chiang, M. Seck, V. Tsoi, and P. Wyder, Excitation of a Magnetic Multilayer by an Electric Current, Phys. Rev. Lett. **80**, 4281–4284 (1998).

[18] J. A. Katine, F. J. Albert, R. A. Buhrman, E. B. Myers, and D. C. Ralph, Current-Driven Magnetization Reversal and Spin-Wave Excitations in Co/Cu/Co Pillars, Phys. Rev. Lett. **84**, 3149–3152 (2000).

[19] M. D. Stiles and A. Zangwill, Anatomy of spin-transfer torque, Phys. Rev. B **66**, 014407 (2002).

[20] D. C. Ralph and M. D. Stiles, Spin transfer torques, J. Magn. Magn. Mater. **320**, 1190–1216 (2008).

[21] M. I. Dyakonov and V. I. Perel, Current-induced spin orientation of electrons in semiconductors, Physics Letters A **35**, 459–460 (1971).

[22] J. E. Hirsch, Spin Hall Effect, Phys. Rev. Lett. **83**, 1834–1837 (1999).

[23] Y. K. Kato, R. C. Myers, A. C. Gossard, and D. D. Awschalom, Observation of the Spin Hall Effect in Semiconductors, Science **306**, 1910–1913 (2004).

[24] J. Wunderlich, B. Kaestner, J. Sinova, and T. Jungwirth, Experimental Observation of the Spin-Hall Effect in a Two-Dimensional Spin-Orbit Coupled Semiconductor System, Phys. Rev. Lett. **94**, 047204 (2005).

[25] Jairo Sinova, Sergio O. Valenzuela, J. Wunderlich, C. H. Back, and T. Jungwirth, Spin Hall effects, Rev. Mod. Phys. **87**, 1213–1260 (2015).

[26] E. Saitoh, M. Ueda, H. Miyajima, and G. Tatara, Conversion of spin current into charge current at room temperature: Inverse spin-Hall effect, Appl. Phys. Lett. **88**, 182509 (2006).

[27] S. O. Valenzuela and M. Tinkham, Direct electronic measurement of the spin Hall effect, Nature **442**, 176–179 (2006).

[28] Claude Chappert, Albert Fert, and Frédéric Nguyen Van Dau, The emergence of spin electronics in data storage, Nat. Mater. **6**, 813–823 (2007).

[29] B. N. Engel, J. Akerman, B. Butcher, R. W. Dave, M. DeHerrera, M. Durlam, G. Grynkewich, J. Janesky, S. V. Pietambaram, N. D. Rizzo, J. M. Slaughter, K. Smith, J. J. Sun, and S. Tehrani, A 4-Mb toggle MRAM based on a novel bit and switching method, IEEE Transactions on Magnetics **41**, 132–136 (2005).

[30] Sabpreet Bhatti, Rachid Sbiaa, Atsufumi Hirohata, Hideo Ohno, Shunsuke Fukami, and S. N. Piramanayagam, Spintronics based random access memory: A review, Materials Today 10.1016/j.mattod.2017.07.007 (2017).

[31] Felix Bloch, Zur theorie des ferromagnetismus, Zeitschrift für Physik **61**, 206–219 (1930).

[32] V. V. Kruglyak, S. O. Demokritov, and D. Grundler, Magnonics, Journal of Physics D: Applied Physics **43**, 264001 (2010).

[33] A. V. Chumak, V. I. Vasyuchka, A. A. Serga, and B. Hillebrands, Magnon spintronics, Nat. Phys. **11**, 453–461 (2015).

[34] Ken-ichi Uchida, Hiroto Adachi, Takeru Ota, Hiroyasu Nakayama, Sadamichi Maekawa, and Eiji Saitoh, Observation of longitudinal spin-Seebeck effect in magnetic insulators, Appl. Phys. Lett. **97**, 172505 (2010).

[35] S. Y. Huang, W. G. Wang, S. F. Lee, J. Kwo, and C. L. Chien, Intrinsic Spin-Dependent Thermal Transport, Phys. Rev. Lett. **107**, 216604 (2011).

[36] Mathias Weiler, Matthias Althammer, Franz D. Czeschka, Hans Huebl, Martin S. Wagner, Matthias Opel, Inga-Mareen Imort, Günter Reiss, Andy Thomas, Rudolf Gross, and Sebastian T. B. Goennenwein, Local Charge and Spin Currents in Magnetothermal Landscapes, Phys. Rev. Lett. **108**, 106602 (2012).

[37] K. Uchida, T. Nonaka, T. Kikkawa, Y. Kajiwara, and E. Saitoh, Longitudinal spin Seebeck effect in various garnet ferrites, Phys. Rev. B **87**, 104412 (2013).

[38] Hailong Wang, Chunhui Du, P. Chris Hammel, and Fengyuan Yang, Antiferromagnonic spin transport from Y 3 Fe 5 O 12 into NiO, Phys. Rev. Lett. **113**, 097202 (2014).

[39] Christian Hahn, Grégoire de Loubens, Vladimir V. Naletov, Jamal Ben Youssef, Olivier Klein, and Michel Viret, Conduction of spin currents through insulating antiferromagnetic oxides, EPL (Europhysics Letters) **108**, 57005 (2014).

[40] L. J. Cornelissen, J. Liu, R. A. Duine, J. Ben Youssef, and B. J. van Wees, Long-distance transport of magnon spin information in a magnetic insulator at room temperature, Nat. Phys. **11**, 1022–1026 (2015).

[41] Weiwei Lin, Kai Chen, Shufeng Zhang, and C. L. Chien, Enhancement of Thermally Injected Spin Current through an Antiferromagnetic Insulator, Phys. Rev. Lett. **116**, 186601 (2016).

[42] Zhiyong Qiu, Jia Li, Dazhi Hou, Elke Arenholz, Alpha T. N'Diaye, Ali Tan, Ken-ichi Uchida, Koji Sato, Satoshi Okamoto, Yaroslav Tserkovnyak, Z. Q. Qiu, and Eiji Saitoh, Spin-current probe for phase transition in an insulator, Nat. Commun. **7**, ncomms12670 (2016).

[43] Yu-Ming Hung, Christian Hahn, Houchen Chang, Mingzhong Wu, Hendrik Ohldag, and Andrew D. Kent, Spin transport in antiferromagnetic NiO and magnetoresistance in Y3Fe5O12/NiO/Pt structures, AIP Advances **7**, 055903 (2016).

[44] Junxue Li, Yadong Xu, Mohammed Aldosary, Chi Tang, Zhisheng Lin, Shufeng Zhang, Roger Lake, and Jing Shi, Observation of magnon-mediated current drag in Pt/yttrium iron garnet/Pt(Ta) trilayers, Nat. Commun. **7**, 10858 (2016).

[45] H. Wu, C. H. Wan, X. Zhang, Z. H. Yuan, Q. T. Zhang, J. Y. Qin, H. X. Wei, X. F. Han, and S. Zhang, Observation of magnon-mediated electric current drag at room temperature, Phys. Rev. B **93**, 060403 (2016).

[46] Yihong Cheng, Kai Chen, and Shufeng Zhang, Giant magneto-spin-Seebeck effect and magnon transfer torques in insulating spin valves, Appl. Phys. Lett. **112**, 052405 (2018).

[47] Ran Cheng, Di Xiao, and Jian-Gang Zhu, Antiferromagnet-based magnonic spin-transfer torque, Phys. Rev. B **98**, 020408 (2018).

[48] Yi Wang, Dapeng Zhu, Yumeng Yang, Kyusup Lee, Rahul Mishra, Gyungchoon Go, Se-Hyeok Oh, Dong-Hyun Kim, Kaiming Cai, Enlong Liu, Shawn D. Pollard, Shuyuan Shi, Jongmin Lee, Kie Leong Teo, Yihong Wu, Kyung-Jin Lee, and Hyunsoo Yang, Magnetization switching by magnon-mediated spin torque through an antiferromagnetic insulator, Science **366**, 1125–1128 (2019).

[49] T. Valet and A. Fert, Theory of the perpendicular magnetoresistance in magnetic multilayers, Phys. Rev. B **48**, 7099–7113 (1993).

[50] M. Julliere, Tunneling between ferromagnetic films, Physics Letters A **54**, 225–226 (1975).

[51] A. Brataas, Y. V. Nazarov, and G. E. W. Bauer, Spin-transport in multi-terminal normal metal-ferromagnet systems with non-collinear magnetizations, The European Physical Journal B **22**, 99–110 (2001).

[52] Ryogo Kubo, The Spin-Wave Theory of Antiferromagnetics, Physical Review **87**, 568–580 (1952).

[53] F. Keffer and C. Kittel, Theory of Antiferromagnetic Resonance, Physical Review **85**, 329–337 (1952).

[54] F. Keffer, H. Kaplan, and Y. Yafet, Spin Waves in Ferromagnetic and Antiferromagnetic Materials, American Journal of Physics **21**, 250–257 (1953).

[55] J. VAN KRANENDONK and J. H. VAN VLECK, Spin Waves, Rev. Mod. Phys. **30**, 1–23 (1958).

[56] T. Holstein and H. Primakoff, Field Dependence of the Intrinsic Domain Magnetization of a Ferromagnet, Physical Review **58**, 1098–1113 (1940).

[57] E. V. Gomonay and V. M. Loktev, Spintronics of antiferromagnetic systems, Low Temperature Physics **40**, 17–35 (2014).

[58] T. Jungwirth, X. Marti, P. Wadley, and J. Wunderlich, Antiferromagnetic spintronics, Nat. Nano. **11**, 231–241 (2016).

[59] V. Baltz, A. Manchon, M. Tsoi, T. Moriyama, T. Ono, and Y. Tserkovnyak, Antiferromagnetic spintronics, Rev. Mod. Phys. **90**, 015005 (2018).

[60] R. A. Duine, Kyung-Jin Lee, Stuart S. P. Parkin, and M. D. Stiles, Synthetic antiferromagnetic spintronics, Nat. Phys. **14**, 217–219 (2018).

[61] O. Gomonay, V. Baltz, A. Brataas, and Y. Tserkovnyak, Antiferromagnetic spin textures and dynamics, Nat. Phys. **14**, 213–216 (2018).

[62] Matthias B. Jungfleisch, Wei Zhang, and Axel Hoffmann, Perspectives of antiferromagnetic spintronics, Physics Letters A **382**, 865–871 (2018).

[63] P. Němec, M. Fiebig, T. Kampfrath, and A. V. Kimel, Antiferromagnetic optospintronics, Nat. Phys. , 1 (2018).

[64] P. W. Anderson, An Approximate Quantum Theory of the Antiferromagnetic Ground State, Physical Review **86**, 694–701 (1952).

[65] Th. Jolicoeur and J. C. Le Guillou, Spin-wave results for the triangular Heisenberg antiferromagnet, Phys. Rev. B **40**, 2727–2729 (1989).

[66] Rajiv R. P. Singh and David A. Huse, Three-sublattice order in triangular- and kagomé-lattice spin-half antiferromagnets, Phys. Rev. Lett. **68**, 1766–1769 (1992).

[67] Luca Capriotti, Adolfo E. Trumper, and Sandro Sorella, Long-range Néel order in the triangular Heisenberg model, Phys. Rev. Lett. **82**, 3899–3902 (1999).

[68] T. Inami, M. Nishiyama, S. Maegawa, and Y. Oka, Magnetic structure of the kagomé lattice antiferromagnet potassium jarosite KFe 3 (OH) 6 (SO 4) 2, Phys. Rev. B **61**, 12181–12186 (2000).

[69] T. Yildirim and A. B. Harris, Magnetic structure and spin waves in the Kagomé jarosite compound K Fe 3 (SO 4) 2 (OH) 6, Phys. Rev. B **73**, 214446 (2006).

[70] Steven R. White and A. L. Chernyshev, Neél order in square and triangular lattice Heisenberg models, Phys. Rev. Lett. **99**, 127004 (2007).

[71] A. L. Chernyshev and M. E. Zhitomirsky, Spin waves in a triangular lattice antiferromagnet: Decays, spectrum renormalization, and singularities, Phys. Rev. B **79**, 144416 (2009).

[72] Joosung Oh, Manh Duc Le, Jaehong Jeong, Jung-hyun Lee, Hyungje Woo, Wan-Young Song, T. G. Perring, W. J. L. Buyers, S.-W. Cheong, and Je-Geun Park, Magnon breakdown in a two dimensional triangular lattice Heisenberg antiferromagnet of multiferroic LuMnO 3, Phys. Rev. Lett. **111**, 257202 (2013).

[73] R. Urban, G. Woltersdorf, and B. Heinrich, Gilbert Damping in Single and Multilayer Ultrathin Films: Role of Interfaces in Nonlocal Spin Dynamics, Phys. Rev. Lett. **87**, 217204 (2001).

[74] Yaroslav Tserkovnyak, Arne Brataas, and Gerrit E. W. Bauer, Enhanced Gilbert Damping in Thin Ferromagnetic Films, Phys. Rev. Lett. **88**, 117601 (2002).

[75] Yaroslav Tserkovnyak, Arne Brataas, and Gerrit E. W. Bauer, Spin pumping and magnetization dynamics in metallic multilayers, Phys. Rev. B **66**, 224403 (2002).

[76] Sadamichi Maekawa, Sergio O Valenzuela, Eiji Saitoh, and Takashi Kimura, *Spin current* (Oxford University Press, 2017).

[77] Lars Onsager, Reciprocal Relations in Irreversible Processes. I., Physical Review **37**, 405–426 (1931).

[78] Lars Onsager, Reciprocal Relations in Irreversible Processes. II., Physical Review **38**, 2265–2279 (1931).

[79] Steven S.-L. Zhang and Shufeng Zhang, Magnon Mediated Electric Current Drag Across a Ferromagnetic Insulator Layer, Phys. Rev. Lett. **109**, 096603 (2012).

[80] Steven S.-L. Zhang and Shufeng Zhang, Spin convertance at magnetic interfaces, Phys. Rev. B **86**, 214424 (2012).

[81] K. Uchida, J. Xiao, H. Adachi, J. Ohe, S. Takahashi, J. Ieda, T. Ota, Y. Kajiwara, H. Umezawa, H. Kawai, G. E. W. Bauer, S. Maekawa, and E. Saitoh, Spin Seebeck insulator, Nat. Mater. **9**, 894–897 (2010).

[82] H. Wu, L. Huang, C. Fang, B. S. Yang, C. H. Wan, G. Q. Yu, J. F. Feng, H. X. Wei, and X. F. Han, Magnon Valve Effect between Two Magnetic Insulators, Phys. Rev. Lett. **120**, 097205 (2018).

[83] Junxue Li, Zhong Shi, Victor H. Ortiz, Mohammed Aldosary, Cliff Chen, Vivek Aji, Peng Wei, and Jing Shi, Spin Seebeck Effect from Antiferromagnetic Magnons and Critical Spin Fluctuations in Epitaxial FeF 2 Films, Phys. Rev. Lett. **122**, 217204 (2019).

[84] S. Y. Huang, X. Fan, D. Qu, Y. P. Chen, W. G. Wang, J. Wu, T. Y. Chen, J. Q. Xiao, and C. L. Chien, Transport Magnetic Proximity Effects in Platinum, Phys. Rev. Lett. **109**, 107204 (2012).

[85] S. Takahashi, E. Saitoh, and S. Maekawa, Spin current through a normal-metal/insulating-ferromagnet junction, Journal of Physics: Conference Series **200**, 062030 (2010).

[86] Jiang Xiao, Gerrit E. W. Bauer, Ken-chi Uchida, Eiji Saitoh, and Sadamichi Maekawa, Theory of magnon-driven spin Seebeck effect, Phys. Rev. B **81**, 214418 (2010).

[87] S. M. Rezende, R. L. Rodríguez-Suárez, and A. Azevedo, Diffusive magnonic spin transport in antiferromagnetic insulators, Phys. Rev. B **93**, 054412 (2016).

[88] S. M. Rezende, R. L. Rodríguez-Suárez, R. O. Cunha, A. R. Rodrigues, F. L. A. Machado, G. A. Fonseca Guerra, J. C. Lopez Ortiz, and A. Azevedo, Magnon spin-current theory for the longitudinal spin-Seebeck effect, Phys. Rev. B **89**, 014416 (2014).

[89] Kai Chen, Weiwei Lin, C. L. Chien, and Shufeng Zhang, Temperature dependence of angular momentum transport across interfaces, Phys. Rev. B **94**, 054413 (2016).

[90] Y. Kajiwara, S. Takahashi, S. Maekawa, and E. Saitoh, Detection of Spin-Wave Spin Current in a Magnetic Insulator, IEEE Transactions on Magnetics **47**, 1591–1594 (2011).

[91] E. B. Sonin, Spin currents and spin superfluidity, Adv. Phys. **59**, 181–255 (2010).

[92] Andreas Rückriegel and Peter Kopietz, Spin currents, spin torques, and the concept of spin superfluidity, Phys. Rev. B **95**, 104436 (2017).

[93] Tadao Kasuya, Electrical Resistance of Ferromagnetic Metals, Progress of Theoretical Physics **16**, 58–63 (1956).

[94] L. C. Davis and S. H. Liu, Electron-Magnon Interaction in Ferromagnetic Transition Metals, Physical Review **163**, 503–505 (1967).

[95] A. Fert, Two-current conduction in ferromagnetic metals and spin wave-electron collisions, Journal of Physics C: Solid State Physics **2**, 1784 (1969).

[96] J. Barnas, O. Baksalary, and Y. Bruynseraede, Effects of interchannel transitions in the current-in-plane giant magnetoresistance, Journal of Physics: Condensed Matter **7**, 6437 (1995).

[97] Tadao Kasuya, Effects of s-d Interaction on Transport Phenomena, Progress of Theoretical Physics **22**, 227–246 (1959).

[98] Isao Mannari, Electrical Resistance of Ferromagnetic Metals, Progress of Theoretical Physics **22**, 335–343 (1959).

[99] D. A. Goodings, Electrical Resistivity of Ferromagnetic Metals at Low Temperatures, Physical Review **132**, 542–558 (1963).

[100] D. L. Mills, A. Fert, and I. A. Campbell, Temperature Dependence of the Electrical Resistivity of Dilute Ferromagnetic Alloys, Phys. Rev. B **4**, 196–201 (1971).

[101] J. Bass, Giant magnetoresistance: Experiment, in *Handbook of Spin Transport and Magnetism*, edited by E.Y. Tsymbal and I. Zutic (CRC Press, 2012) pp. 69–93.

[102] M. A. M. Gijs, S. K. J. Lenczowski, and J. B. Giesbers, Perpendicular giant magnetoresistance of microstructured Fe/Cr magnetic multilayers from 4.2 to 300 K, Phys. Rev. Lett. **70**, 3343–3346 (1993).

[103] K. Liu, K. Nagodawithana, P. C. Searson, and C. L. Chien, Perpendicular giant magnetoresistance of multilayered Co/Cu nanowires, Phys. Rev. B **51**, 7381–7384 (1995).

[104] L. J. Cornelissen, K. J. H. Peters, G. E. W. Bauer, R. A. Duine, and B. J. van Wees, Magnon spin transport driven by the magnon chemical potential in a magnetic insulator, Phys. Rev. B **94**, 014412 (2016).

[105] Scott A. Bender and Yaroslav Tserkovnyak, Thermally driven spin torques in layered magnetic insulators, Phys. Rev. B **93**, 064418 (2016).

[106] John C. Slonczewski, Initiation of spin-transfer torque by thermal transport from magnons, Phys. Rev. B **82**, 054403 (2010).

[107] Yiming Huai, Frank Albert, Paul Nguyen, Mahendra Pakala, and Thierry Valet, Observation of spin-transfer switching in deep submicron-sized and low-resistance magnetic tunnel junctions, Appl. Phys. Lett. **84**, 3118–3120 (2004).

[108] Zhitao Diao, Dmytro Apalkov, Mahendra Pakala, Yunfei Ding, Alex Panchula, and Yiming Huai, Spin transfer switching and spin polarization in magnetic tunnel junctions with MgO and AlOx barriers, Appl. Phys. Lett. **87**, 232502 (2005).

[109] Zhitao Diao, Alex Panchula, Yunfei Ding, Mahendra Pakala, Shengyuan Wang, Zhanjie Li, Dmytro Apalkov, Hideyasu Nagai, Alexander Driskill-Smith, Lien-Chang Wang, Eugene Chen, and Yiming Huai, Spin transfer switching in dual MgO magnetic tunnel junctions, Appl. Phys. Lett. **90**, 132508 (2007).

[110] Scott A. Bender, Rembert A. Duine, and Yaroslav Tserkovnyak, Electronic Pumping of Quasiequilibrium Bose-Einstein-Condensed Magnons, Phys. Rev. Lett. **108**, 246601 (2012).

[111] S. M. Rezende, R. L. Rodríguez-Suárez, and A. Azevedo, Theory of the spin Seebeck effect in antiferromagnets, Phys. Rev. B **93**, 014425 (2016).

[112] Yuichi Ohnuma, Hiroto Adachi, Eiji Saitoh, and Sadamichi Maekawa, Spin Seebeck effect in antiferromagnets and compensated ferrimagnets, Phys. Rev. B **87**, 014423 (2013).

[113] J. Barnaś, A. Fert, M. Gmitra, I. Weymann, and V. K. Dugaev, From giant magnetoresistance to current-induced switching by spin transfer, Phys. Rev. B **72**, 024426 (2005).

[114] Arne Brataas, Yu. V. Nazarov, and Gerrit E. W. Bauer, Finite-Element Theory of Transport in Ferromagnet-Normal Metal Systems, Phys. Rev. Lett. **84**, 2481–2484 (2000).

[115] J. C. Slonczewski, Conductance and exchange coupling of two ferromagnets separated by a tunneling barrier, Phys. Rev. B **39**, 6995–7002 (1989).

[116] W. H. Butler, X.-G. Zhang, T. C. Schulthess, and J. M. MacLaren, Spin-dependent tunneling conductance of Fe—MgO—Fe sandwiches, Phys. Rev. B **63**, 054416 (2001).

[117] J. Mathon and A. Umerski, Theory of tunneling magnetoresistance of an epitaxial Fe/MgO/Fe(001) junction, Phys. Rev. B **63**, 220403 (2001).

[118] D. Apalkov, B. Dieny, and J. M. Slaughter, Magnetoresistive Random Access Memory, Proceedings of the IEEE **104**, 1796–1830 (2016).

[119] S. Ikeda, J. Hayakawa, Y. Ashizawa, Y. M. Lee, K. Miura, H. Hasegawa, M. Tsunoda, F. Matsukura, and H. Ohno, Tunnel magnetoresistance of 604% at 300 K by suppression of Ta diffusion in Co Fe B/ Mg O/ Co Fe B pseudo-spin-valves annealed at high temperature, Appl. Phys. Lett. **93**, 082508 (2008).

[120] G. D. Fuchs, N. C. Emley, I. N. Krivorotov, P. M. Braganca, E. M. Ryan, S. I. Kiselev, J. C. Sankey, D. C. Ralph, R. A. Buhrman, and J. A. Katine, Spin-transfer effects in nanoscale magnetic tunnel junctions, Appl. Phys. Lett. **85**, 1205–1207 (2004).

[121] M. Hosomi, H. Yamagishi, T. Yamamoto, K. Bessho, Y. Higo, K. Yamane, H. Yamada, M. Shoji, H. Hachino, C. Fukumoto, H. Nagao, and H. Kano, A novel nonvolatile memory with spin torque transfer magnetization switching: spin-ram, in *IEEE International Electron Devices Meeting, 2005. IEDM Technical Digest.* (2005) pp. 459–462.

[122] S. Ikeda, K. Miura, H. Yamamoto, K. Mizunuma, H. D. Gan, M. Endo, S. Kanai, J. Hayakawa, F. Matsukura, and H. Ohno, A perpendicular-anisotropy CoFeB–MgO magnetic tunnel junction, Nat. Mater. **9**, 721–724 (2010).

[123] D. C. Worledge, G. Hu, David W. Abraham, J. Z. Sun, P. L. Trouilloud, J. Nowak, S. Brown, M. C. Gaidis, E. J. O'Sullivan, and R. P. Robertazzi, Spin torque switching of perpendicular Ta|CoFeB|MgO-based magnetic tunnel junctions, Appl. Phys. Lett. **98**, 022501 (2011).

[124] Jisang Hong and D. L. Mills, Theory of the spin dependence of the inelastic mean free path of electrons in ferromagnetic metals: A model study, Phys. Rev. B **59**, 13840–13848 (1999).

[125] Jisang Hong and D. L. Mills, Spin dependence of the inelastic electron mean free path in Fe and Ni: Explicit calculations and implications, Phys. Rev. B **62**, 5589–5600 (2000).

[126] R. C. Sousa, I. L. Prejbeanu, D. Stanescu, B. Rodmacq, O. Redon, B. Dieny, Jianguo Wang, and P. P. Freitas, Tunneling hot spots and heating in magnetic tunnel junctions, Journal of Applied Physics **95**, 6783–6785 (2004).

[127] E. Gapihan, J. Hérault, R. C. Sousa, Y. Dahmane, B. Dieny, L. Vila, I. L. Prejbeanu, C. Ducruet, C. Portemont, K. Mackay, and J. P. Nozières, Heating asymmetry induced by tunneling current flow in magnetic tunnel junctions, Appl. Phys. Lett. **100**, 202410 (2012).

[128] Hiroto Adachi, Jun-ichiro Ohe, Saburo Takahashi, and Sadamichi Maekawa, Linear-response theory of spin Seebeck effect in ferromagnetic insulators, Phys. Rev. B **83**, 094410 (2011).

[129] Hiroto Adachi, Ken-ichi Uchida, Eiji Saitoh, and Sadamichi Maekawa, Theory of the spin Seebeck effect, Reports on Progress in Physics **76**, 036501 (2013).

[130] M Beens, J P Heremans, Yaroslav Tserkovnyak, and R A Duine, Magnons versus electrons in thermal spin transport through metallic interfaces, Journal of Physics D: Applied Physics **51**, 394002 (2018).

[131] E. Beaurepaire, J.-C. Merle, A. Daunois, and J.-Y. Bigot, Ultrafast Spin Dynamics in Ferromagnetic Nickel, Phys. Rev. Lett. **76**, 4250–4253 (1996).

[132] Austin Deschenes, Sadid Muneer, Mustafa Akbulut, Ali Gokirmak, and Helena Silva, Analysis of self-heating of thermally assisted spin-transfer torque magnetic random access memory, Beilstein Journal of Nanotechnology **7**, 1676–1683 (2016).

[133] Stephen M. Wu, Wei Zhang, Amit KC, Pavel Borisov, John E. Pearson, J. Samuel Jiang, David Lederman, Axel Hoffmann, and Anand Bhattacharya, Antiferromagnetic Spin Seebeck Effect, Phys. Rev. Lett. **116**, 097204 (2016).

[134] S. Maekawa and U. Gafvert, Electron tunneling between ferromagnetic films, IEEE Transactions on Magnetics **18**, 707–708 (1982).

[135] T. Jungwirth, J. Sinova, A. Manchon, X. Marti, J. Wunderlich, and C. Felser, The multiple directions of antiferromagnetic spintronics, Nat. Phys. **14**, 200–203 (2018).

[136] A. Manchon, J. Železný, I. M. Miron, T. Jungwirth, J. Sinova, A. Thiaville, K. Garello, and P. Gambardella, Current-induced spin-orbit torques in ferromagnetic and antiferromagnetic systems, Rev. Mod. Phys. **91**, 035004 (2019).

[137] Ran Cheng, Jiang Xiao, Qian Niu, and Arne Brataas, Spin Pumping and Spin-Transfer Torques in Antiferromagnets, Phys. Rev. Lett. **113**, 057601 (2014).

[138] Wei Zhang, Matthias B. Jungfleisch, Wanjun Jiang, John E. Pearson, Axel Hoffmann, Frank Freimuth, and Yuriy Mokrousov, Spin Hall Effects in Metallic Antiferromagnets, Phys. Rev. Lett. **113**, 196602 (2014).

[139] Yongxi Ou, Shengjie Shi, D. C. Ralph, and R. A. Buhrman, Strong spin Hall effect in the antiferromagnet PtMn, Phys. Rev. B **93**, 220405 (2016).

[140] Hua Chen, Qian Niu, and A. H. MacDonald, Anomalous Hall Effect Arising from Noncollinear Antiferromagnetism, Phys. Rev. Lett. **112**, 017205 (2014).

[141] J. Kübler and C. Felser, Non-collinear antiferromagnets and the anomalous Hall effect, EPL (Europhysics Letters) **108**, 67001 (2014).

[142] Ajaya K. Nayak, Julia Erika Fischer, Yan Sun, Binghai Yan, Julie Karel, Alexander C. Komarek, Chandra Shekhar, Nitesh Kumar, Walter Schnelle, Jürgen Kübler, Claudia Felser, and Stuart S. P. Parkin, Large anomalous Hall effect driven by a nonvanishing Berry curvature in the noncolinear antiferromagnet Mn3Ge, Sci. Adv. **2**, e1501870 (2016).

[143] Benedetta Flebus, Yaroslav Tserkovnyak, and Gregory A. Fiete, Interfacial spin Seebeck effect in noncollinear magnetic systems, Phys. Rev. B **99**, 224410 (2019).

[144] Alexander Mook, Jürgen Henk, and Ingrid Mertig, Thermal Hall effect in noncollinear coplanar insulating antiferromagnets, Phys. Rev. B **99**, 014427 (2019).

[145] Kyung-Su Kim, Ki Hoon Lee, Suk Bum Chung, and Je-Geun Park, Magnon topology and thermal Hall effect in trimerized triangular lattice antiferromagnet, Phys. Rev. B **100**, 064412 (2019).

[146] Alexander Mook, Robin R. Neumann, Jürgen Henk, and Ingrid Mertig, Spin Seebeck and spin Nernst effects of magnons in noncollinear antiferromagnetic insulators, Phys. Rev. B **100**, 100401 (2019).

[147] Motoi Kimata, Hua Chen, Kouta Kondou, Satoshi Sugimoto, Prasanta K. Muduli, Muhammad Ikhlas, Yasutomo Omori, Takahiro Tomita, Allan H. MacDonald, Satoru Nakatsuji, and Yoshichika Otani, Magnetic and magnetic inverse spin Hall effects in a non-collinear antiferromagnet, Nature **565**, 627–630 (2019).

[148] P. K. Muduli, T. Higo, T. Nishikawa, D. Qu, H. Isshiki, K. Kondou, D. Nishio-Hamane, S. Nakatsuji, and YoshiChika Otani, Evaluation of spin diffusion length and spin Hall angle of the antiferromagnetic Weyl semimetal Mn 3 Sn, Phys. Rev. B **99**, 184425 (2019).

[149] Nobuyuki Okuma, Magnon Spin-Momentum Locking: Various Spin Vortices and Dirac magnons in Noncollinear Antiferromagnets, Phys. Rev. Lett. **119**, 107205 (2017).

[150] M. Elhajal, B. Canals, and C. Lacroix, Symmetry breaking due to Dzyaloshinsky-Moriya interactions in the kagomé lattice, Phys. Rev. B **66**, 014422 (2002).

[151] T. Yildirim and A. B. Harris, Magnetic structure and spin waves in the Kagomé jarosite compound K Fe 3 (SO 4) 2 (OH) 6, Phys. Rev. B **73**, 214446 (2006).

[152] K. Matan, D. Grohol, D. G. Nocera, T. Yildirim, A. B. Harris, S. H. Lee, S. E. Nagler, and Y. S. Lee, Spin waves in the frustrated kagomé lattice antiferromagnet KFe 3 (OH) 6 (SO 4) 2, Phys. Rev. Lett. **96**, 247201 (2006).

[153] N. D. Mermin and H. Wagner, Absence of Ferromagnetism or Antiferromagnetism in One- or Two-Dimensional Isotropic Heisenberg Models, Phys. Rev. Lett. **17**, 1133–1136 (1966).

[154] Jakub Železný, Yang Zhang, Claudia Felser, and Binghai Yan, Spin-Polarized Current in Noncollinear Antiferromagnets, Phys. Rev. Lett. **119**, 187204 (2017).